TRANSNUCLEAR

# CALCULATION PACKAGE



| | |
|---|---|
| CALCULATION NO: SCE-23.0411 NP | PROJECT NAME: San Onofre Unit 2/3 Dry Cask Storage |
| PROJECT NO: SCE-23 | CLIENT: Southern California Edision |

CALCULATION TITLE:

Thermal Analysis of NUHOMS® 24PT4-DSC Using CFD Method

SUMMARY DESCRIPTION:

The NUHOMS® 24PT4 dry shielded canister (DSC) is designed to serve as the containment and confinement boundary for up to twenty-four (24) spent nuclear fuel assemblies (FAs) during operations in the Advanced NUHOMS® Horizontal Storage Module (AHSM) and the OS197 transfer cask. The design of the 24PT4-DSC provides for the passive rejection of the decay heat from the FAs. This calculation provides a design basis evaluation of the thermal performance of the 24PT4-DSC, including the effects of convection heat transfer, using a computational fluid dynamics (CFD) methodology.

NON-PROPRIETARY
FOR INFORMATION ONLY

| REVISION | TOTAL PAGES AND DISKS (IF ANY) | NAMES AND INITIALS OF PREPARERS & DATES | NAMES AND INITIALS OF VERIFIERS & DATES | APPROVER NAME AND SIGNATURE | APPROVAL DATE |
|---|---|---|---|---|---|
| 0 | 75 + A1 + B1 to B9 | Gregory J. Banken Gregory Banken 6/28/04 | Marcel D. Berz Marcel Berz 6/28/04 | Ian McInnes for Joginder Bandra | 6/30/04 |
| | | | | | |
| | | | | | |
| | | | | | |

## REVISION SUMMARY

| REV. | DATE | DESCRIPTION | AFFECTED PAGES | AFFECTED DISKS |
|---|---|---|---|---|
| 0 | 6/30/04 | Initial Release | ALL | |
| | | | | |
| | | | | |

TABLE OF CONTENTS

## LIST OF TABLES



## LIST OF FIGURES

# 1. INTRODUCTION

## 1.1 Objective

The NUHOMS® 24PT4 dry shielded canister (DSC) is designed to serve as the containment and confinement boundary for up to twenty-four (24) spent nuclear fuel assemblies (FAs) during all operations in the Advanced NUHOMS® Horizontal Storage Module (AHSM) and the OS197 transfer cask. The design of the 24PT4-DSC provides for the passive rejection of the decay heat from the FAs to the surrounding environment. The objective of this calculation is to develop a thermal model of the heat transfer mechanisms within the NUHOMS® 24PT4-DSC using a computational fluid dynamics (CFD) methodology and provide evaluations of the thermal performance at selected conditions of storage and transfer. The model encompasses a section of the fuel basket located at the axial location of the peak heat flux from the fuel assemblies. Symmetry conditions are assumed on either side of the modeled basket section.

## 1.2 Purpose of Revision 0

The purpose of Revision 0 is to develop a thermal model of the NUHOMS® 24PT4-DSC using a CFD methodology and provide an evaluation of the thermal performance of the 24PT4-DSC with heat load configuration #1 for the bounding design basis thermal conditions of storage and transfer. In addition, the thermal performance of the 24PT4-DSC with heat load configuration #1 is evaluated at the off-normal cold condition of transfer and at the conditions existing for the helium leak check operations following vacuum drying.

The sensitivity of the thermal performance of the NUHOMS® 24PT4-DSC to the distribution of the heat load within the DSC is evaluated by analyzing heat load configuration #3 for the bounding design basis thermal condition of storage.

The bounding design basis condition of storage is the normal hot day condition with a peak ambient air temperature of 104°F and 24-hour averaged insolation loading. The bounding design basis condition of transfer is the off-normal hot condition with a peak ambient air temperature of 117°F and with the use of a sunshade. These conditions are bounding in that each yields the lowest thermal margin for the predicted fuel cladding temperature. The off-normal cold conditions of transfer assume an ambient temperature of -40°F and no insolation, while the helium lead check operations assume a constant shell temperature of 230°F.

## 1.3 Scope

The scope of this calculation is limited to the NUHOMS® 24PT4-DSC design as defined by its design drawings [6.2]. Further, the calculation is valid for steady-state operations with an internal DSC

decay heat loading of 24 kW or less and for DSC shell temperatures that are encompassed by those associated for the analyzed normal hot condition of storage, the off-normal hot condition of transfer with sunshade, the off-normal cold condition of transfer, and the helium leak check condition following vacuum drying.

## 2. ASSUMPTIONS AND CONSERVATISMS

### 2.1 General Assumptions

2.1.1 The geometry of the NUHOMS® 24PT4-DSC for this analysis is defined by the [6.2] design drawings.

2.1.2 The design basis operating conditions used for this calculation are the normal hot storage condition with a maximum daily ambient air temperature of 104°F and the off-normal hot transfer condition with sunshade with a maximum daily ambient air temperature of 117°F. The DSC shell temperatures that result for these conditions and the off-normal cold condition of transfer, as determined by other analyses, are used as a boundary condition for this calculation.

2.1.3 The helium leak check operations are conducted with the DSC in the vertical orientation, in the transfer cask, and with the annulus between the DSC and the transfer cask filled with water. The DSC shell temperature is assumed to be 230°F or less, corresponding to the boiling point of water at an average head pressure of approximately 14 feet of water.

2.1.4 The design decay heat loading for the 24PT4-DSC is 24 kW. The analysis assumes this heat loading is distributed over the active fuel length of 150" for the CE 16x16 fuel assemblies (FAs) with a peaking factor of 1.08. Heat load configuration #1 assumes 1.0 kW per fuel assembly, while heat load configuration #3 assumes 1.3 kW/assembly for 16 fuel assemblies, 0.8 kW/assembly for 4 fuel assemblies, and no fuel assemblies in the 4 center guide sleeve positions.

2.1.5 The 24PT4-DSC is backfilled with a minimum of 248.1 g-moles of helium gas per [6.7]. The void volume within the 24PT4-DSC cavity is 409,000 $in^3$. The helium leak check operations are conducted with the helium backfill pressure maintained at a maximum of 13 psig.

2.1.6 The basket is in the horizontal orientation for the storage and transfer operations and in the vertical orientation for the helium leak check operations. The same model and methodology are used to predict the convection driven temperatures in either orientation with the change in orientation simulated by simply by changing the orientation of the gravity vector. The FLUENT™ code is not well suited to analyzing operations during vacuum drying since no convection is present.

2.1.7 For the purposes of modeling, the nominal ligament sizes are assumed for the spacer discs. This is a valid approach since each cutout in a spacer disc is produced independently of the other cutouts and each spacer disc is fabricated independently from the other spacer discs.

2.1.8 With the exception of the BORAL™/aluminum composite plates and the fuel assemblies, the thermal conductivity properties for the various materials are assumed to be isotropic (i.e., independent of the direction of heat flow). Due to the non-uniform composition and geometry of the BORAL™/aluminum composite plates and the fuel assemblies with direction, anisotropic thermal conductivity properties exist for these materials.

2.1.9 For the purposes of computing the peak cladding temperature, the fuel assemblies are modeled as a homogenous material within each guide sleeve region.

2.1.10 Given the separation distance between the support rods and the adjacent surfaces, the size of the rods, and the circulation patterns within the DSC the presence support rods has little effect on the convection flow within the DSC. As such, the rods can be ignored for the purposes of this model.

2.2 Conservatisms

2.2.1 No credit is taken for contact heat transfer from the lower horizontal surfaces of the guide sleeves to the spacer discs (i.e., the guide sleeves are assumed to be centered within their respective cutout in the spacer disc) and from the fuel assembly to the guide sleeve.

2.2.2 The spacer discs are assumed to be centered within the DSC shell. Ignoring the direct contact between the lower edges of the spacer discs and the DSC shell is conservative for computing the peak temperatures within the canister.

2.2.3 Nominal dimensions are assumed in the analysis. Ignoring the reduction in the gap between the spacer discs and the canister shell and between the guide sleeves and the spacer disc cutouts due to differential thermal expansion is conservative for computing the peak temperatures within the canister.

## 3. 24PT4-DSC DESIGN

### 3.1 24PT4-DSC Geometry

The 24PT4-DSC (see Figure 3-1) uses a spacer disc and guide sleeve type of fuel basket to position and restrain the fuel assemblies within the canister. Since this type of fuel basket is not directly attached to the canister wall, the principal means of heat transfer between the fuel assemblies and the canister shell is via radiation and convection. Each canister assembly consists of the same major components: a cylindrical shell, top end inner and outer cover plates, bottom end inner closure plate, bottom end outer closure plate, top and bottom end shield plugs, and vent and drain ports. The fuel basket assembly consists of twenty four (24) guide sleeves containing fixed borated neutron absorbing material (BORAL™), circular spacer discs, and support rods. As illustrated in Figure 3-2, cutouts in the 1.25 inch thick spacer discs provide the means for supporting the individual fuel guide sleeves and for maintaining a minimum separation between the walls of neighboring guide sleeves.

The type 'X' cutouts are slightly smaller than the type 'Y' cutouts due to the presence of the BORAL™ material on only 2 sides versus all 4 sides. Four support rod assemblies are used to maintain the axial separation between the individual spacer discs.

The canister shell, the inner and outer cover plates for the top closure, and the inner and outer cover plates for the bottom closure are fabricated of Type 316 stainless steel. Type 304 stainless steel is used for the fabrication of the 0.125" thick guide sleeves and the 0.018" thick over sleeves which encase the 0.20" thick BORAL™ neutron absorbing material. The spacer discs for the 24PT4 design are fabricated of SA-533 carbon steel and are electroless nickel coated for corrosion control. SA-564, Type 630 stainless steel is used to fabricate the support rods and spacer sleeves. Lead is used for the top and bottom shield plugs of the 24PT4-DSC. The [6.2] drawings and the [6.4] calculation provide additional details regarding the design and the materials used in the fabrication of the DSC.

The DSCs are stored horizontally within the AHSM during storage conditions and within the OS197 transfer cask during transfer operations. The temperatures predicted for the DSC shell as obtained from a separate analysis of the DSC in the AHSM [6.5] and the DSC in the transfer cask [6.4] are used as boundary conditions for this analysis.

## 3.2 Material Properties

Table 3-1 lists the thermal conductivity and specific heat as a function of temperature for SA-240, Type 304/304L stainless steel used for the guide sleeves and the BORAL™ over sleeves. The values listed in the table are taken from [6.3]. The thermal emissivity of the Type 304/304L stainless steel is assumed to be 0.4 per [6.4]. Per the same reference, the Type 316 stainless steel used for the canister shell is assumed to have an emissivity of 0.587. Material properties for the Type 316 stainless steel are not needed since the canister shell is represented in the model as a boundary condition with no heat transfer within the material. Similarly, the thermal properties for lead are not required since the model does not encompass the top and bottom shield plugs.

The spacer discs are fabricated of SA-533, Grade B carbon steel. The thermal conductivity of this material as a function of temperature is provided in Table 3-1, with the listed data taken from [6.3]. The SA-533 carbon steel spacer discs have an electroless nickel coating applied to control corrosion. An emissivity value of 0.15 is assumed for the electroless nickel coating [6.4].

The thermal conductivity in the radial or 'through' direction for the CE 16x16 PWR fuel assemblies is computed using a detailed model of the fuel assembly geometry (see Appendix B). The model accounts for conduction and radiation heat transfer between the individual pins of the fuel assembly, and across the gap between the edge of the fuel assembly and the guide sleeve wall. The results of this detailed modeling are used to compute an 'effective thermal conductivity' for the fuel assembly wherein the assembly is treated as a homogenized solid that extends to fill the interior of the guide sleeve. Since the effective thermal conductivity values are computed assuming no convection within the fuel assembly, the same thermal properties can be conservatively applied to both the vertical and horizontal orientations of the fuel assembly.

The axial heat transfer within the fuel assembly is assumed to be limited to that occurring within the cladding. This approach is in keeping with conservatism since there is no guarantee that the individual fuel pellets would not have experienced cracking during operations in the reactor and/or that gaps between the fuel pellets would not exist. The axial thermal conductivity values presented in Table 3-1 assume the pin geometry and number of fueled pins for the CE 16x16 Zircaloy clad fuel assembly for the 24PT4-DSC (see Appendix B) and are adjusted by the cross-sectional area of the fuel region to account for the fact that the fuel assemblies are treated as homogenized regions within this modeling.

Table 3-2 lists the thermal conductivity and specific heat as a function of temperature for air and helium gas. The values listed in the table are taken from [6.13].

The allowable temperature limits associated with the various DSC components are listed in Table 3-3.

## 3.3 Thermal Load

The thermal loads imposed on the fuel basket arise from the decay heat within the fuel assemblies. Two heat load configurations are considered for this analysis. Heat load configuration #1 (see Figure 3-3) assumes a decay heat load of 1.0 kW for each of the twenty-four (24) fuel assemblies, while heat load configuration #3 (see Figure 3-4) assumes a decay heat load of 1.3 kW in sixteen (16) fuel assemblies, 0.8 kW in four (4) fuel assemblies, and no fuel assemblies in the four (4) center positions of the basket. Both heat load configurations yield a total decay heat load of 24 kW. The active fuel length of the CE 16x16 fuel assembly (i.e., 150") and a peaking factor of 1.08 are used to computing the maximum heat load at the modeled canister section. As such, the heat source assumed for each fuel assembly in the 6.8" long modeled section of the 24PT4-DSC under heat load configuration #1 is computed as:

Q = 24,000 W/24 FAs/150" active fuel length*1.08 peaking factor * 6.8" model length
= 48.96 watts/assembly

Similarly, the heat source assumed for the fuel assemblies with 1.3 kW and 0.8 kW decay heat load under heat load configuration #3 is computed as:

Q = 1,300 W/150" active fuel length*1.08 peaking factor * 6.8" model length
= 63.648 watts/assembly

and

Q = 800 W/150" active fuel length*1.08 peaking factor * 6.8" model length
= 39.168 watts/assembly

## 3.4 DSC Pressure

Determination of the convection heat transfer within the DSC requires calculating the gas density within the canister since the strength of the convection flow is greater for higher gas densities (i.e.,

higher mass flow rate for a given flow velocity). In turn, gas density is a function of the initial fill pressure and the bulk average gas temperature within the DSC cavity at the operating condition. Per [6.7], the design fill gas quantity in the DSC is 248.1 g-moles of helium, based on the minimum fill pressure of 6 psig. For conservatism, the contribution to the DSC gas quantity due to potential fuel rod failures is ignored.

Determination of the bulk average gas temperature within the DSC cavity requires a 3-dimensional analysis of the length of the DSC. Since this model encompasses only a section of the fuel basket, the results from Table 9-6 of [6.4] are used to provide the average temperature of the gas within the DSC for the analyzed conditions. Per [6.4], the average gas temperature within the DSC cavity is 494°F for the normal storage condition with a 104°F ambient air temperature and 550°F for the off-normal transfer condition with a 117°F ambient air temperature. As such, the minimum expected pressure within the DSC at the design basis storage condition is estimated as follows:

$$P_{104F-normal-storage} = \frac{(1.4504 \bullet 10^{-4})(248.1\,\text{g mol})(8.314\,\text{J/g mol-K})(494^{\circ}\text{F} + 460^{\circ}\text{R})}{(409{,}000\,\text{in}^3)(1.6387 \bullet 10^{-5}\,\text{m}^3/\text{in}^3)(1.8^{\circ}\text{R/K})}$$

$$P_{104F-normal-storage} = 23.7\,psia\,(9\,psig)$$

The DSC at the design basis transfer condition is estimated as follows:

$$P_{117F-off-normal-transfer} = \frac{(1.4504 \bullet 10^{-4})(248.1\,\text{g mol})(8.314\,\text{J/g mol-K})(550^{\circ}\text{F} + 460^{\circ}\text{R})}{(409{,}000\,\text{in}^3)(1.6387 \bullet 10^{-5}\,\text{m}^3/\text{in}^3)(1.8^{\circ}\text{R/K})}$$

$$P_{117F-off-normal-transfer} = 25.0\,psia\,(10.3\,psig)$$

For conservatism, a 9 psig pressure will also be used for the design basis transfer condition.

The helium pressure during the helium leak check operation is maintained within a relatively narrow pressure range by adding or removing gas as required. Since the intent of the thermal evaluation of the leak check operation is to determine the minimum temperature achieved, the maximum 13 psig pressure permitted during this operation is assumed for this evaluation.

**Table 3-1 - Canister Material Properties, Solids**

| Material | Temperature (°F) | Thermal Conductivity (BTU/min-in-°F) | Density [1] (lb/in$^3$) | Specific Heat (BTU/lb-°F) |
|---|---|---|---|---|
| Type 304/304L Stainless Steel [2] | 70 | 0.0119 | 0.285 | 0.116 |
| | 100 | 0.0121 | | 0.116 |
| | 200 | 0.0129 | | 0.121 |
| | 300 | 0.0136 | | 0.124 |
| | 400 | 0.0144 | | 0.128 |
| | 500 | 0.0151 | | 0.130 |
| | 600 | 0.0157 | | 0.132 |
| | 800 | 0.0169 | | 0.135 |
| Type SA-533 Carbon Steel[2] | 70 | 0.0310 | 0.284 | 0.106 |
| | 100 | 0.0314 | | 0.108 |
| | 200 | 0.0325 | | 0.114 |
| | 300 | 0.0331 | | 0.119 |
| | 400 | 0.0331 | | 0.125 |
| | 500 | 0.0326 | | 0.131 |
| | 600 | 0.0319 | | 0.137 |
| | 700 | 0.0310 | | 0.142 |
| Fuel Assembly Axial Effective k[5] | 122 | 9.374E-04 | not used | not used |
| | 212 | 9.640E-04 | | |
| | 302 | 9.905E-04 | | |
| | 392 | 1.017E-03 | | |
| | 482 | 1.048E-03 | | |
| | 572 | 1.079E-03 | | |
| | 662 | 1.132E-03 | | |
| | 752 | 1.185E-03 | | |
| Radial or 'Through' Effective k[4] | 200 | 3.529E-04 | | |
| | 275 | 3.950E-04 | | |
| | 350 | 4.459E-04 | | |
| | 425 | 5.040E-04 | | |
| | 500 | 5.695E-04 | | |
| | 575 | 6.408E-04 | | |
| | 650 | 7.175E-04 | | |
| | 725 | 8.018E-04 | | |
| | 800 | 8.856E-04 | | |

## Table 3-1 - Canister Material Properties, Solids

| Material | Temperature (°F) | Thermal Conductivity (BTU/min-in-°F) | | Density [1] (lb/in$^3$) | Specific Heat (BTU/lb-°F) |
|---|---|---|---|---|---|
| BORAL™ [6] | 100 | 0.0689 | | 0.0896 | 0.220 |
| | 500 | 0.0617 | | | 0.268 |
| Composite Guide Sleeves | | Through | Along | | |
| & BORAL™ Plates [3] | 200 | 3.555E-03 | 4.568E-02 | not used | not used |
| | 300 | 3.869E-03 | 4.482E-02 | | |
| | 400 | 4.202E-03 | 4.400E-02 | | |
| | 500 | 4.564E-03 | 4.314E-02 | | |
| | 600 | 4.996E-03 | 4.336E-02 | | |
| | 700 | 5.248E-03 | 4.360E-02 | | |

Table 3-1 Notes:

(1) Single values are shown since this material property does not vary significantly with temperature.
(2) Material properties are obtained from [6.3].
(3) From Tables 5-2 and 5-3 of [6.4].
(4) From Appendix B.
(5) Heat transfer through cladding of 236 fueled pins for CE 16x16. See Appendix B for fuel geometry. Computed conductivity adjusted for homogenization of fuel assembly as a solid region
(6) From [6.8].

## Table 3-2 - Canister Material Properties, Gas

| Material | Temp. (°F) | Thermal Conductivity (BTU/min-in-°F) | Specific Heat (BTU/lbm-°F) | Density ($lbm/ft^3$) | Dynamic Viscosity (lbm/hr-ft) |
|---|---|---|---|---|---|
| Helium [1,2,3] | 0 | 1.089E-04 | 1.24 | Ideal gas law used to establish operating density, Boussinesq approximation used to compute buoyancy forces | 0.04306 |
| | 50 | 1.162E-04 | 1.24 | | 0.04634 |
| | 100 | 1.230E-04 | 1.24 | | 0.04944 |
| | 200 | 1.362E-04 | 1.24 | | 0.05520 |
| | 300 | 1.493E-04 | 1.24 | | 0.06088 |
| | 400 | 1.635E-04 | 1.24 | | 0.06643 |
| | 500 | 1.794E-04 | 1.24 | | 0.07153 |
| | 600 | 1.949E-04 | 1.24 | | 0.07640 |
| | 700 | 2.094E-04 | 1.24 | | 0.08116 |
| | 800 | 2.232E-04 | 1.24 | | 0.08580 |
| Air [1,2,3] | 107 | 2.156E-05 | 0.241 | Ideal gas law used to establish operating density | 0.04633 |
| | 206 | 2.470E-05 | 0.242 | | 0.05227 |
| | 296 | 2.769E-05 | 0.243 | | 0.05724 |
| | 404 | 3.055E-05 | 0.245 | | 0.06278 |
| | 512 | 3.333E-05 | 0.248 | | 0.06808 |
| | 602 | 3.603E-05 | 0.251 | | 0.07218 |
| | 692 | 3.866E-05 | 0.253 | | 0.07614 |
| | 800 | 4.124E-05 | 0.257 | | 0.08060 |
| | 1000 | 4.620E-05 | 0.262 | | 0.08887 |

Table 3-2 Notes:

(1) Properties based on curve fits from [6.13].

(2) The associated Prandtl number at each temperature point can be computed from the given table values via the equation: Prandtl number = specific heat*viscosity*2.41909/conductivity.

(3) The coefficient of thermal expansion for an ideal gas is 1/(T+459.67), where T is the gas temperature in degrees F.

**Table 3-3 - DSC Component Allowable Temperatures**

| Component | Max. Long Term Temperature Limit, °F | Off-normal/Accident Temperature Limit, °F |
|---|---|---|
| Zircaloy Fuel Cladding | 752°F | 1058°F |
| Load Bearing Carbon Steel | 700°F | 700°F |
| Load Bearing Stainless Steel | 800°F | 800°F |
| Type 630 Stainless Steel (used for support rods) | 650°F | 650°F |
| BORAL™ | 850°F | 1000°F |

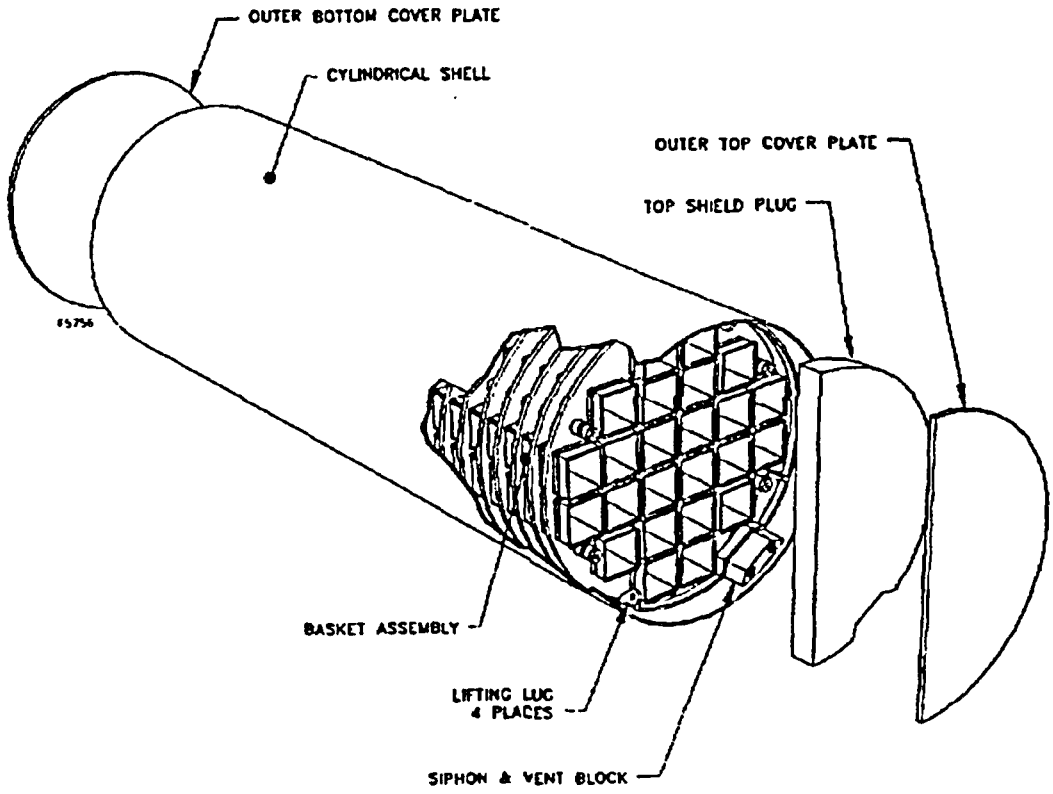


**Figure 3-1 - General Design Configuration for 24PT DSC**

Figure removed under 10 CFR 2.390

**Figure 3-2 - Layout Fuel Assemblies within 24PT4-DSC**

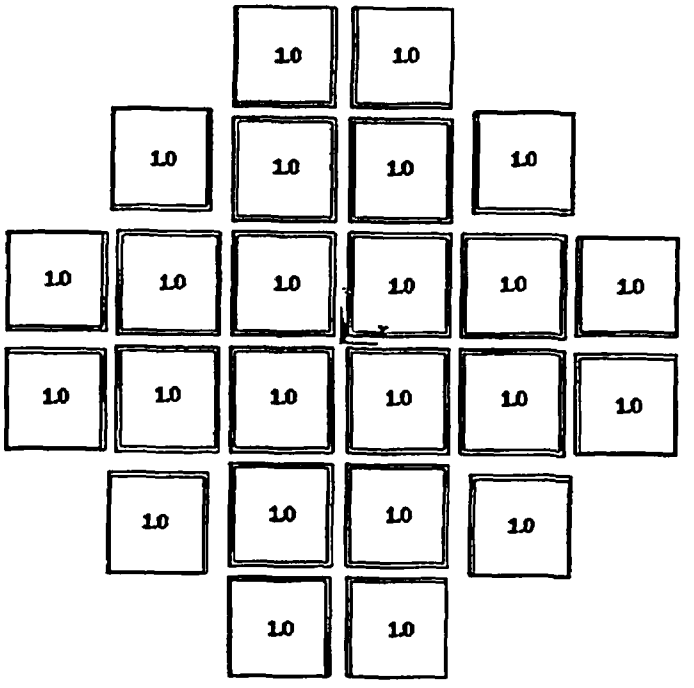


Figure 3-3 - 24PT4 DSC Heat Load Configurations #1, kW/Assembly

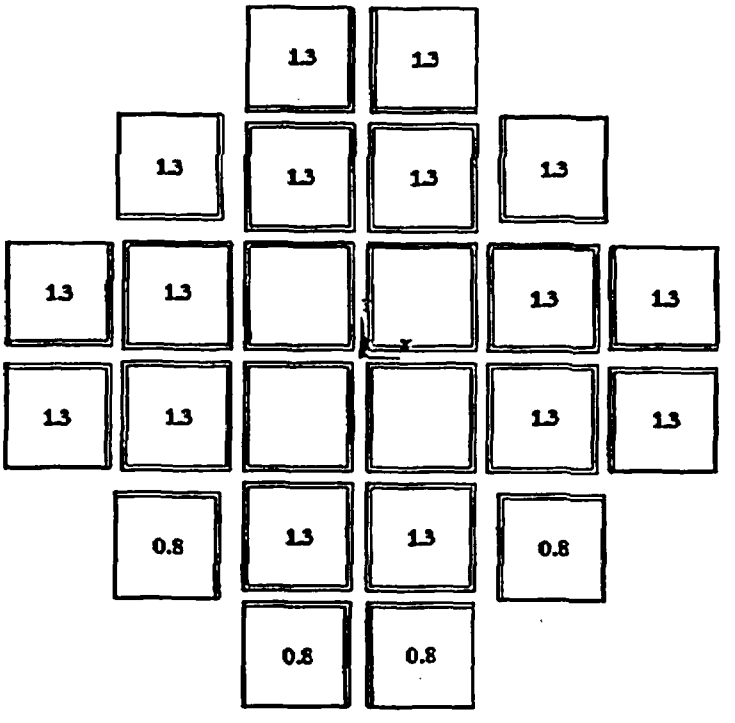


Figure 3-4 - 24PT4 DSC Heat Load Configurations #3, kW/Assembly

# 4. CALCULATIONS

## 4.1 Fluent™/ Icepak™ Model

Based on the 24PT4-DSC geometry summarized in Section 3.1 and detailed in the [6.2] drawing set, the thermal-hydraulic environment within the DSC is evaluated for the bounding storage and transfer conditions and a decay heat loading of 24 kW. The program selected for this evaluation is the Fluent™ code [6.9] with the Icepak™ module [6.10]. The Fluent™ code is a general purpose computational fluid dynamics (CFD) code that is recognized internationally as one of the premier codes in its class. The general modeling capabilities of the code as they relate to this application include:

- Meshing flexibility using structured and unstructured mesh generation with hexahedra, non-hexahedra, and tetrahedral mesh types
- Capability to model low speed, buoyancy driven flow regimes
- Steady-state and transient flows
- Inviscid, laminar, and turbulent flows
- Heat transfer including forced, natural, and mixed convection, conjugate heat transfer, and radiation
- Custom materials property database
- Integrated problem set-up and post-processing

The Icepak™ module is a fully interactive, object-based graphical interface that allows complex geometries to be modeled and meshed using a combination of shapes in a 'building block' approach. The Icepak™ module does not perform any CFD related numerical calculations itself, but only serves as a pre- and post-processor to the Fluent™ code. While the Icepak™ module is specifically designed for the analysis of electronic enclosures, its operational features are fully capable of handling the geometry for this application. The verification and validation of the Icepak™ and Fluent™ codes for the computation of generic buoyancy driven convection heat transfer within an enclosure is documented in [6.11].

Figure 4-1 illustrates an isometric wire frame view of the thermal-hydraulic model developed to simulate a representative segment of the fuel basket along its axial length. The modeled segment spans from the mid-plane on one spacer disc to the mid-plane on an adjacent spacer disc (a 6.8" length) and is centered on the section of the active fuel length exhibiting the peak heat flux. The thermal model encompasses a 360° segment of the basket cross-section with symmetry conditions assumed to exist at the axial boundaries of the model. The x-axis of the model's coordinate system is aligned with the horizontal axis and the y-axis is aligned with the vertical axis of the horizontally oriented DSC. The z- axis is aligned along the length of the DSC. The origin of the coordinate system is at the center of the modeled canister segment.

Figure 4-2 illustrates the twenty-four (24) plate sections used to approximate the curved geometry of the DSC shell. Individual plate segments are used in order to facilitate the imposition of a variable

boundary temperature condition at the shell of the DSC as a function of the circumferential position. Table 4-1 lists the shell temperatures used as a boundary condition in this calculation as a function of angle. These temperatures are taken from [6.5] and [6.6].

Figure 4-3 illustrates the modeling of the fuel assemblies as solids with anisotropic effective thermal properties portions. Table 3-1 presents the thermal conductivity values assumed for the fuel assemblies as a function of temperature and the heat transfer direction. The radial or 'through' direction of the fuel is across the width of the fuel assembly (i.e., in the x-axis and y-axis directions), while the 'axial' direction is in the z-axis direction. For simplicity, the thermal model approximated that thermal conductivity in the axial direction as 1.5 times that of the radial or 'through' direction. This simplification is acceptable since the heat flow is principally in the radial direction given that symmetry conditions exist at the axial ends of the model.

Figure 4-4 illustrates the modeling of the composite BORAL™ sheets (i.e., poison sheets) used for criticality control within the DSC. The poison sheets are modeled as a composite material consisting of the BORAL™, the stainless steel wrapper, and the assumed gaps in the interfaces between theses materials. Given the limited change in the thermal conductivity with temperature, a fixed conductivity of 0.043 Btu/min-in-°F is used for the material properties in the 'along' direction. The same fixed conductivity value is used in the 'through' direction for simplicity. While this level of thermal conductivity for the 'through' is approximately 10 times higher than the listed Table 3-1 values, the effect on the model results are negligible (i.e., < 1°F) given that the thermal resistance through the thickness of the poison sheets is small in either case due to the thinness of the sheets. Further, the principal reason that the computed thermal conductivity in the 'through' direction is low compared to the 'axial' direction is that the computed values conservatively assume a uniform helium filled gap between the guide sleeves and the BORAL™ and between the BORAL™ and the stainless steel wrapper. Direct contact over even a small portion of the surface area will significantly increase the 'through' conductivity values to near that of the 'axial' direction.

Figure 4-5 illustrates the model geometry for the spacer discs. Both the placement and the size of the disc cutouts are accurately reflected in the model geometry.

Figure 4-6 to Figure 4-9 illustrate the meshing used for this modeling. A total of approximately 1,050,000 mesh elements are used for the analysis to represent the various components of the DSC shell, the fuel basket, and the fuel assemblies. Figure 4-6 presents a perspective view of the mesh profile along the x-y plane through the center of the module. Figure 4-7 illustrates a plan view of the mesh for the spacer discs, while Figure 4-8 presents an enlarged view of the spacer disc mesh in the vicinity of the center fuel assemblies. Figure 4-9 illustrates an elevation view of the mesh along the y-z plane.

The CFD analysis is conducted with radiation and turbulent flow enabled. The radiation view factors were calculated using the 'hemicube' methodology, with the mesh coarsening option disabled to avoid lessening the resolution for the curved and angled surface shapes. The effects of flow turbulence are calculated using the 'mixing-length zero-equation' turbulence model, while the temperature-dependent fluid density is computed using the Boussinesq model. Both of these

computational options represent the FLUENT recommendations for natural convection, buoyancy driven problems. The use of the Boussinesq model was validated via a sensitivity run wherein the use of the ideal gas option to compute density produced similar peak temperatures.

## 4.2 Thermal Analysis for the Bounding Design Basis AHSM Condition

### 4.2.1 Heat Load Configuration #1

The design basis analysis of the thermal performance of the 24PT4-DSC in the AHSM is conducted for the normal condition of storage with a peak daily temperature of 104°F, a 24-hour average of 97°F, solar insolation, and heat load configuration #1 with a decay heat loading of 24 kW within the DSC. This condition yields the lowest thermal margin for the fuel cladding temperature. Figure 4-10 illustrates the DSC shell temperatures, as obtained from the [6.5] analysis of the DSC in the AHSM (see Table 4-1), that were imposed as a boundary condition to the model. The operating density in the DSC for the analyzed condition is estimated using the ideal gas relationship. For this calculation, a canister pressure of 23.7 psia (see Section 3.4) and a bulk average gas temperature of 520°F (a value that conservatively bounds the 494°F used to determine the operating pressure) are assumed. Based on these parameters and a molecular weight of 4.003 for helium, the operating density is computed as:

$$\rho_{104F-normal-storage} = \frac{P_{104F-normal-storage}}{\frac{\text{Universal Gas Constant}}{\text{molecular wt}} T_{absolute}}$$

$$\rho_{104F-normal-storage} = \frac{23.7\,\text{psia} \times 144 \frac{\text{in}^2}{\text{ft}^2}}{\frac{1545}{4.003}(520°\text{F} + 460°\text{R})}$$

$$\rho_{104F-normal-storage} = 0.00902\,\text{lb}_m/\text{ft}^3$$

The local density, $\rho$, is calculated from the operating density, $\rho_0$, via the Boussinesq relationship:

The Boussinesq relationship is valid if $(T - T_0)/(T + 460°R) << 1$. For this application this parameter is < 0.2, thus the validity of the Boussinesq relationship is established.

Figure 4-11 to Figure 4-13 present a summary of the temperature distributions predicted for the analyzed condition. As seen from Figure 4-11, the maximum fuel cladding temperature predicted is 697°F, while Figure 4-12 and Figure 4-13 show that the predicted maximum spacer disc temperature is 653°F and the peak poison sheet temperature is 662°F.

Examination of Figure 4-11 to Figure 4-13 revels that the analysis predicts a slightly non-symmetric temperature distribution about the y-axis when symmetry should clearly occur given the condition evaluated. The worst case magnitude of this non-symmetry (approximately 30°F) occurs between the extreme left side and the extreme right side of the distributions illustrated in Figure 4-11 and Figure 4-12. The cause of the non-symmetric distribution was not identified. A review of the applied heat loads, the imposed DSC shell temperatures, the geometry of the model, and the meshing revealed no obvious reason for the non-symmetric result. The velocity profiles illustrated in Figure 4-15 to Figure 4-17 do show that a larger component of the flow entering and exiting the vertical channel at the canister centerline is from the right side of the plot (i.e., the side showing the lower temperature) and higher flow rates will reduce the peak component temperatures. However, it is uncertain whether the flow imbalance is a cause or the result of the non-symmetry condition.

Given the relatively low magnitude of the non-symmetric temperature condition and the fact that (for energy balanced solution) a symmetric solution should yield peak temperatures that are an average of the corresponding left and right side components, the use of the peak temperatures from Figure 4-11 to Figure 4-13 will bound those achieved from a fully symmetrical solution.

Figure 4-14 illustrates the temperature profile along vertical lines through the spacer discs and the fuel assemblies. One of the profiles passes through the vertical centerline of the horizontal DSC, while the second profile passes through the location of the peak FA temperature (i.e., 5.16" from the centerline), as indicated by the model. The profiles show the expected trend of a temperature distribution skewed to the top of the DSC cross section due to the presence of convection within the basket. Further, the temperature profile through each FA location shows the characteristic 'hump' associated with a heat generating solid.

Figure 4-15 illustrates the velocity profile through the center of the modeled segment of the DSC. The profile demonstrates the expected result of a global circulation pattern up through the vertical channels between the fuel assemblies and then downward along the shell to the bottoms of the vertical channels. Further, as expected, the flow in the horizontal channels between the fuel assemblies is very limited with the exception of the channels surrounding the fuel assemblies in the corners of the fuel basket. The maximum flow velocity seen in the center of the fuel basket is less than 1 foot per second. The peak flow velocity of approximately 2.3 feet per second occurs on the left and right sides of the basket where the flow is 'choked down' as it passes between the outermost corner of the fuel assemblies and the DSC shell. Figure 4-16 and Figure 4-17 present enlarged views of the velocity profiles within the DSC.

Table 5-1 presents a summary of the DSC component temperatures predicted under this design basis calculation. The predicted peak fuel cladding temperature of 697°F is 55°F below the allowable temperature for the cladding. The predicted peak spacer disc temperature of 653°F is 47°F below the 700°F limit for carbon steel used for structural applications, while the peak temperatures seen for the guide sleeves, the support rods, and the DSC shell are all well within their allowable temperature limits.

4.2.2 Heat Load Configuration #3

The sensitivity of the thermal performance of the 24PT4-DSC in the AHSM to the assumed heat load configuration was evaluated by repeating the design basis analysis for the normal condition of storage as described in Section 4.2.1 with heat load configuration #3. Although heat load configurations #1 and #3 both have a total decay heat loading of 24 kW, the distribution of the heat load within the fuel basket is different. Figure 3-3 and Figure 3-4 illustrate the differences in heat load distribution between these heat load configurations. The DSC shell temperatures illustrated in Figure 4-10 and listed in Table 4-1 again serves as the boundary condition for this analysis. Likewise, the operating density determined in Section 4.2.1 is assumed for this analysis.

Figure 4-18 and Figure 4-19 present a summary of the temperature distributions predicted for the analyzed condition. As seen from the figures, the maximum fuel cladding temperature predicted is 697°F and the predicted maximum spacer disc temperature is 635°F. The peak poison sheet temperature noted for this condition is 650°F. Comparison with the results presented in Section 4.2.1 for heat load configuration #1 shows that the same peak fuel cladding temperature is achieved with either heat load configuration, but that the peak spacer disc and poison sheet temperatures achieved under heat load configuration #3 are 18 and 12°F lower, respectively, than the peaks achieved under heat load configuration #1. As with the analysis for heat load configuration #1, a slight non-symmetric temperature distribution about the y-axis is noted in the solution. Again, the worst case magnitude of this non-symmetry is approximately 30°F between the extreme left side and the extreme right side of the temperature distributions depicted in the figures and 40°F between the peak temperature in the extreme left and right fuel assemblies.

Figure 4-20 illustrates the temperature profile along vertical lines through the spacer discs and the fuel assemblies. One of the profiles passes through the vertical centerline of the horizontal DSC, the second profile passes the first set of FAs adjacent to the basket centerline (i.e., 5.16" from the centerline), and the third profile passes through the location of the peak FA temperature (i.e., 15.9" from the centerline) as indicated by the model. The profiles show the expected trend of a temperature distribution skewed to the top of the DSC cross section due to the presence of convection within the basket and a flat curve adjacent to the empty fuel assembly locations. Further, the temperature profile through each FA location shows the characteristic 'hump' associated with a heat generating solid.

Figure 4-21 illustrates the velocity profile through the center of the modeled segment of the DSC. The same global circulation pattern seen for heat load configuration #1 also exists for heat load configuration #3. The principal differences in the noted flow pattern with heat load configuration #3 is that flow exists within the empty fuel assembly locations and the slightly stronger flow around the outlying FA locations in each quadrant of the basket. It should be noted that this analysis conservatively assumes that the guide sleeves at the empty fuel locations remain in the basket. Removal of the guide sleeves at these locations (logical given the cost of the sleeves and the poison sheets) would decrease the local flow losses and increase the convective heat transfer in this region. A peak flow velocity of approximately 2.3 feet per second occurs on the left and right sides of the basket where the flow is 'choked down' as it passes between the outermost corner of the fuel

assemblies and the DSC shell. Figure 4-22 and Figure 4-23 present enlarged views of the velocity profiles within the DSC.

Table 5-1 presents a summary of the DSC component temperatures predicted for this heat load configuration.

## 4.3 Thermal Analysis at the Bounding Design Basis Transfer Cask Condition

The design basis analysis of the thermal performance in the OS197 transfer cask is conducted for the off-normal hot condition of transfer with a peak daily temperature of 117°F, the use of a sun shade, and a decay heat loading of 24 kW within the DSC. This condition yields the lowest thermal margin for the fuel cladding temperature under transfer conditions. Figure 4-24 illustrates the DSC shell temperatures, as obtained from the [6.6] analysis of the DSC in the transfer cask, that were imposed as a boundary condition to the model. As seen, a uniform DSC shell temperature of 443°F is conservatively used for this condition. In reality, a temperature variation will exist around the circumference of the DSC shell due to the presence of an non-uniform gap between the shell and the transfer cask when in the horizontal position and due to the direct contact between the DSC and the transfer cask at the location of the 'rub rails'.

Figure 4-25 to Figure 4-27 present the temperature distributions predicted for the analyzed condition. As seen from Figure 4-25, the maximum fuel cladding temperature predicted under the analyzed condition is 712°F, while Figure 4-26 shows that the predicted maximum spacer disc temperature is 668°F. The peak poison sheet temperature indicated from Figure 4-27 is 675°F. Examination of the figures again shows the same slight non-symmetric temperature distribution about the y-axis which was noted for the analysis of the storage condition. Again, the worst case magnitude of this non-symmetry is approximately 30°F and occurs between the extreme left side and the extreme right side of the distributions.

Figure 4-28 illustrates the temperature profile along vertical lines through the spacer discs and the fuel assemblies for this condition. Again, one of the profiles passes through the vertical centerline of the horizontal DSC, while the second profile passes through the location of the peak FA temperature, as indicated by the model. The illustrated profiles reflect the expected trend.

Figure 4-29 to Figure 4-31 illustrates the velocity profile through the center of the modeled segment of the DSC. The velocity profiles are essentially the same as those seen in Figure 4-15 for the analyzed condition within the AHSM except for the magnitude of the peak velocity. The peak velocity seen in this analysis is lower than the evaluation for the AHSM due to the absence of a temperature variation around the circumference of the DSC shell. As such, the buoyancy forces available to drive the flow pattern are less. As with the analysis in the AHSM, the peak flow velocity of approximately 2 feet per second seen for the evaluated operation in the transfer cask occurs on the left and right sides of the basket where the flow is choked down as it passes between the outermost corner of the fuel assemblies and the DSC shell. Figure 4-30 and Figure 4-31 present enlarged views of the velocity profiles within the DSC.

4.4 Thermal Analysis at the Off-Normal Cold Transfer Cask Condition

The thermal performance in the OS197 transfer cask for the off-normal cold condition of transfer with an ambient temperature of -40°F and a decay heat loading of 24 kW within the DSC. Figure 4-32 illustrates the associated DSC shell temperatures obtained from the [6.6] analysis of the DSC in the transfer cask. The imposed temperature variation is also listed in Table 4-1 as function of the angle around the circumference. As seen, the DSC shell temperature imposed as a boundary condition varies from a minimum of 146°F at the bottom to 380°F for this condition.

Figure 4-33 and Figure 4-34 present the temperature distributions predicted for the analyzed condition. As seen from the figures, the maximum fuel cladding temperature predicted under the analyzed condition is 636°F and the predicted maximum spacer disc temperature is 590°F. The peak poison sheet temperature is predicted to be 601°F.

Figure 4-35 illustrates the temperature profile along vertical lines through the spacer discs and the fuel assemblies for this condition. One of the profiles passes through the vertical centerline of the horizontal DSC, while the second profile passes through the location of the peak FA temperature, as indicated by the model.

Figure 4-36 illustrates the velocity profile through the center of the modeled segment of the DSC. The velocity profiles is similar to those seen in Figure 4-29 except that the magnitude of the peak velocity is higher since the variation in the DSC shell temperature around the circumference provides a greater buoyancy driven flow than the constant DSC shell temperatures assumed for the off-normal hot transfer condition.

4.5 Thermal Analysis for the Helium Leak Check Condition in a Vertical Transfer Cask

Following vacuum drying, the DSC is backfilled with helium to a maximum pressure of 13 psig and maintained at that pressure while the closure welds are leak tested. The same CFD model used to evaluate the thermal performance at the design basis storage and transfer conditions was used to predict the temperature profile within the DSC for steady-state operations for the helium leak check condition. The changes implemented to the model used to evaluate the storage and transfer conditions consisted of switching the direction of the gravity vector from the negative y-direction to the negative z-direction, changing the DSC shell temperatures to a uniform 230°F, and changing the operating pressure from 9 psig to 13 psig.

Figure 4-37 illustrates the DSC shell temperatures that are imposed on the model as a boundary condition for the helium leak check condition. Figure 4-38 to Figure 4-40 present the temperature distributions predicted for the analyzed condition. As seen from Figure 4-38, the maximum fuel cladding temperature predicted under the analyzed condition is 607°F, while Figure 4-26 shows that the predicted maximum spacer disc temperature is 559°F. The peak poison sheet temperature indicated from Figure 4-27 is 568°F. As with the storage and transfer conditions, a non-symmetric temperature distribution is predicted by the analysis whereas a symmetrical solution should occur. The higher temperatures are used for reporting purposes.

Figure 4-41 illustrates the temperature profile for this condition along radial lines extending outward from the center of the basket to the DSC shell through the spacer discs and the fuel assemblies. One profile passes between the center FAs, while the second profile illustrates the temperature profile along a line through the location of the peak FA temperature, as indicated by the model. The illustrated profiles reflect the expected trend of a larger $\Delta T$ between the DSC shell and the peak FA temperature versus that seen for the storage and transfer conditions. A larger $\Delta T$ required to remove the heat from the basket since the lower overall basket temperatures resulting from the 230°F boundary condition imposed at the DSC shell effectively reduces the contribution of radiation to the total heat transfer rate.

Figure 4-42 to Figure 4-44 illustrates the velocity profiles seen within the modeled segment of the DSC. Figure 4-42 presents a plan view of the velocity profile in the center of the modeled segment (i.e., between the spacer discs). The figure demonstrates that, while the majority of the buoyancy driven flow occurs around the outer perimeter of the basket, a small level of flow will occur at the center of the basket. The flow distribution is more apparent in the Figure 4-43 flow profile which represents the profile along an x-z plane in the center of the basket. The gravity vector points downward in this figure. As seen, despite the limited 5.6" separation distance between the spacer discs, sufficient buoyancy forces will exist to cause flow to extend from the center of the basket to the perimeter of the basket. The strength of the buoyancy driven flow increases as the DSC shell boundary is approached. Figure 4-44 presents an enlarged view of the Figure 4-43 profile.

**Table 4-1 - Imposed DSC Shell Temperatures vs. Circumferential Position**

| Angular Position on DSC (Bottom = 0°, Top = 180°) | DSC Shell Temperature, °F | | | |
|---|---|---|---|---|
| | Operation In AHSM [1] | Off-Normal Hot In Transfer Cask [2] | Off-Normal Cold In Transfer Cask [3] | Helium Leak Check, Vertical Transfer Cask [4] |
| 0° to 7.5° | 367.0 | 443.0 | 146.0 | 230.0 |
| 7.5° to 22.5° | 368.6 | " | 165.5 | " |
| 22.5° to 37.5° | 357.0 | " | 185.0 | " |
| 37.5° to 52.5° | 357.3 | " | 204.5 | " |
| 52.5° to 67.5° | 371.2 | " | 224.0 | " |
| 67.5° to 82.5° | 385.9 | " | 243.5 | " |
| 82.5° to 97.5° | 390.0 | " | 263.0 | " |
| 97.5° to 112.5° | 388.4 | " | 282.5 | " |
| 112.5° to 127.5° | 398.8 | " | 302.0 | " |
| 127.5° to 142.5° | 417.8 | " | 321.5 | " |
| 142.5° to 157.5° | 431.9 | " | 341.0 | " |
| 157.5° to 172.5° | 447.1 | " | 360.5 | " |
| 172.5° to 180° | 459.3 | " | 380.0 | " |

Table Notes: 1) Temperatures for normal hot day condition of 104°F peak ambient in AHSM as obtained from [6.5] analysis. Indicated temperatures represent average of the shell temperatures from 0° to 180° with opposing counterparts from 180° to 360°.

2) Temperatures for off-normal hot day condition of 117°F peak ambient in transfer cask with sunshade.

3) Temperatures for off-normal cold day condition -40°F ambient without insolation in transfer cask.

4) Temperature represent boiling point of water at approx. 14 feet of head.

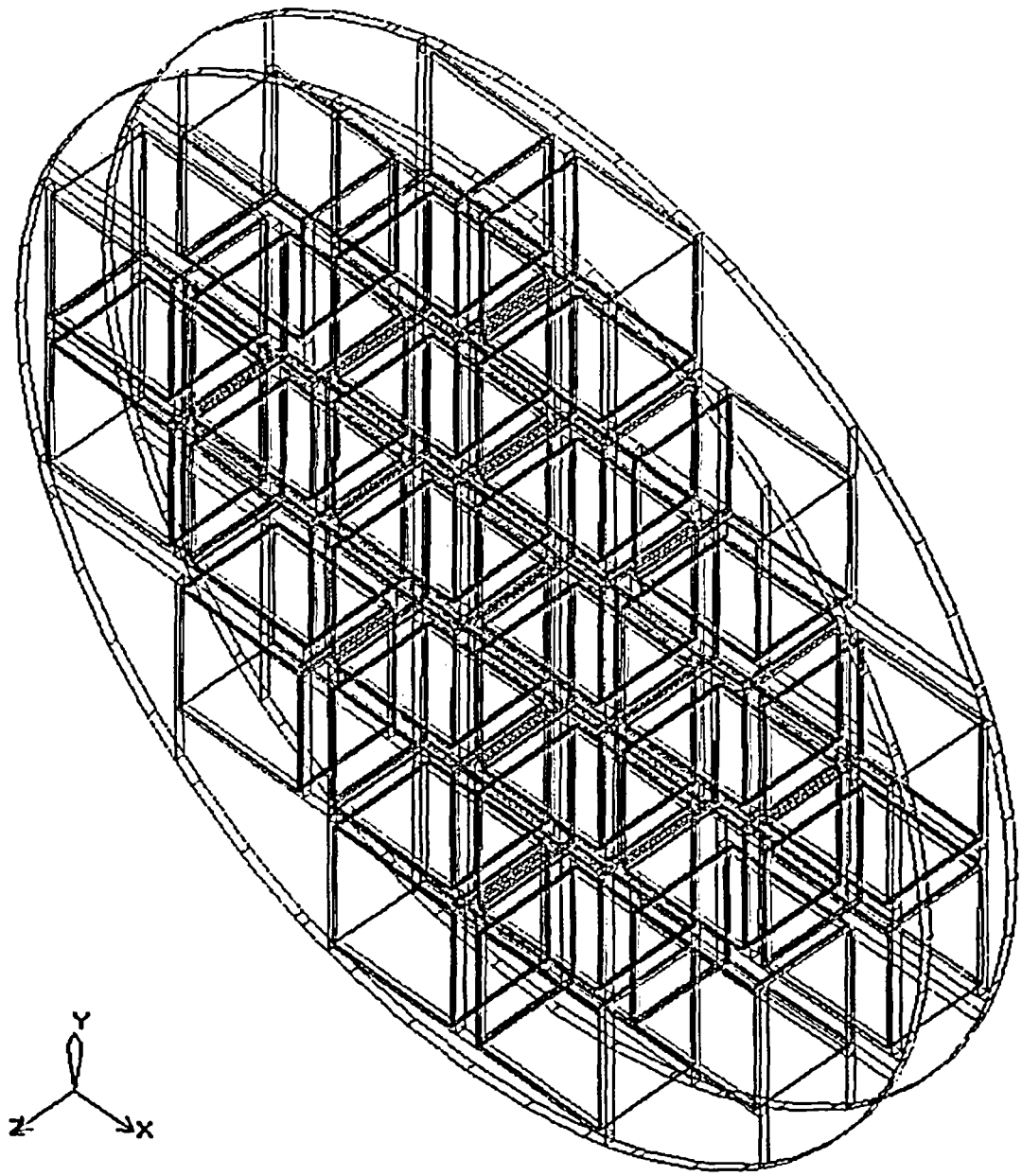


**Figure 4-1 - Isometric, Wireframe View of Model Layout**

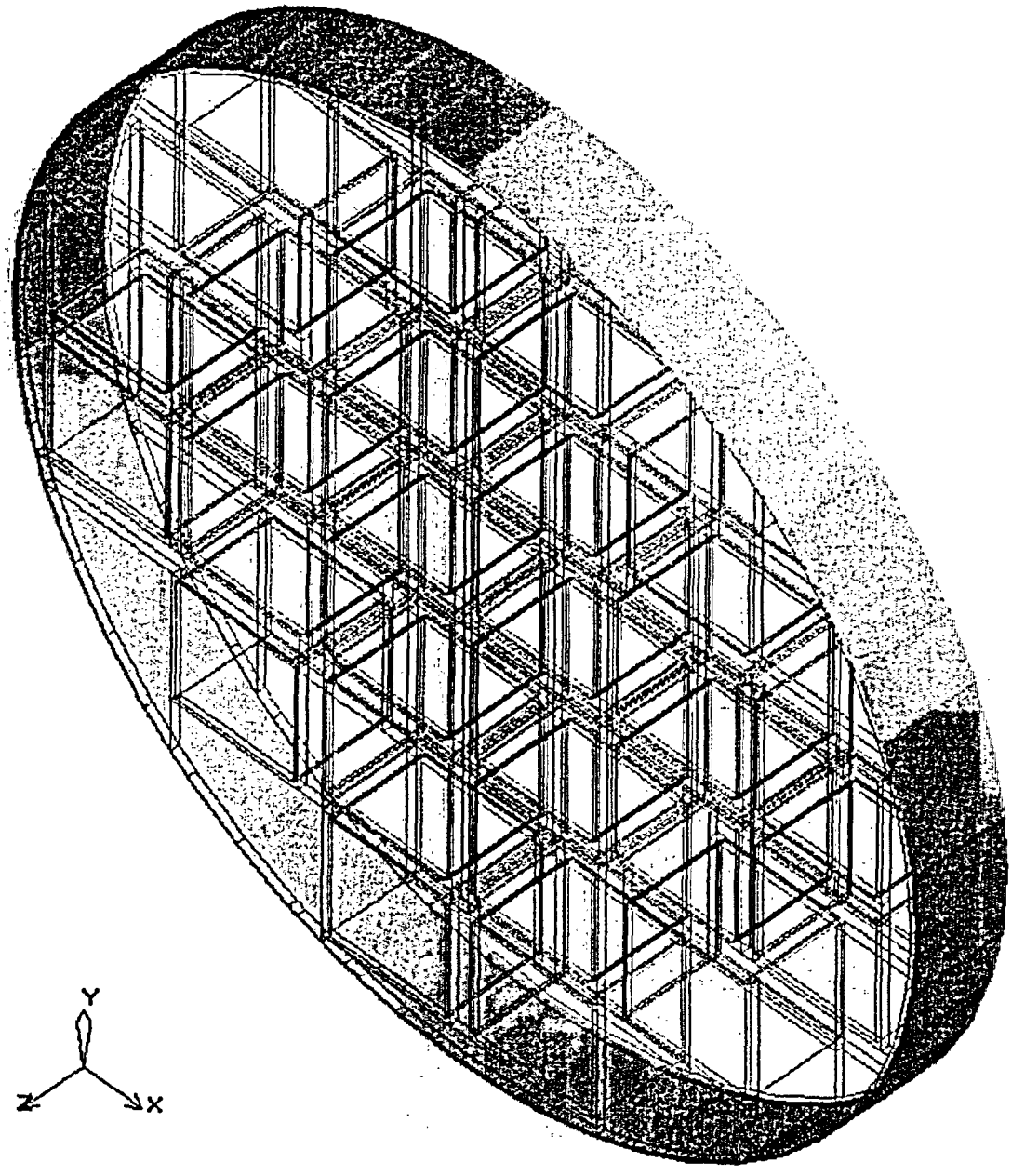


**Figure 4-2 - DSC Shell Model**

C01

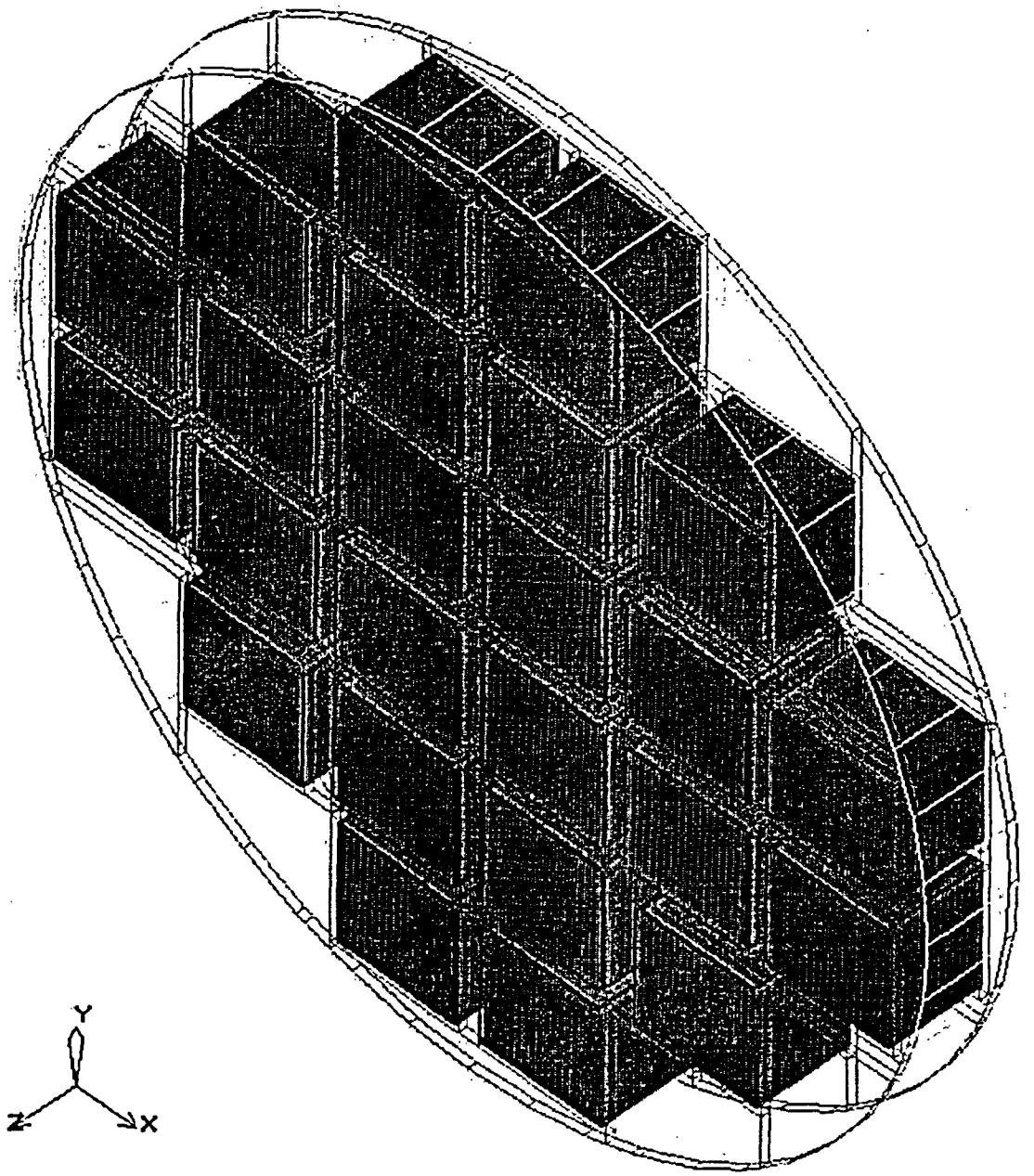


**Figure 4-3 - Fuel Assembly Model**

C02

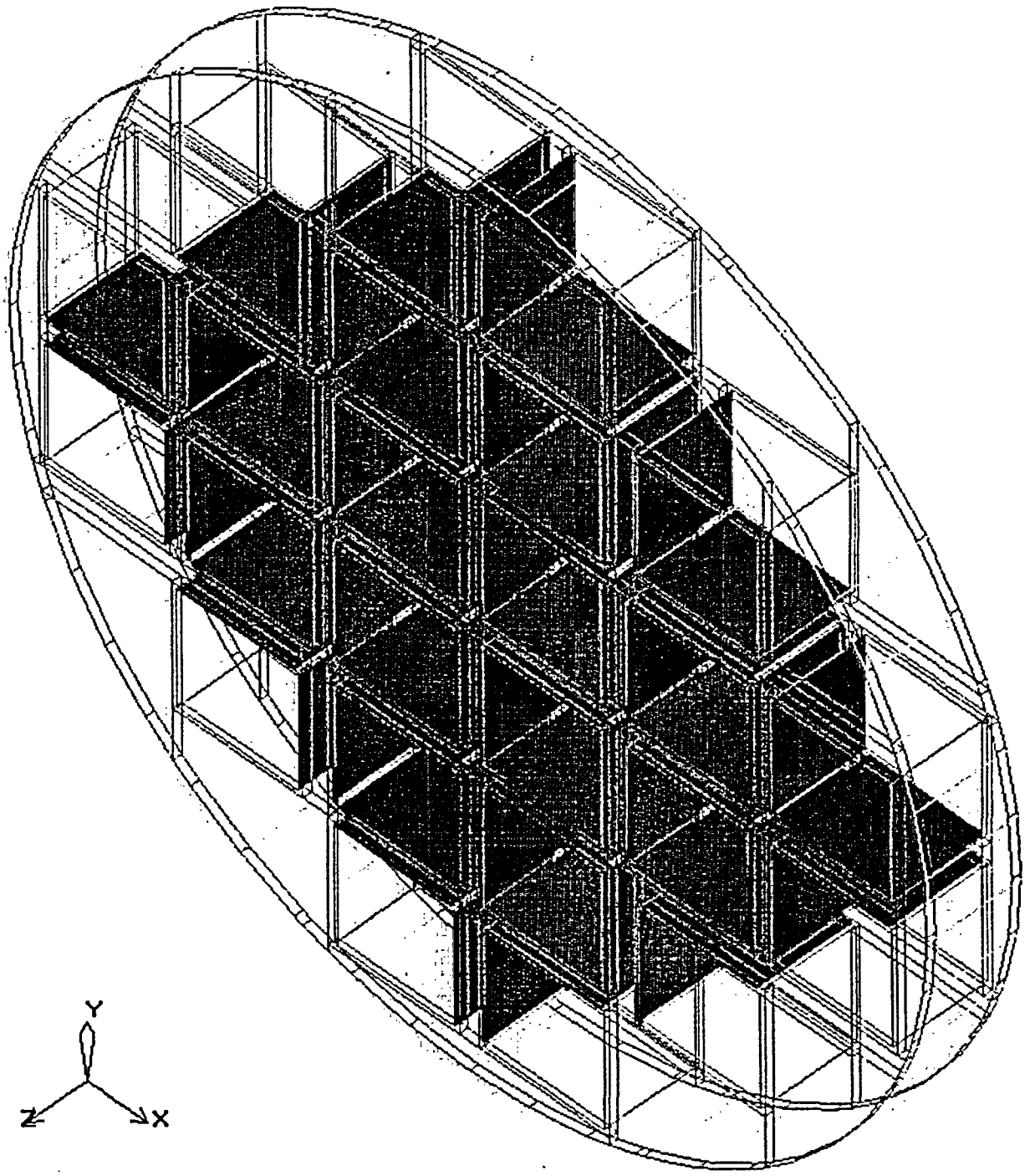


**Figure 4-4 - Poison Sheet Model**

C03

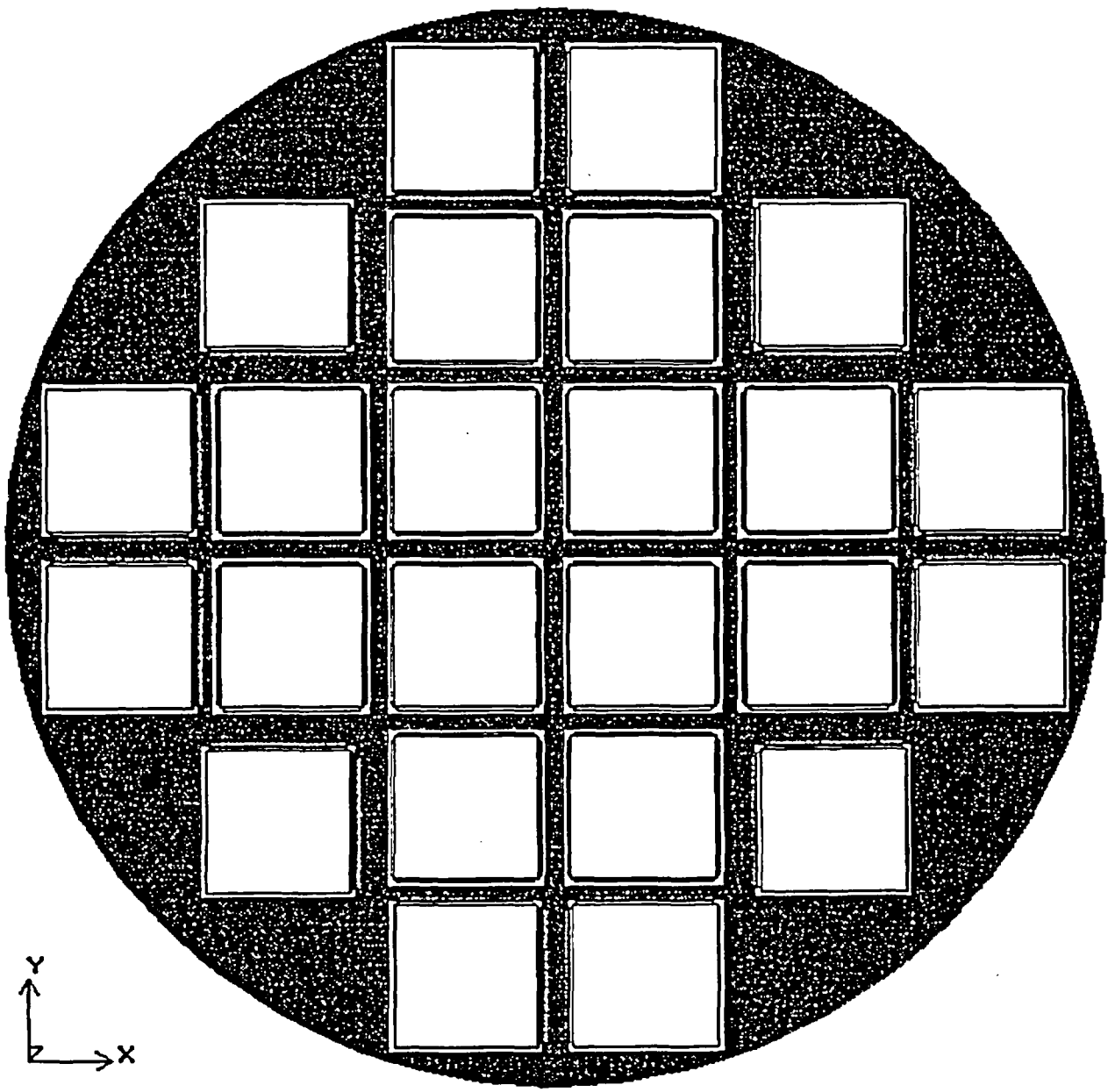


**Figure 4-5 - Spacer Disc Model**

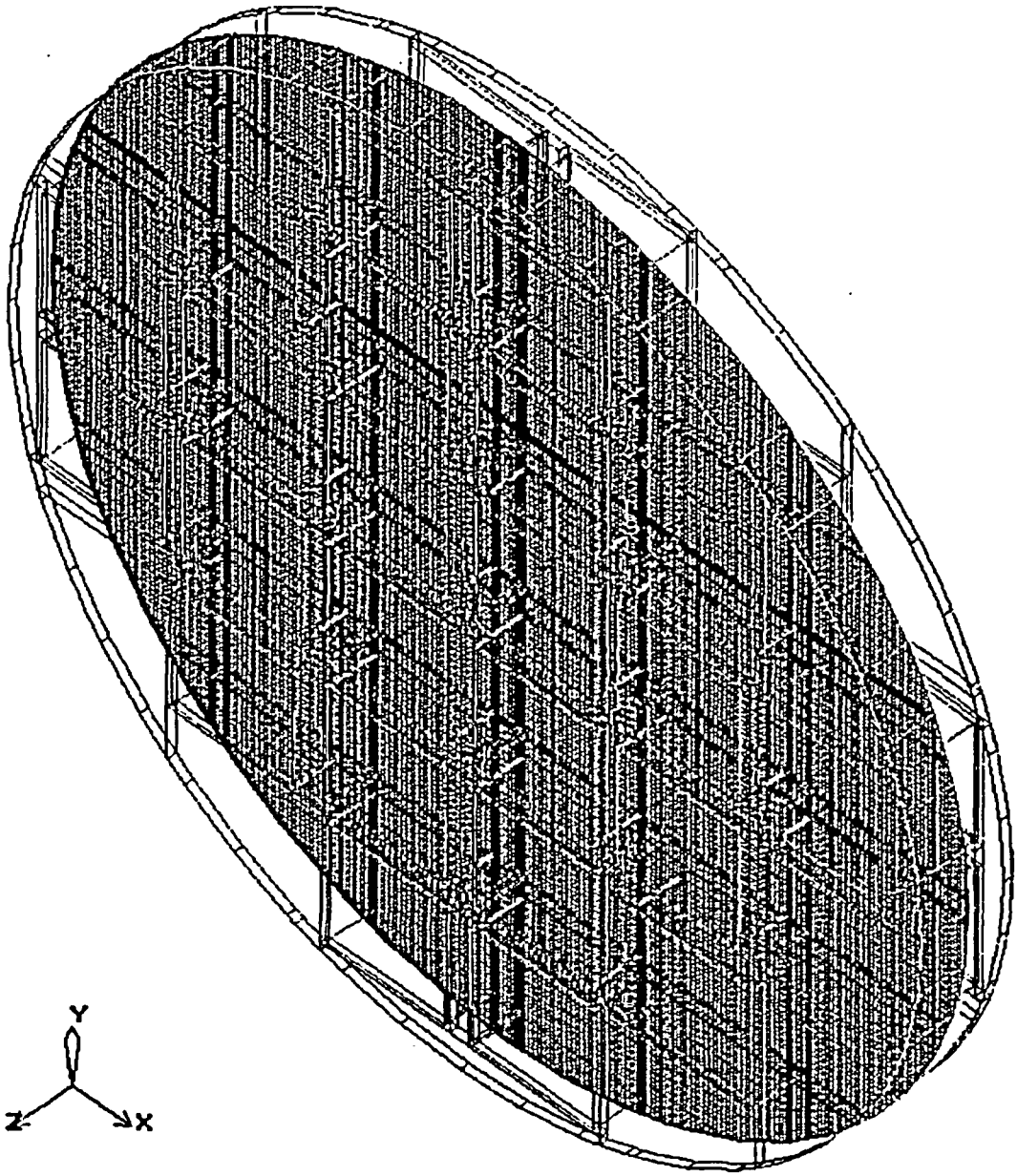


**Figure 4-6 - Perspective View of Meshing At X-Y Plane of 24PT4-DSC**

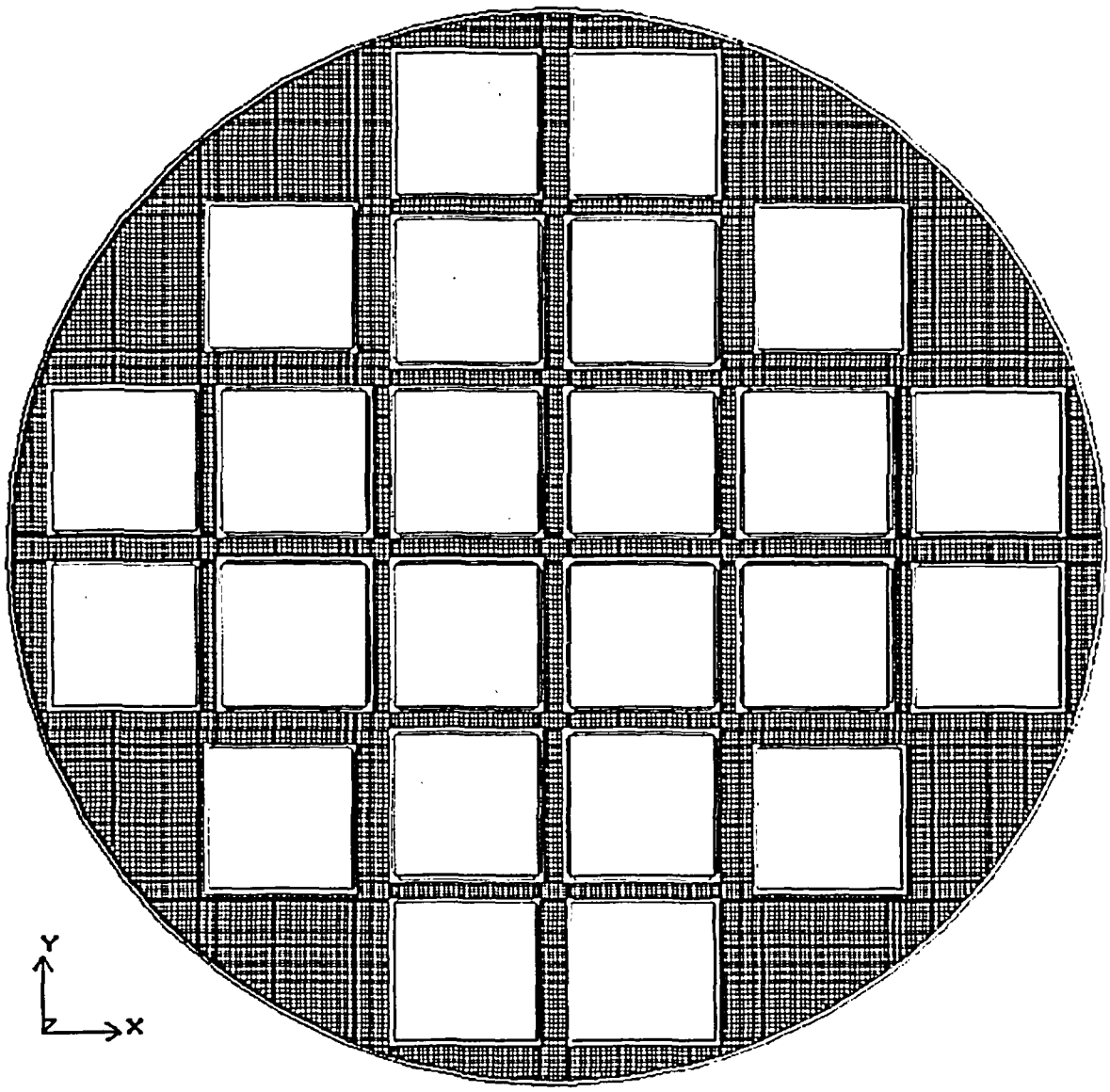


**Figure 4-7 - Plan View of Meshing At Spacer Disc**

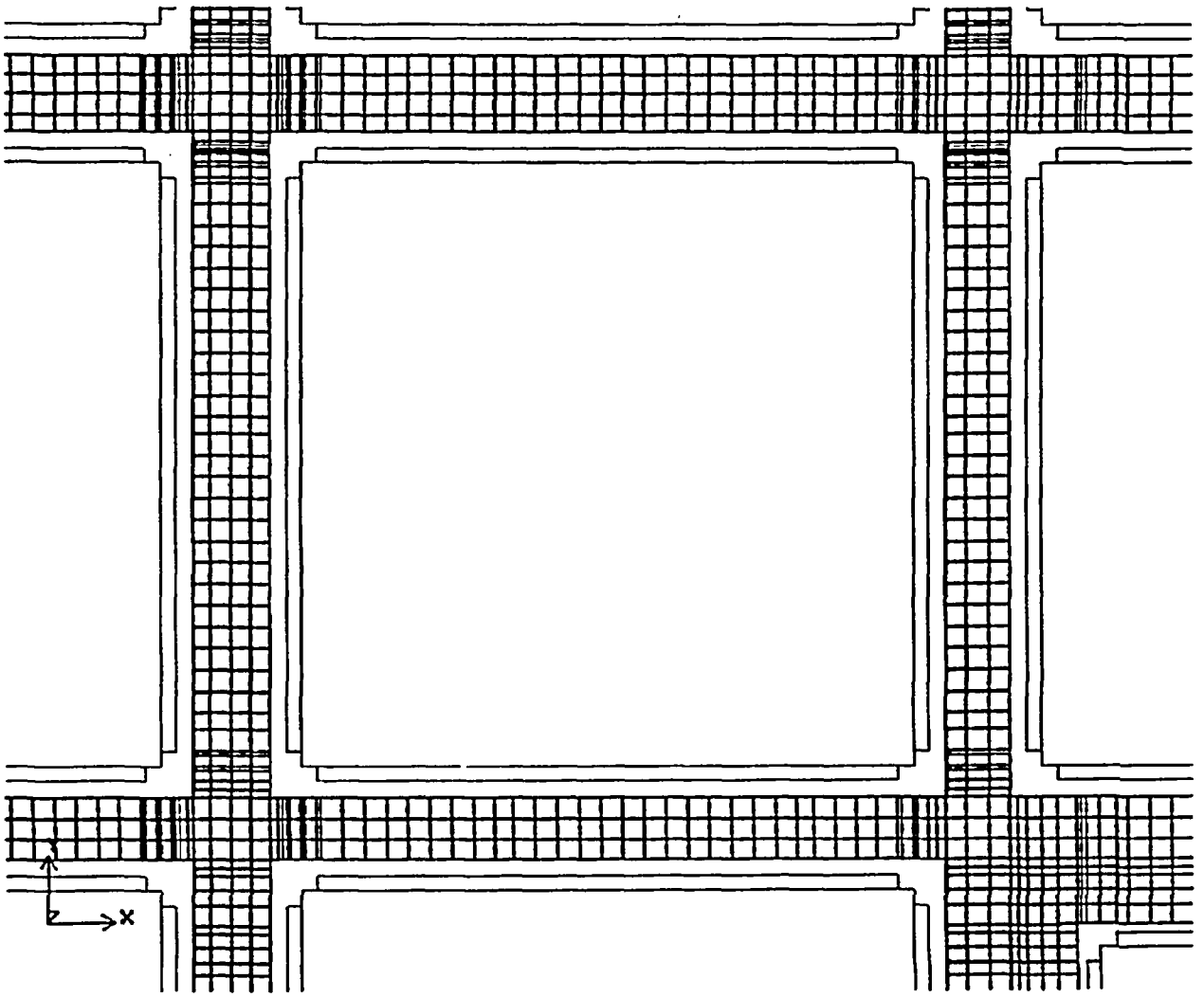


**Figure 4-8 - Enlarged View of Meshing At Spacer Disc**

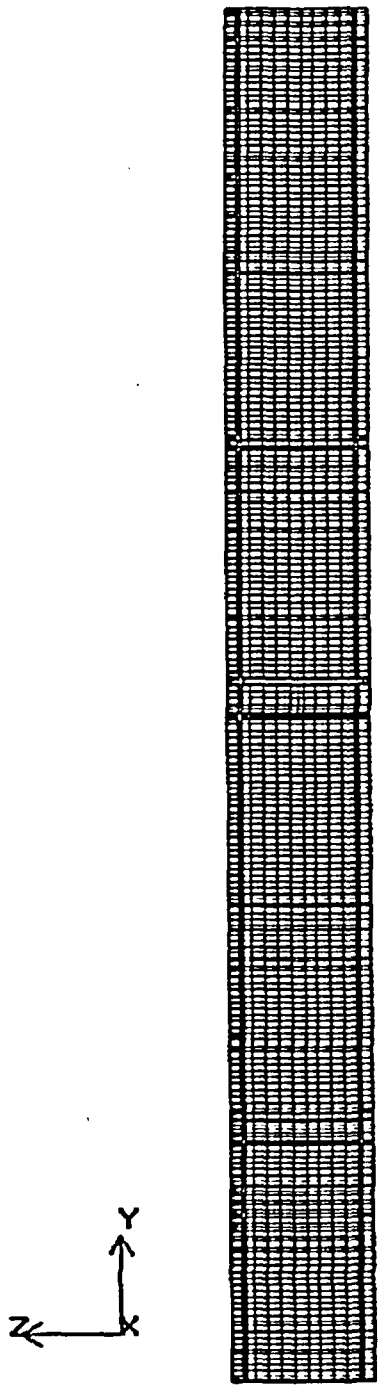


**Figure 4-9 - Elevation View of Meshing At Z-Y Plane of Modeled DSC Segment**

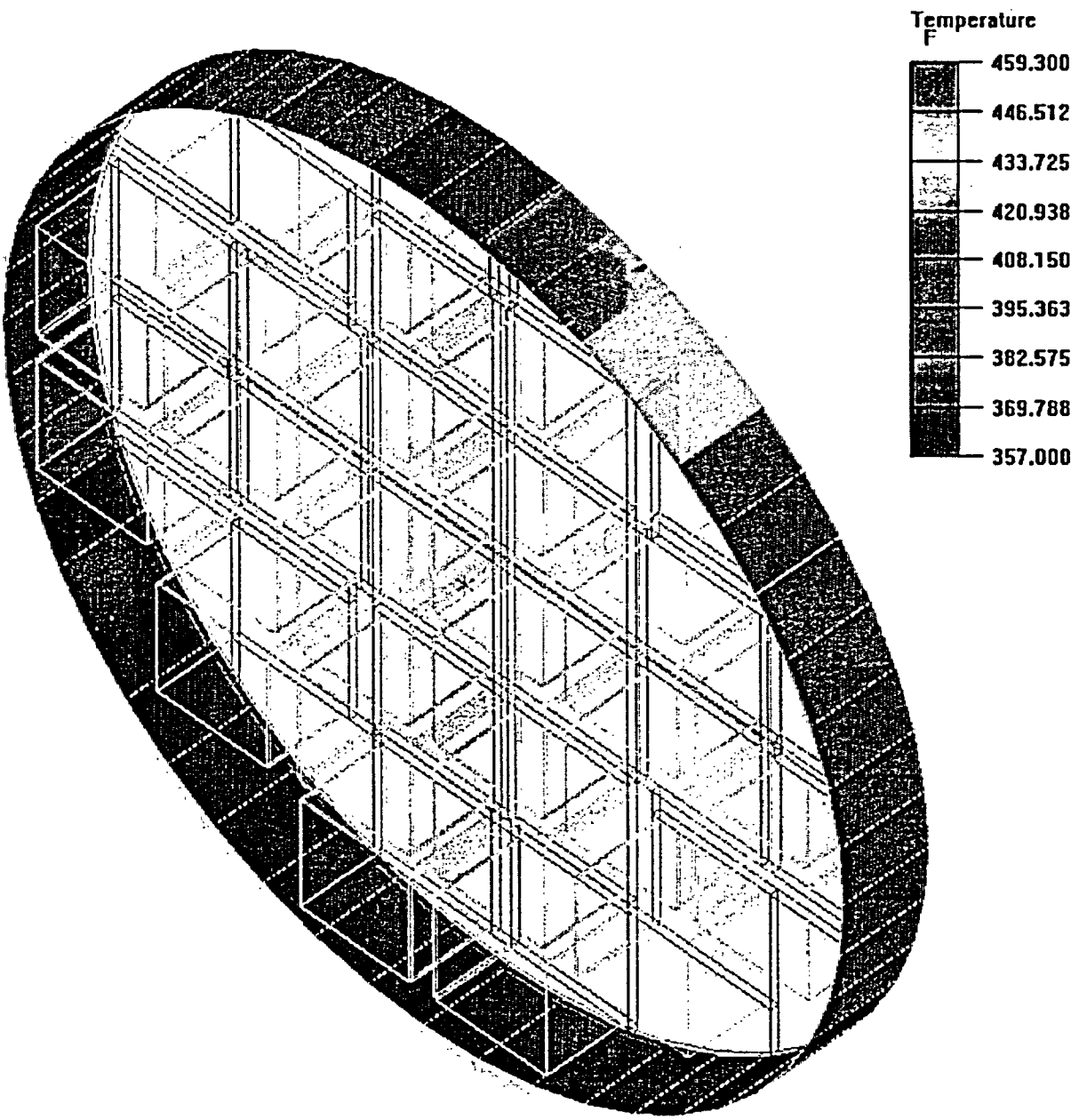


**Figure 4-10 - Imposed Shell Temperatures, Bounding Condition in AHSM**

C04

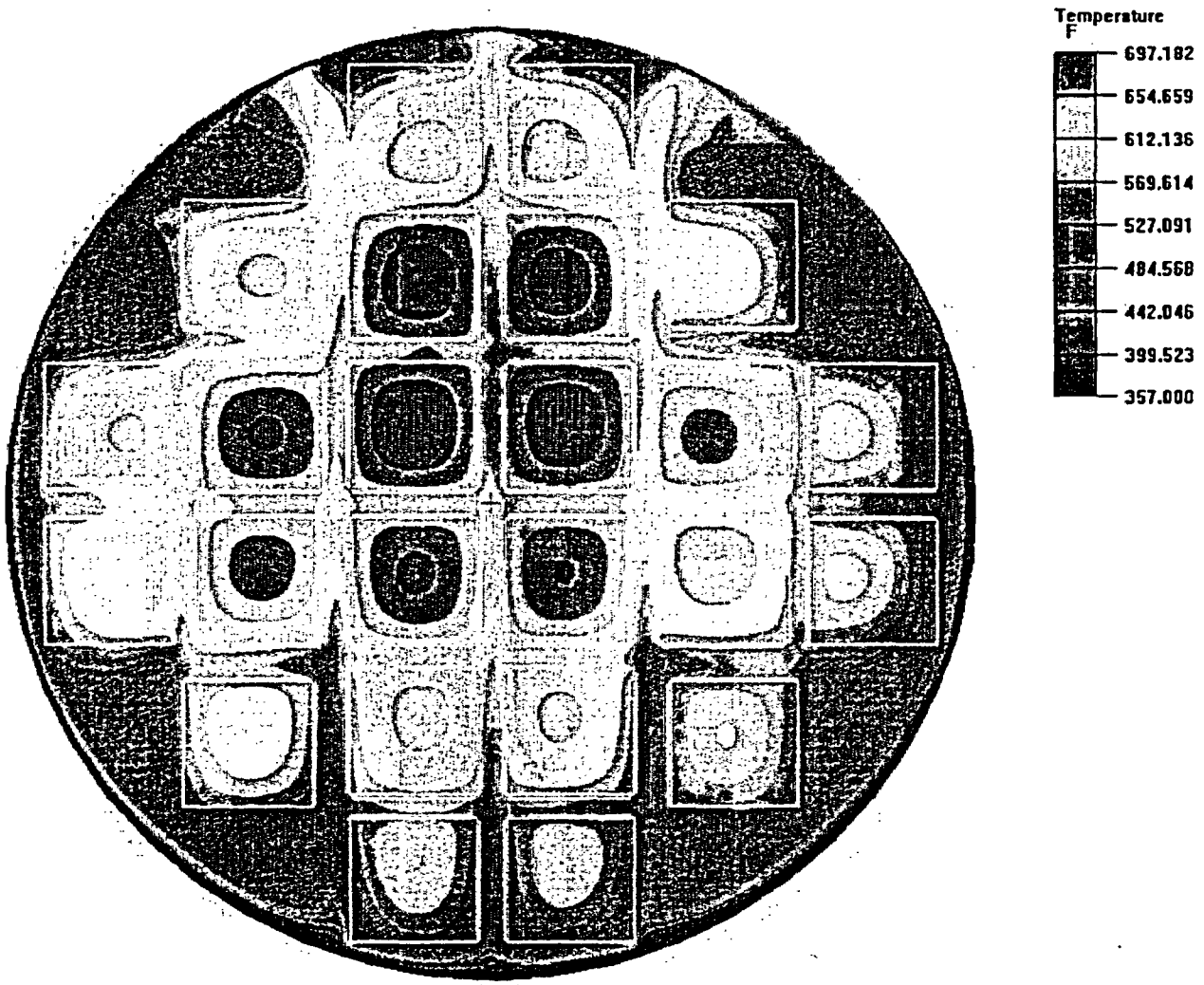


**Figure 4-11 - Temperature Distribution, Bounding Condition in AHSM, Heat Load Configuration #1**

C05

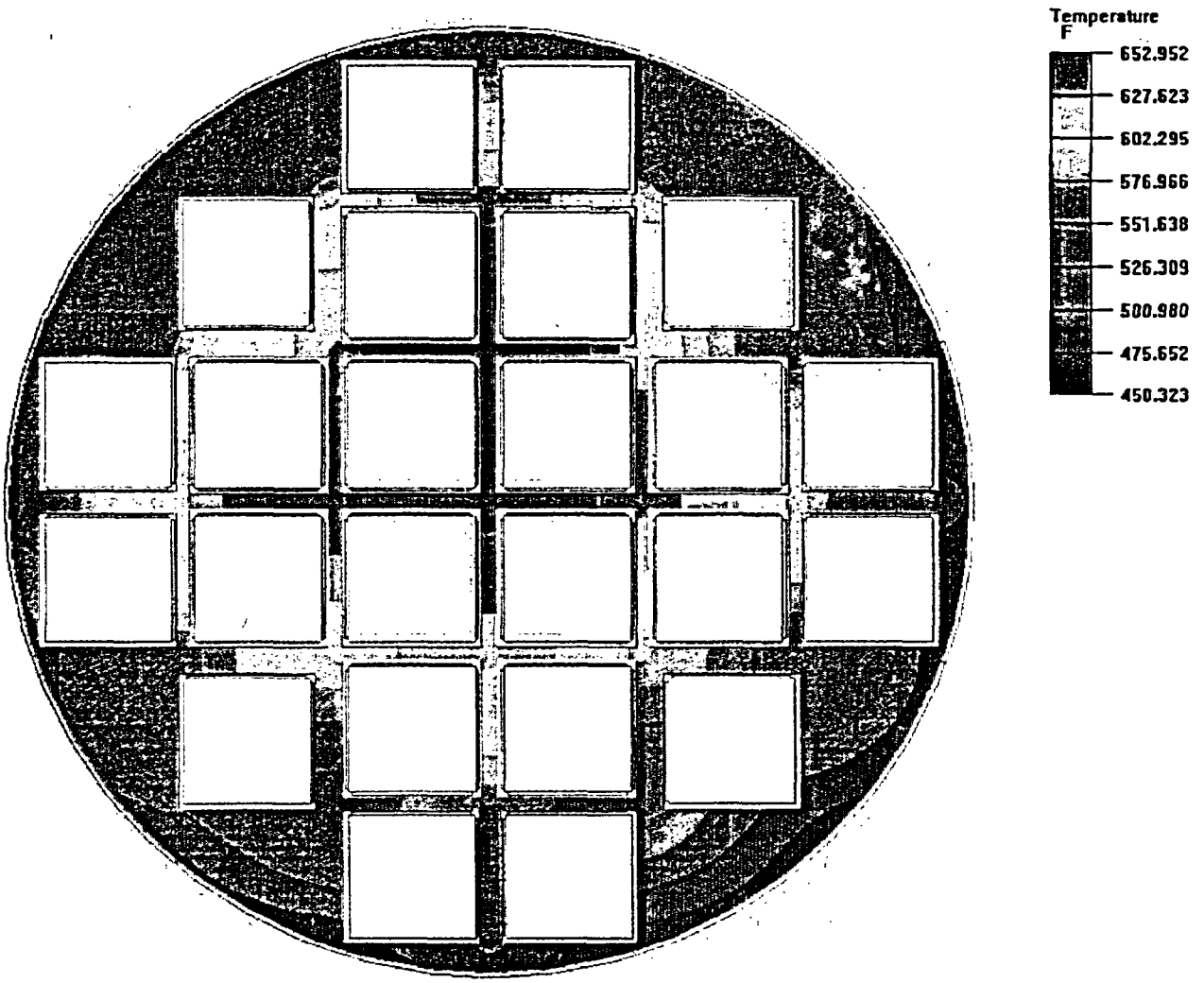


**Figure 4-12 - Spacer Disc Temperature Distribution, Bounding Condition in AHSM, Heat Load Configuration #1**

C06

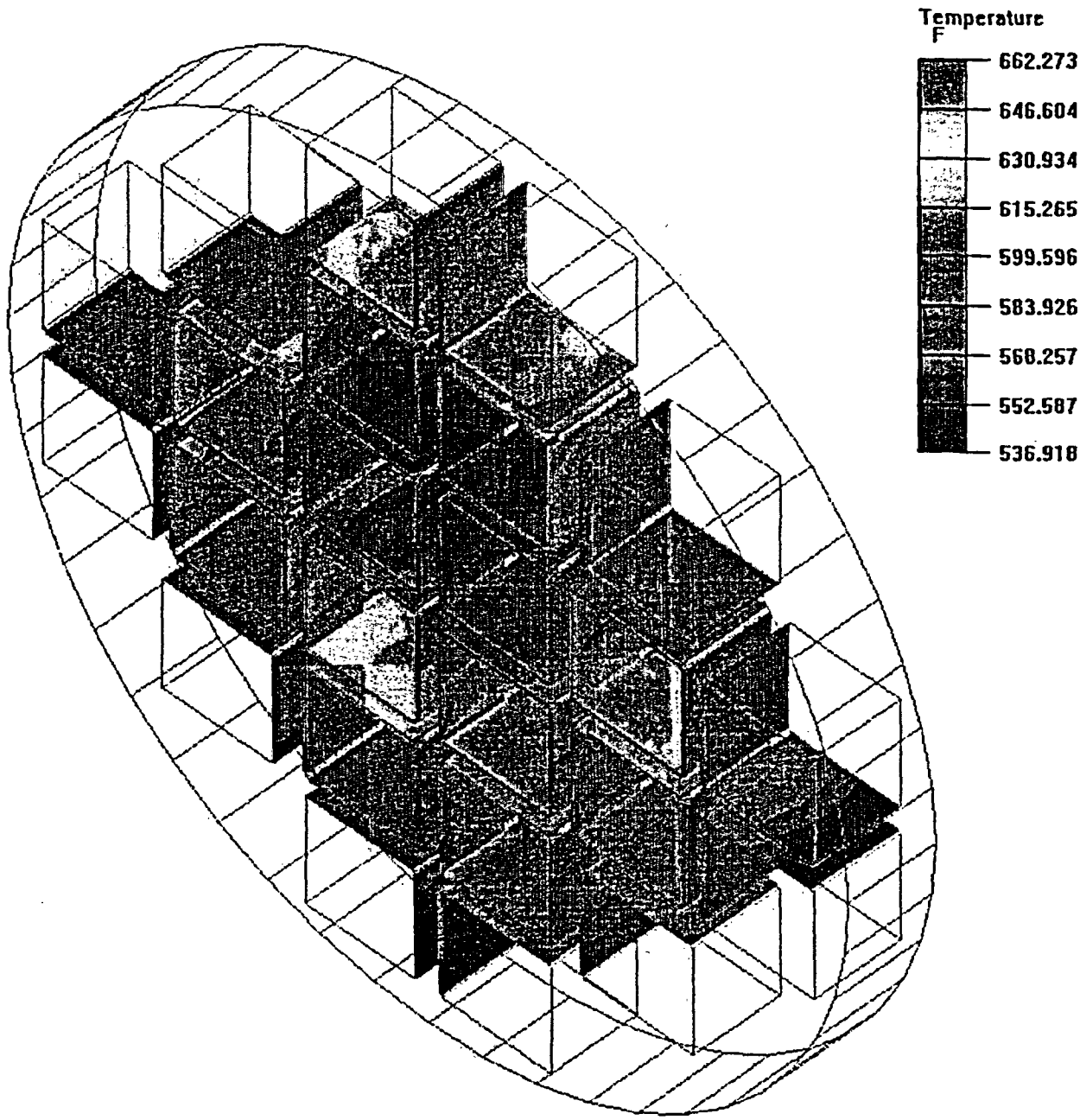


**Figure 4-13 - Poison Sheet Temperature Distribution, Bounding Condition in AHSM, Heat Load Configuration #1**

C07

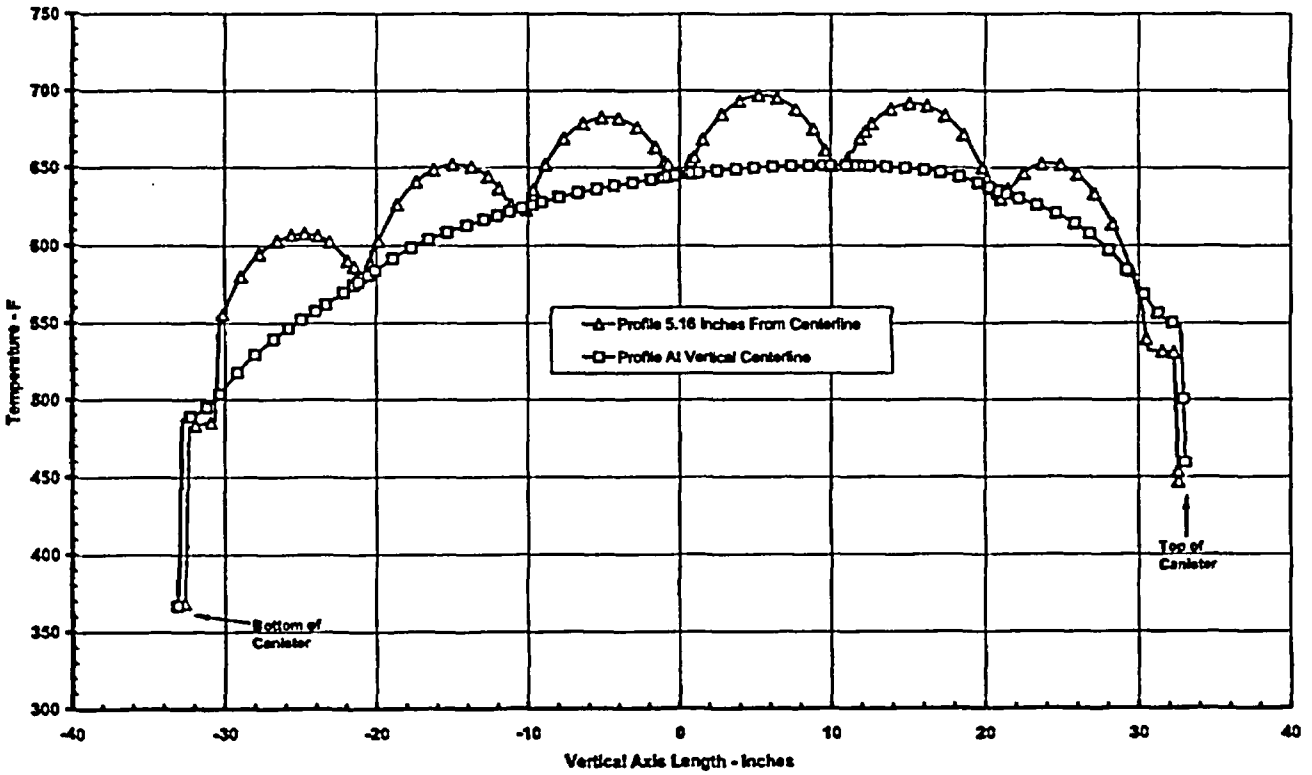


**Figure 4-14 - Temperature Along Vertical Lines Through Basket, Bounding Condition in AHSM, Heat Load Configuration #1**

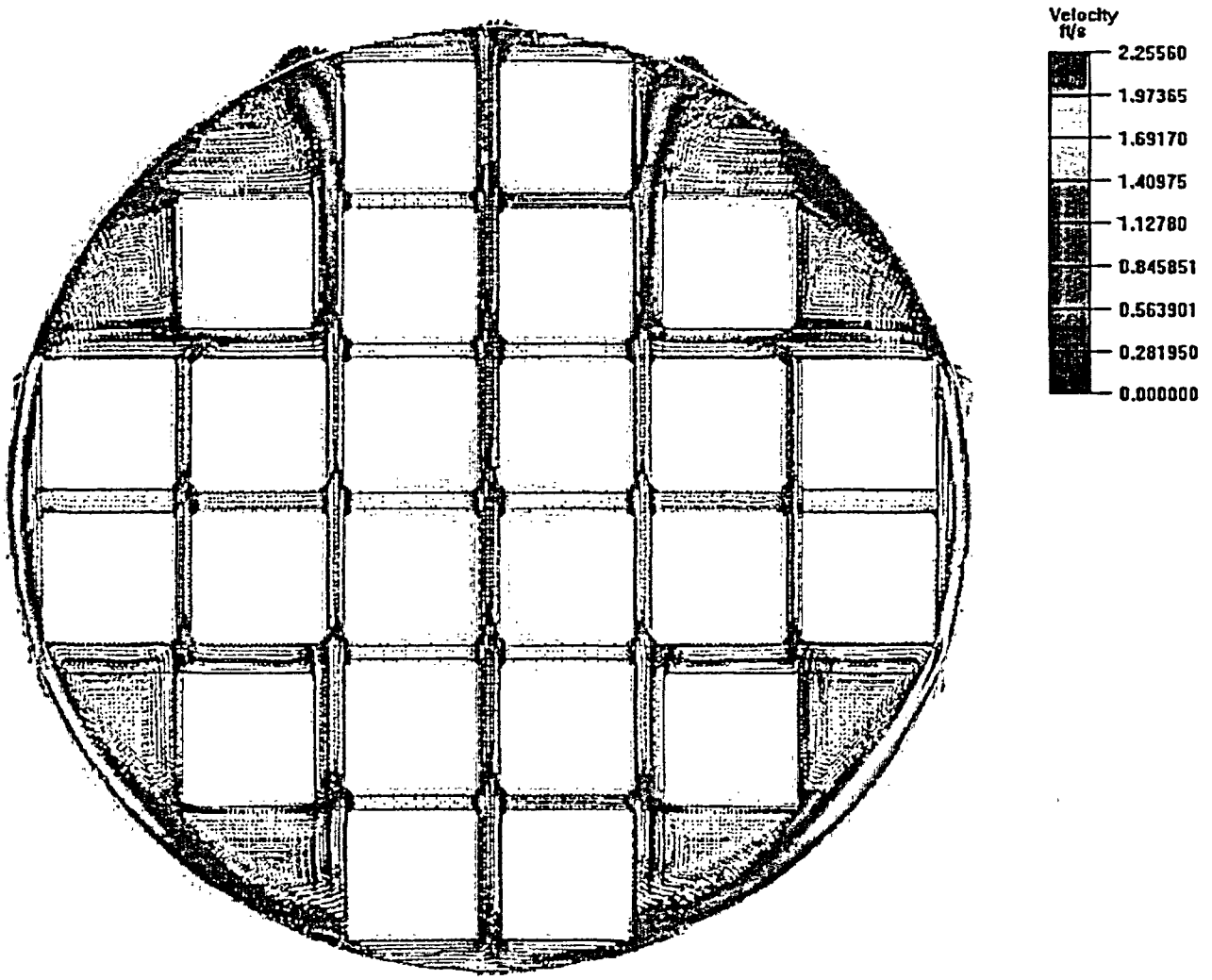


**Figure 4-15 - Velocity Distribution, Bounding Condition in AHSM, Heat Load Configuration #1**

C08

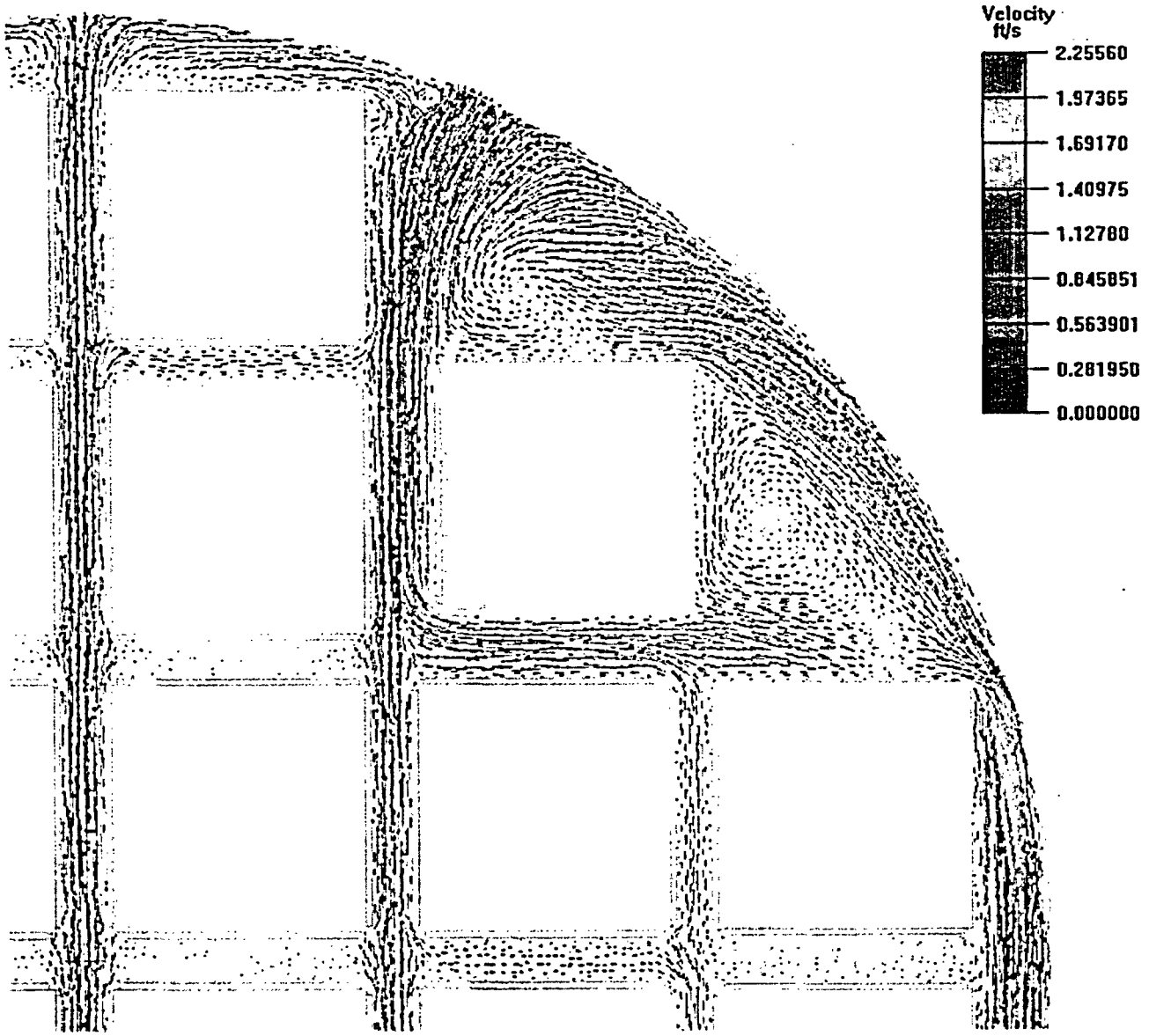


**Figure 4-16 - Velocity Distribution, Bounding Condition in AHSM, Heat Load Configuration #1 (Enlarged View)**

C09


**Figure 4-17 - Velocity Distribution, Bounding Condition in AHSM, Heat Load Configuration #1 (Enlarged View)**

C10

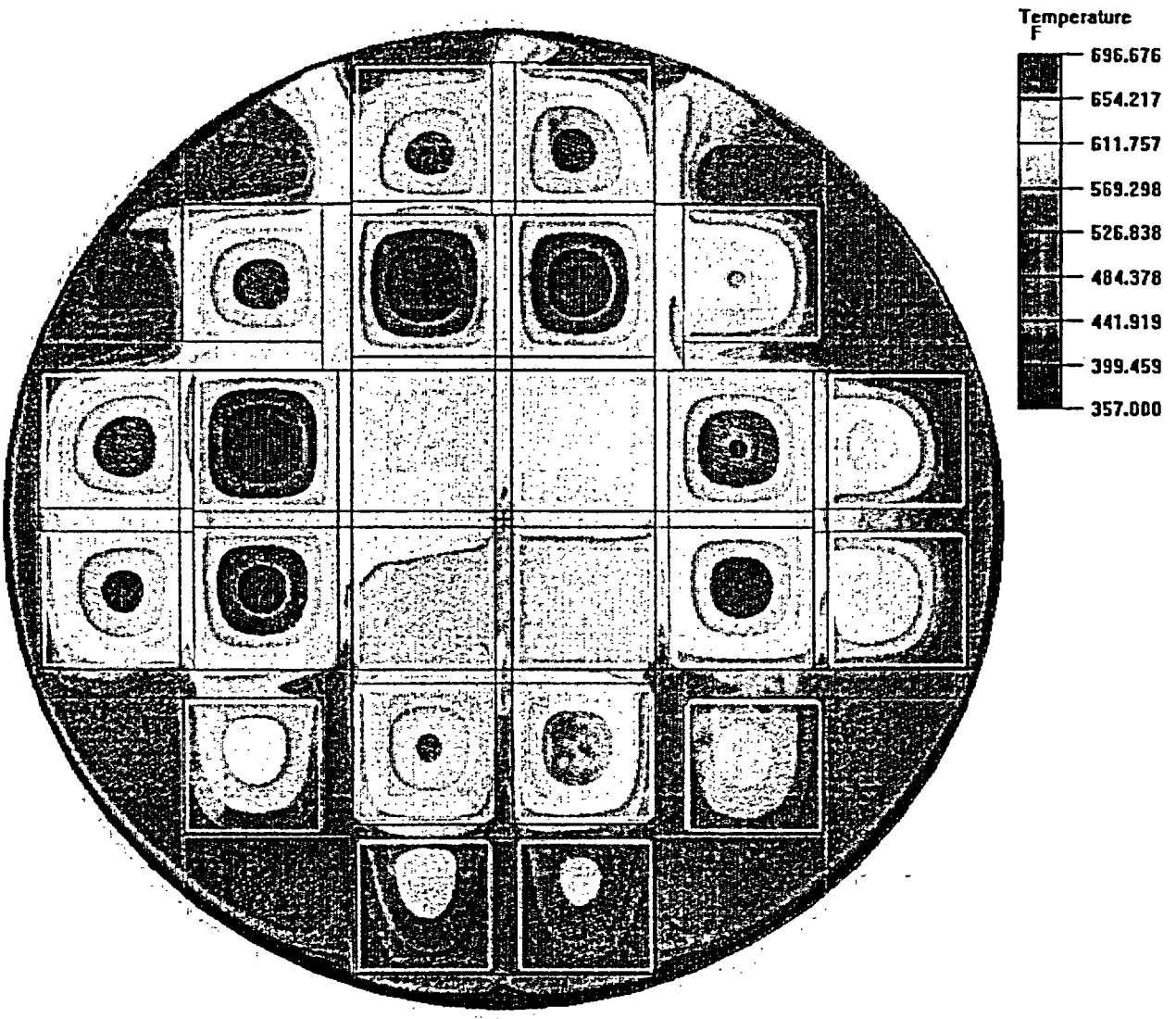


**Figure 4-18 - Temperature Distribution, Bounding Condition in AHSM, Heat Load Configuration #3**

C11

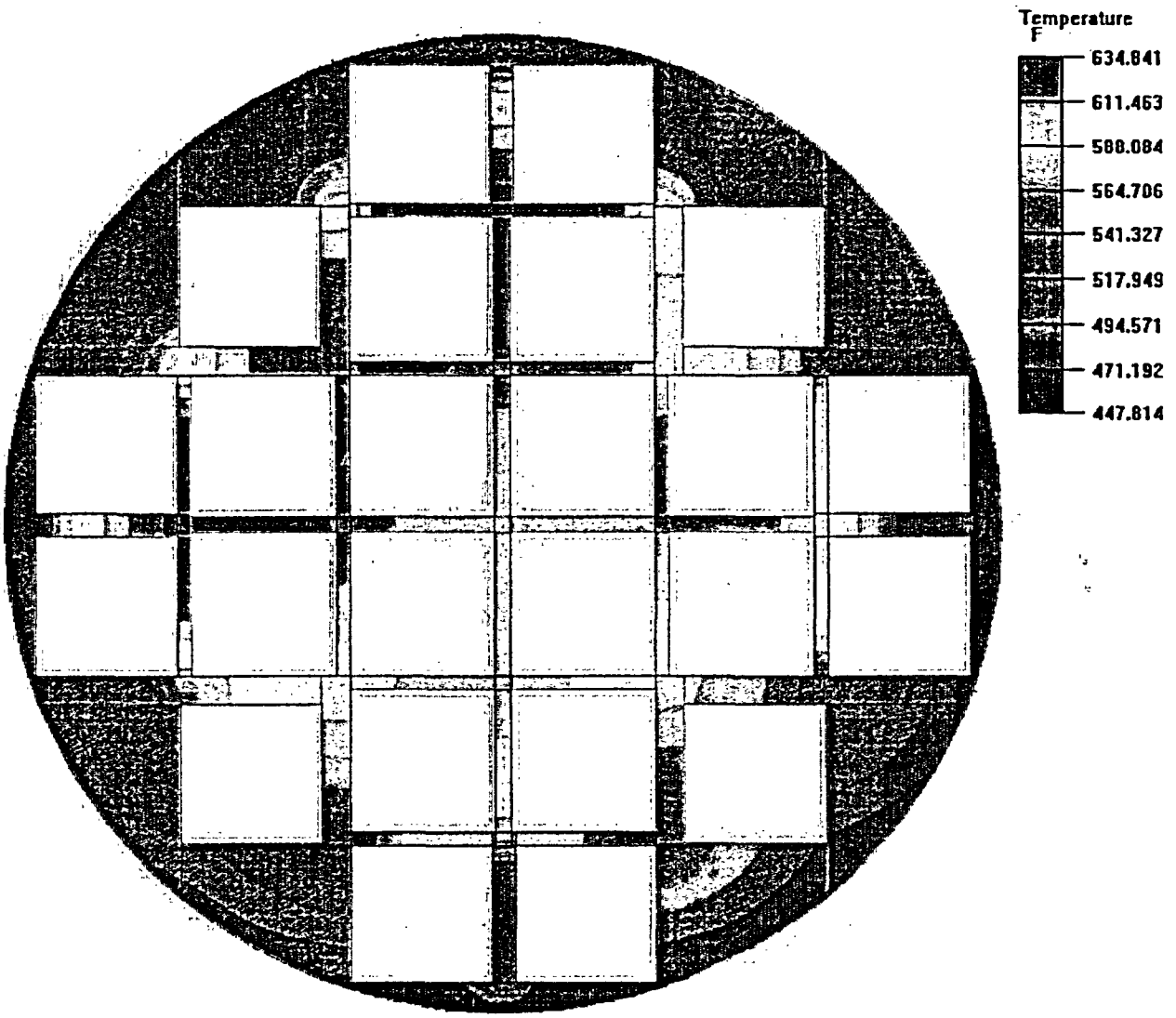


**Figure 4-19 - Spacer Disc Temperature Distribution, Bounding Condition in AHSM, Heat Load Configuration #3**

C 12

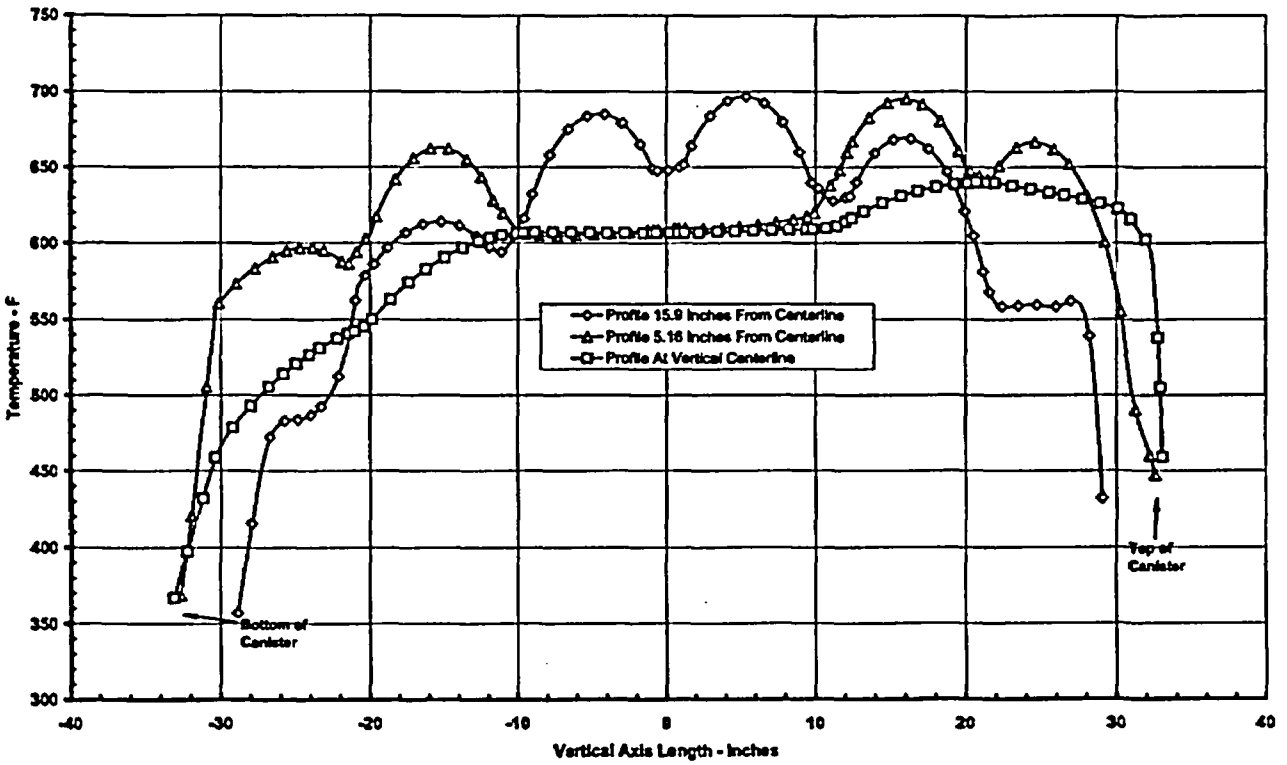


**Figure 4-20 - Temperature Along Vertical Lines Through Basket, Bounding Condition in AHSM, Heat Load Configuration #3**

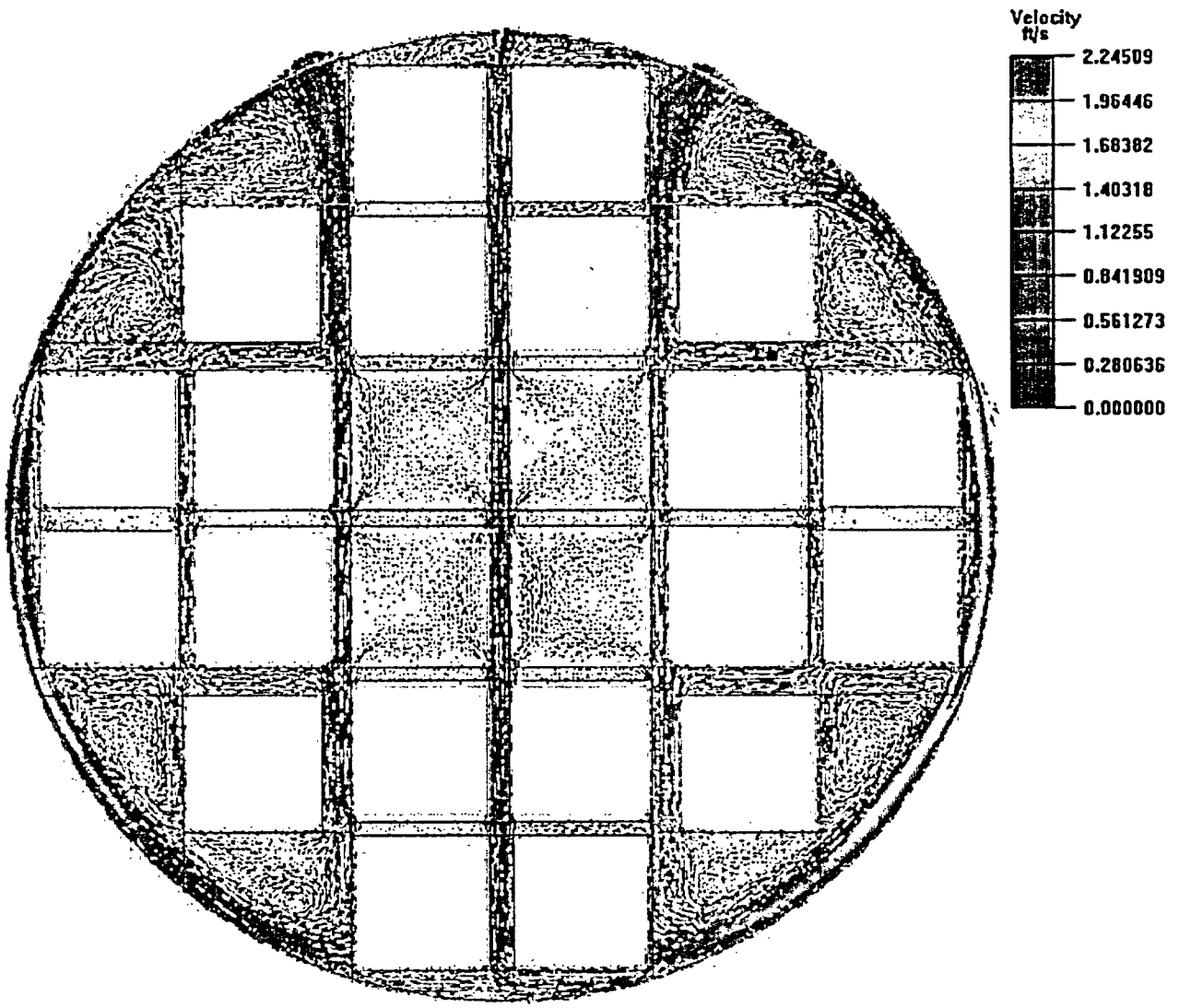


**Figure 4-21 - Velocity Distribution, Bounding Condition in AHSM, Heat Load Configuration #3**

C13

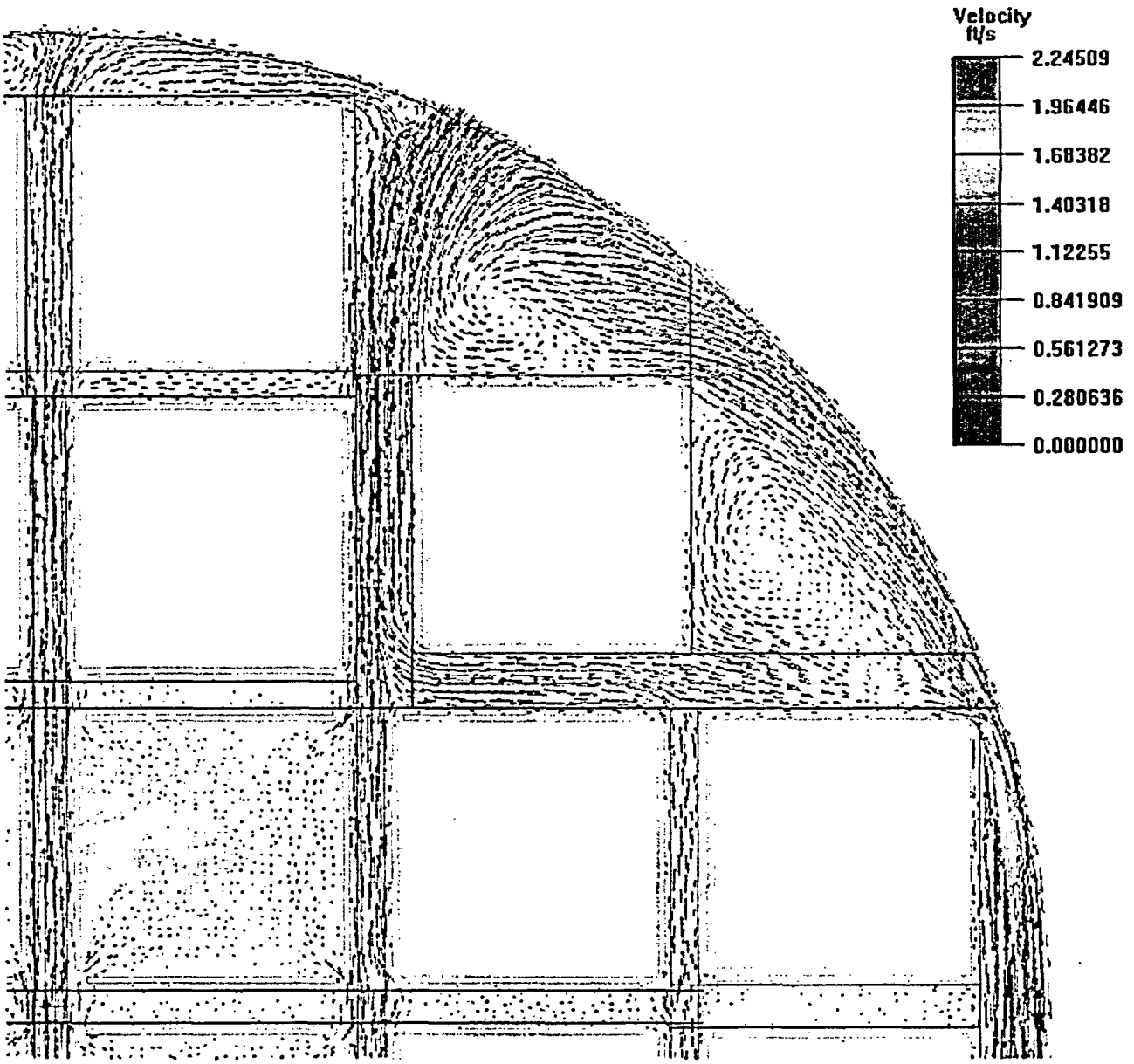


**Figure 4-22 - Velocity Distribution, Bounding Condition in AHSM, Heat Load Configuration #3 (Enlarged View)**

C14

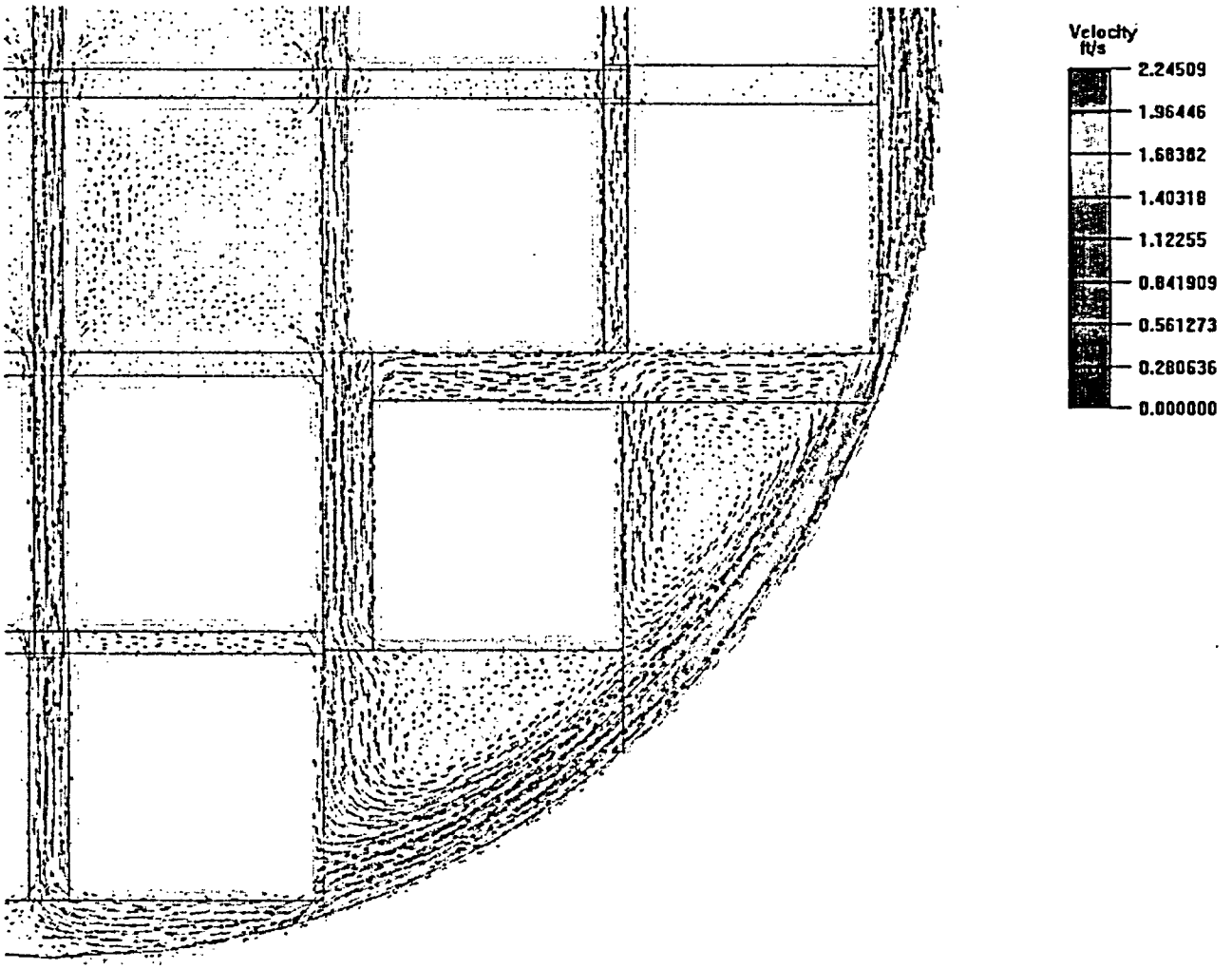


**Figure 4-23 - Velocity Distribution, Bounding Condition in AHSM, Heat Load Configuration #3 (Enlarged View)**

C 15

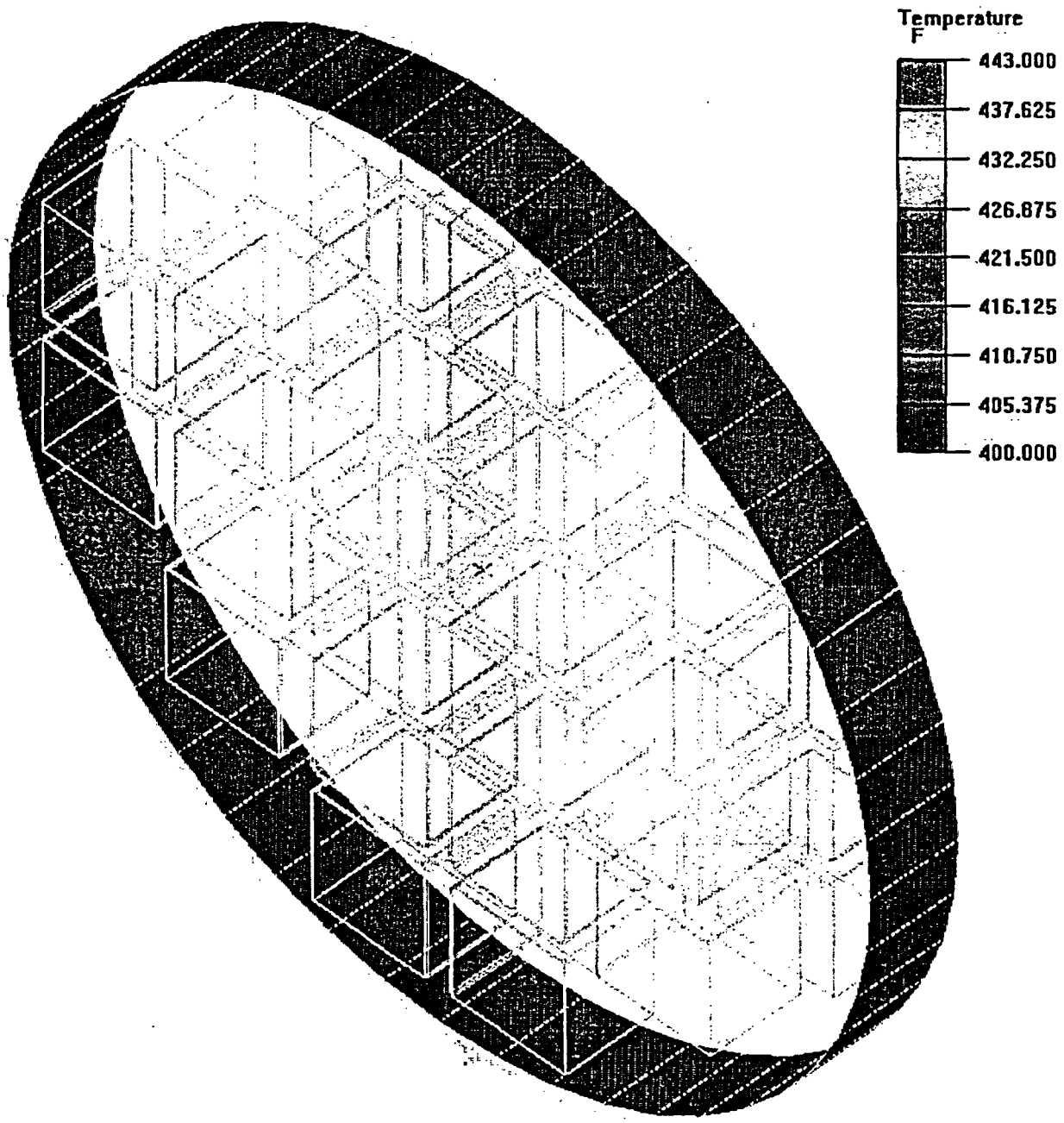


**Figure 4-24 - Imposed Shell Temperatures, Bounding Condition in Transfer Cask**

C16

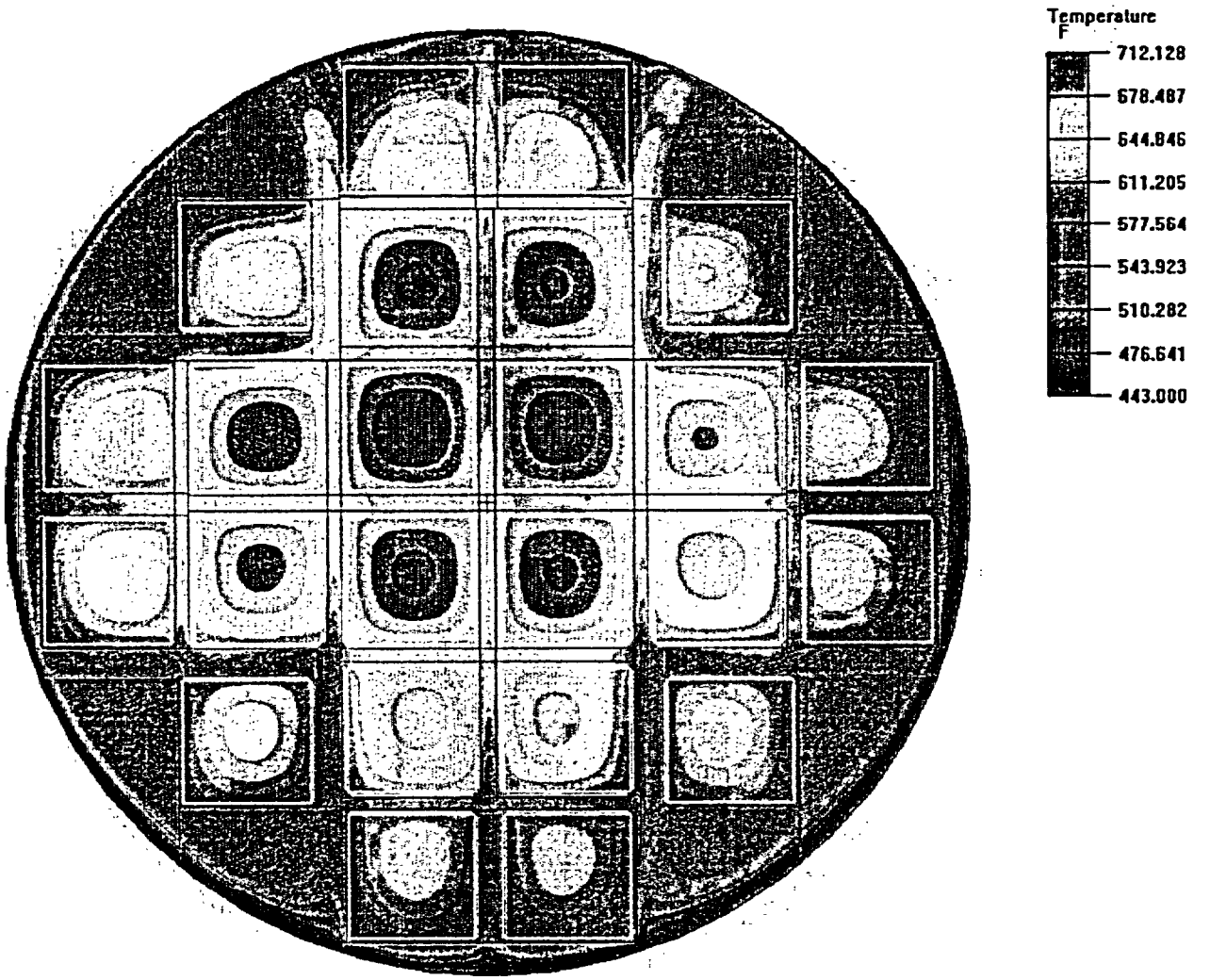


**Figure 4-25 - Temperature Distribution, Bounding Condition in Transfer Cask**

C17

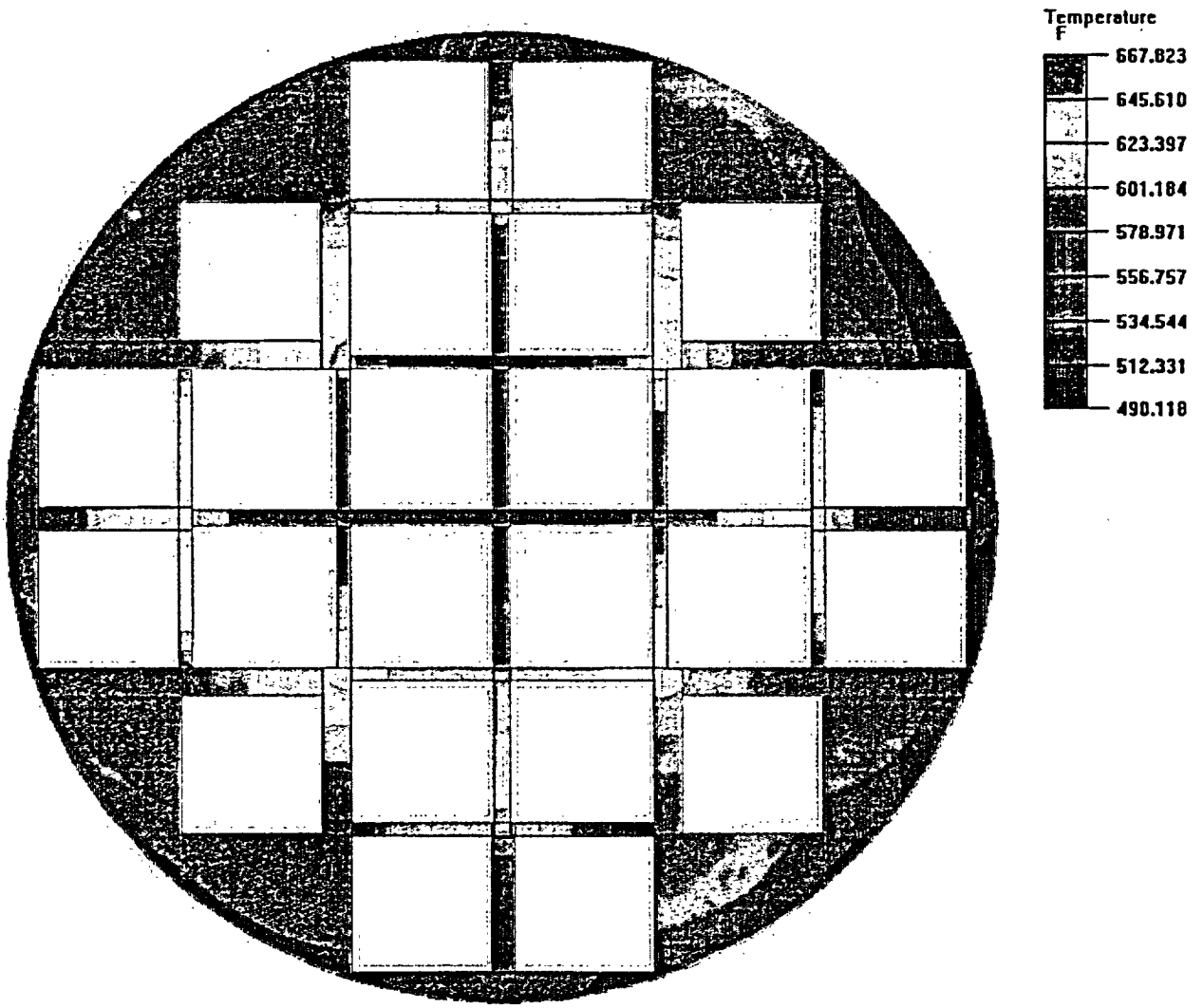


**Figure 4-26 - Spacer Disc Temperature Distribution, Bounding Condition in Transfer Cask**

C18

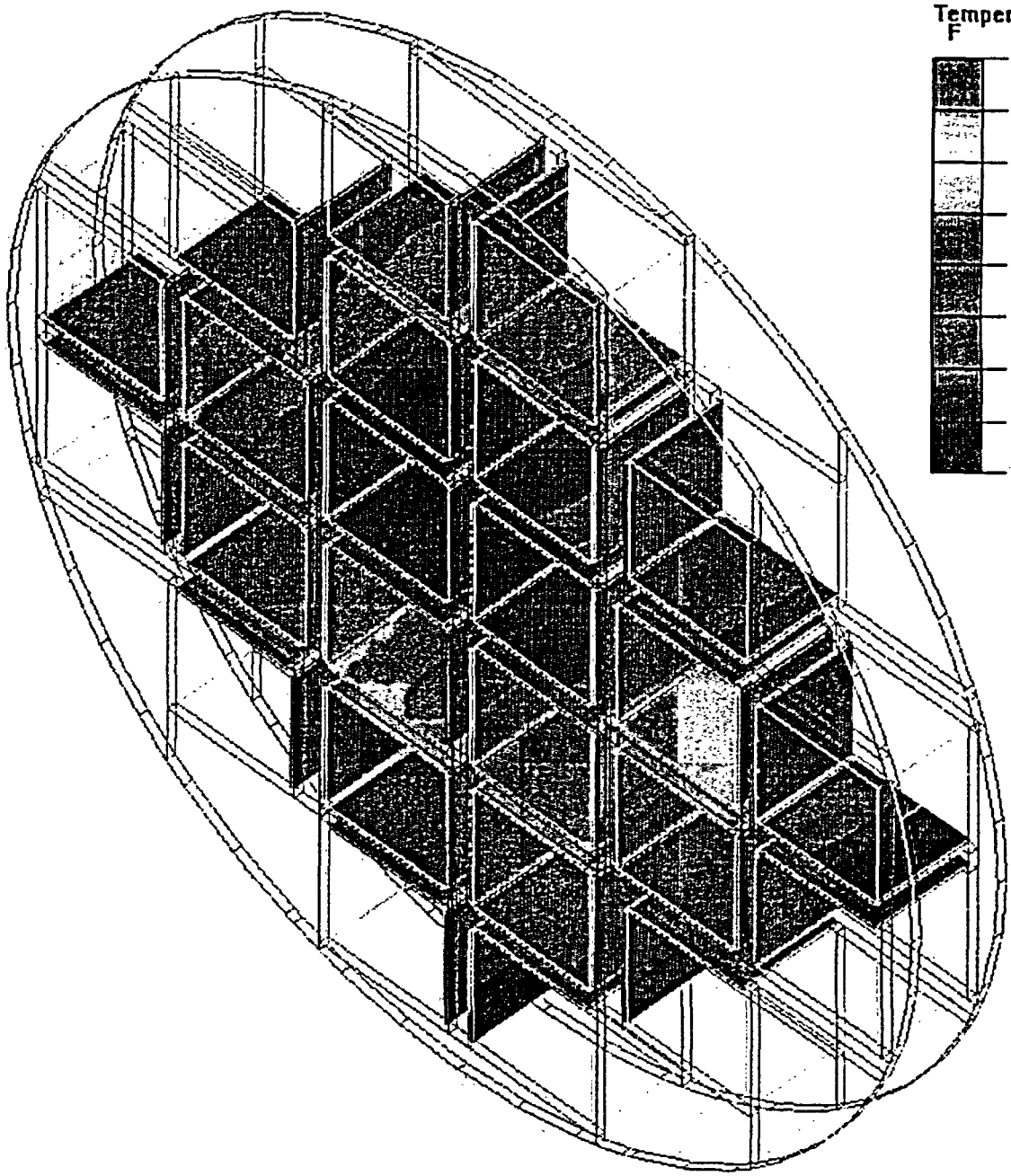


**Figure 4-27 - Poison Sheet Temperature Distribution, Bounding Condition in Transfer Cask**

C19

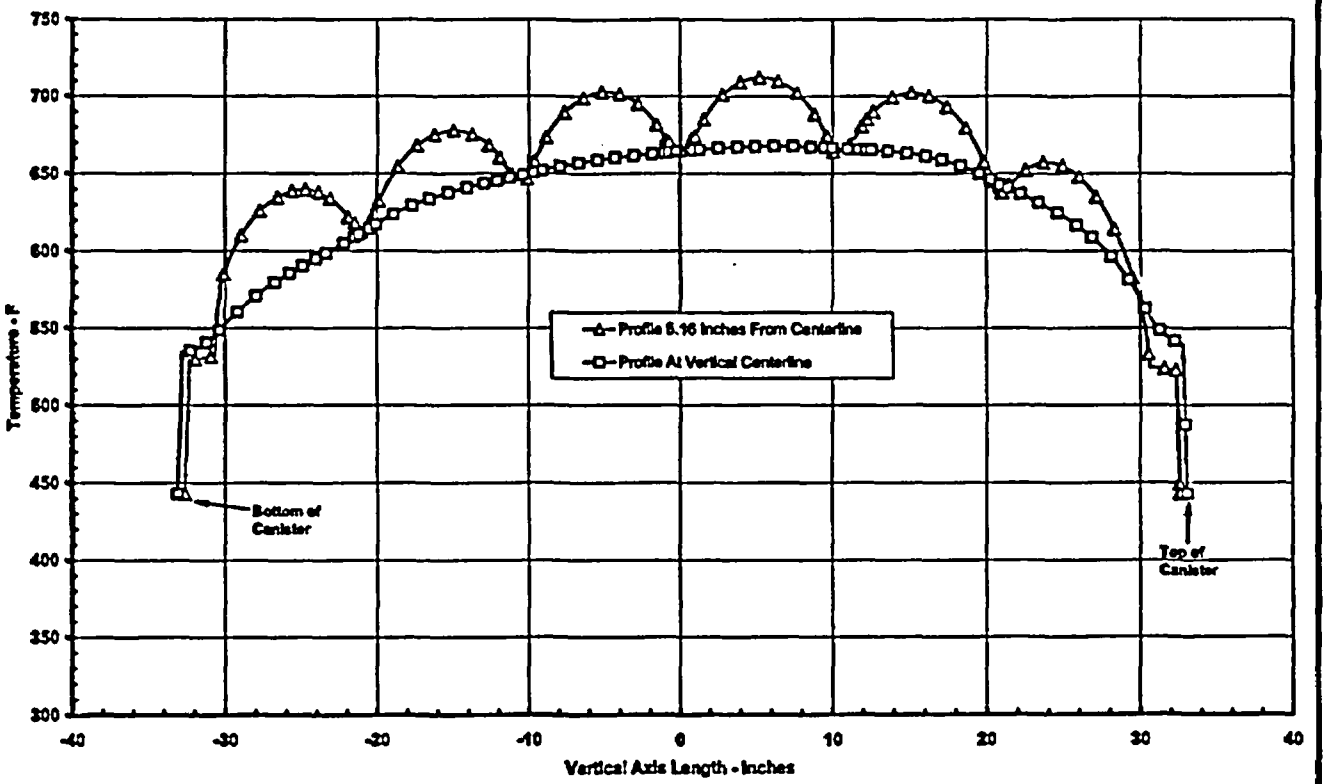


**Figure 4-28 - Temperature Along Vertical Lines Through Basket, Bounding Condition in Transfer Cask**

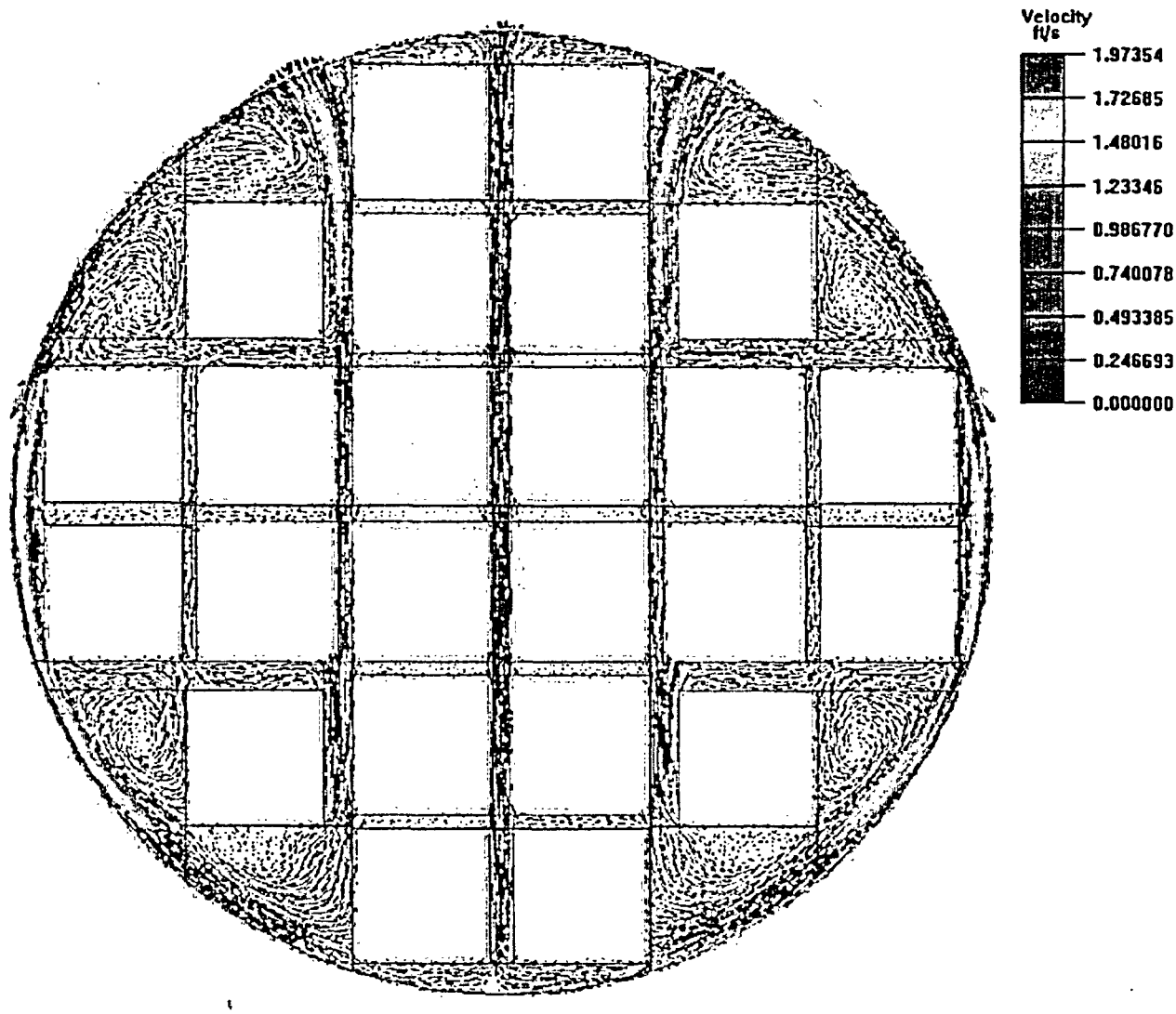


**Figure 4-29 - Velocity Distribution, Bounding Condition in Transfer Cask**

C20

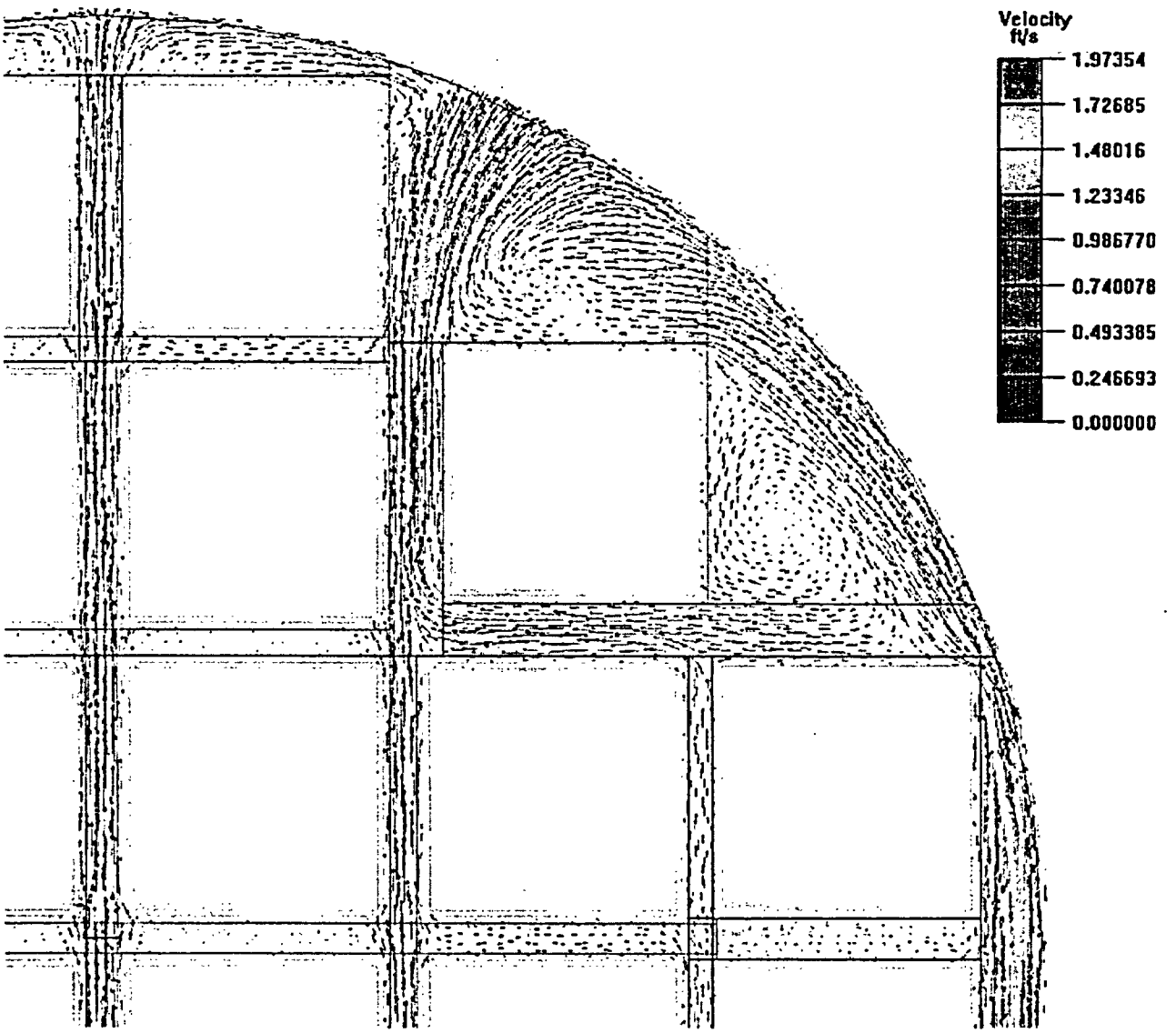


**Figure 4-30 - Velocity Distribution, Bounding Condition in Transfer Cask (Enlarged View)**

C21

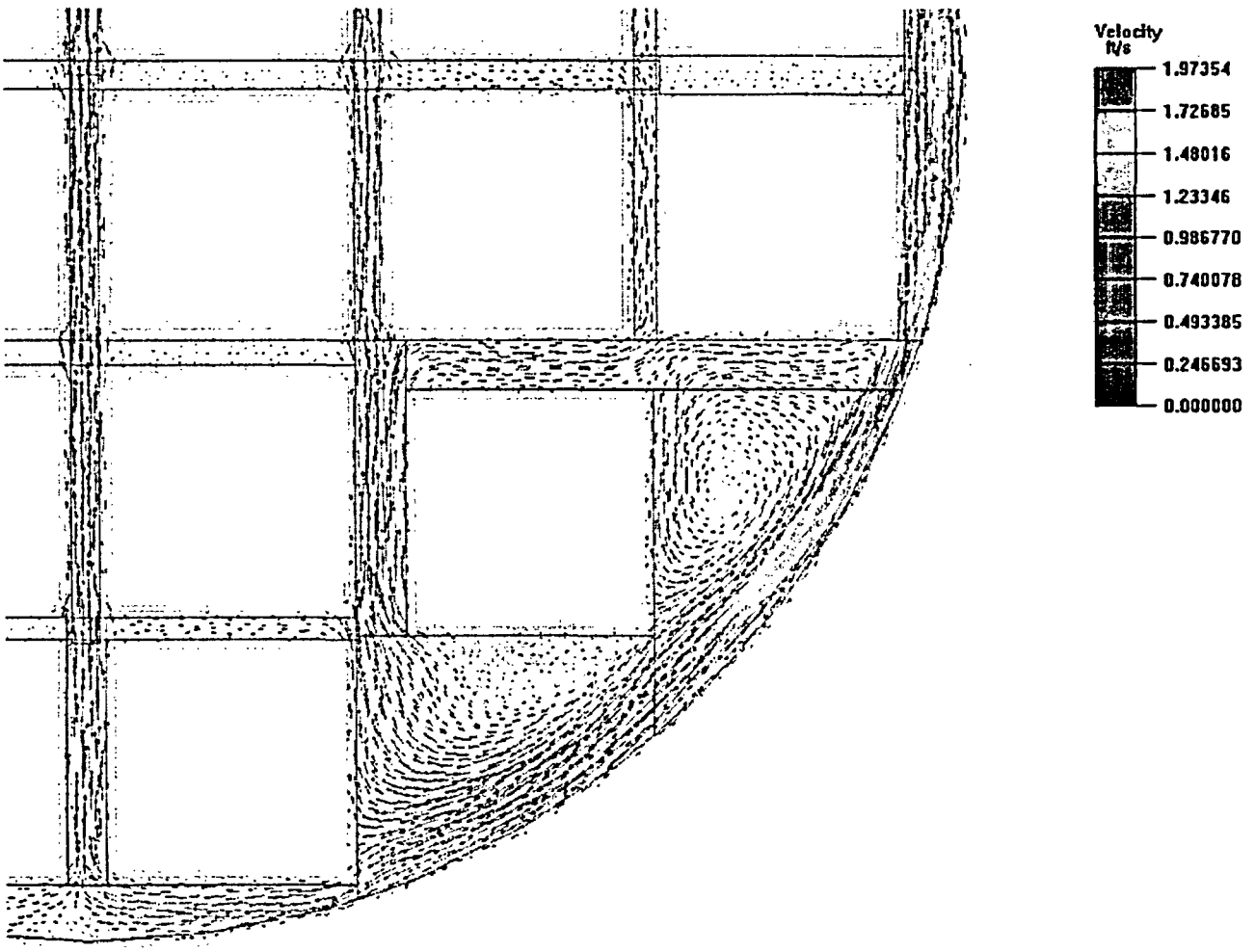


**Figure 4-31 - Velocity Distribution, Bounding Condition in Transfer Cask (Enlarged View)**

C 22

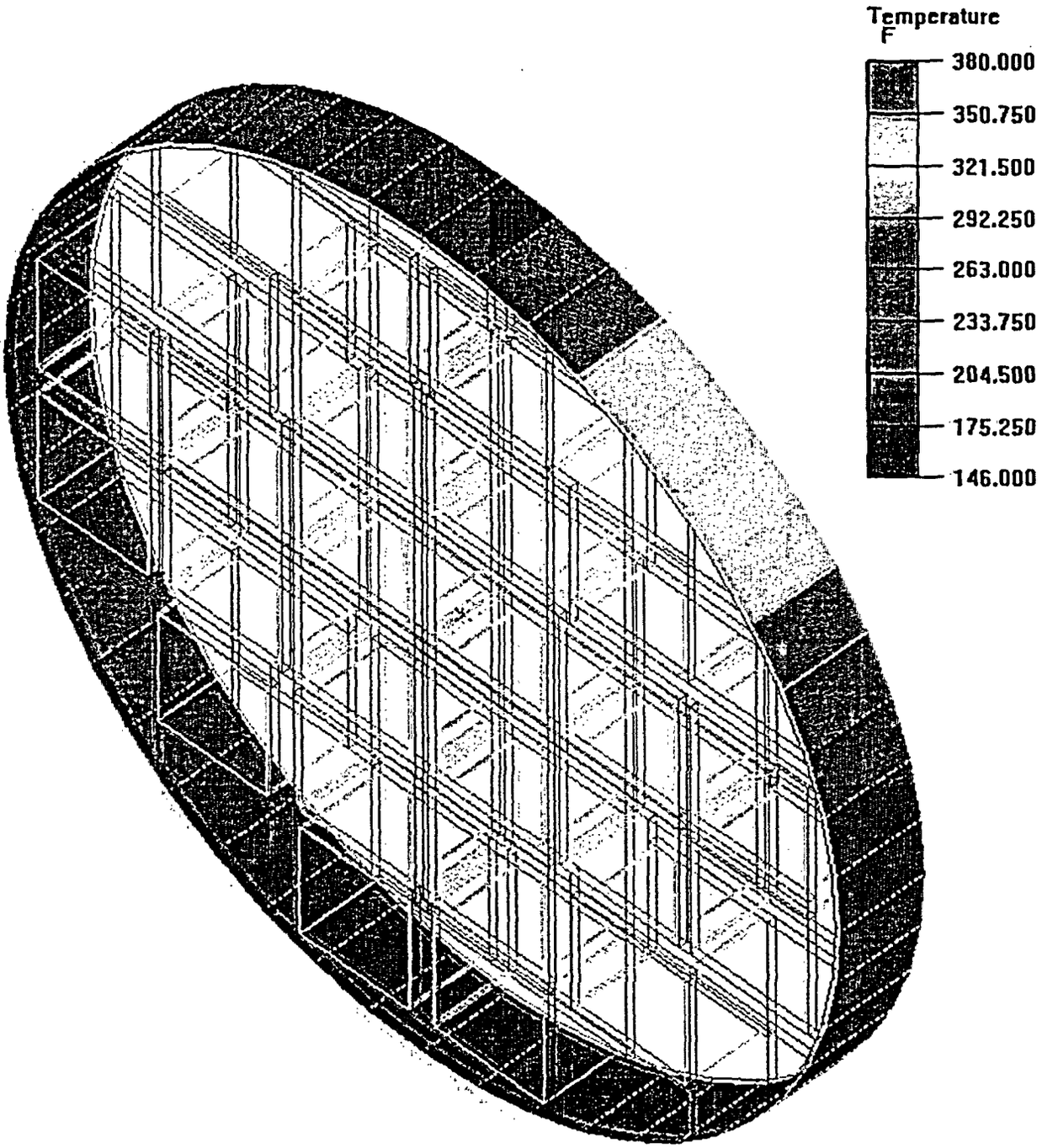


**Figure 4-32 - Imposed Shell Temperatures, Off-Normal Cold Condition in Transfer Cask**

C23

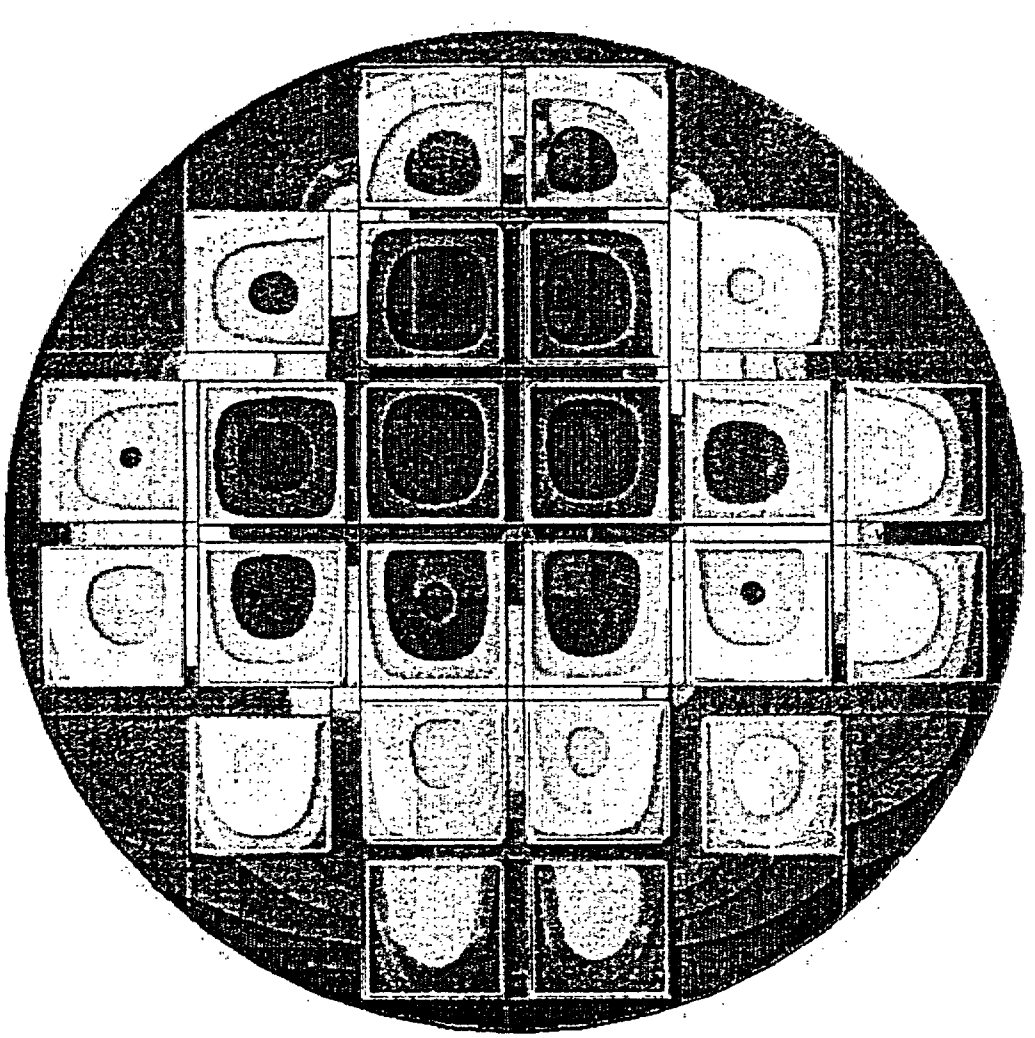


**Figure 4-33 - Temperature Distribution, Off-Normal Cold Condition in Transfer Cask**

C24

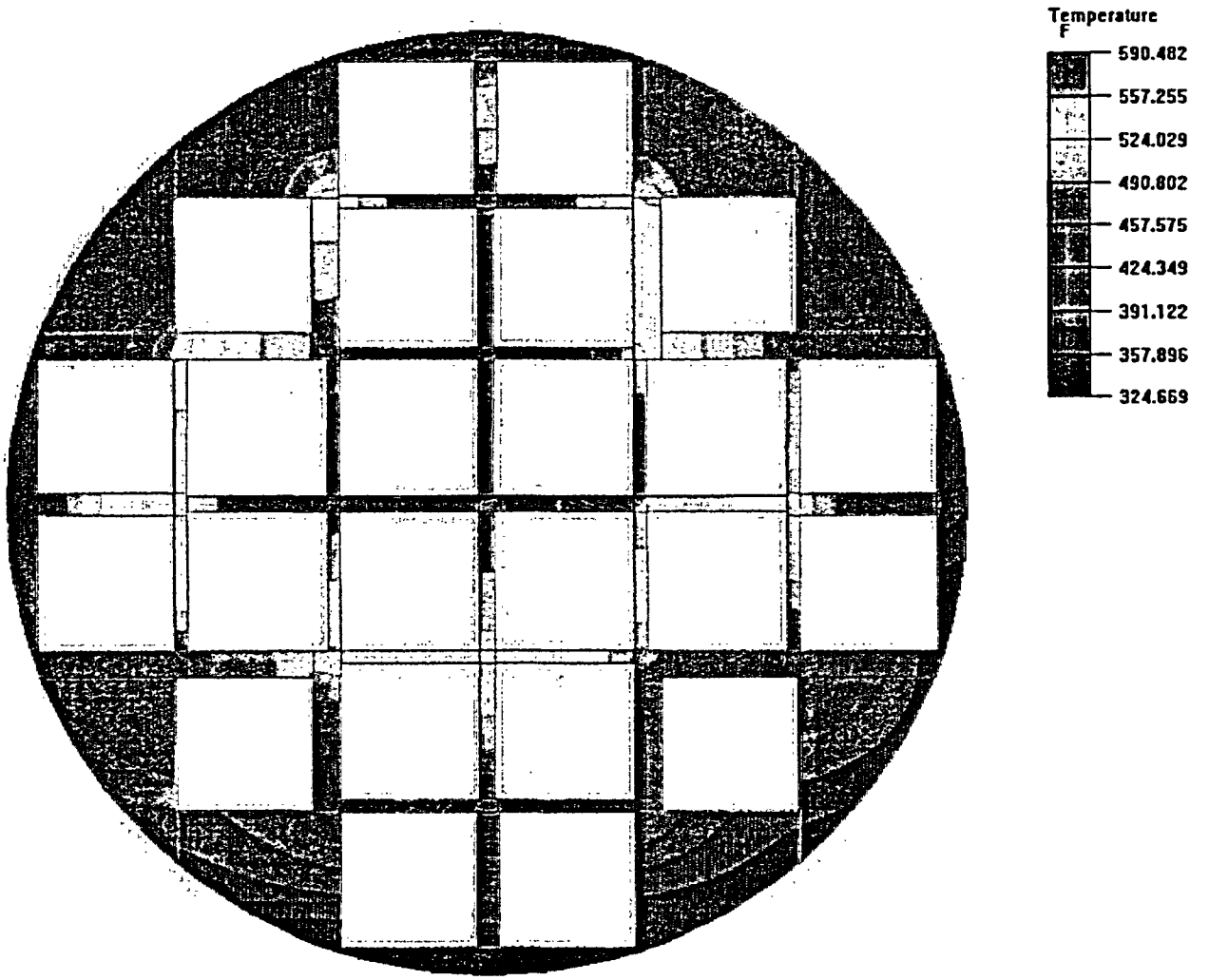


**Figure 4-34 - Spacer Disc Temperature Distribution, Off-Normal Cold Condition in Transfer Cask**

C25

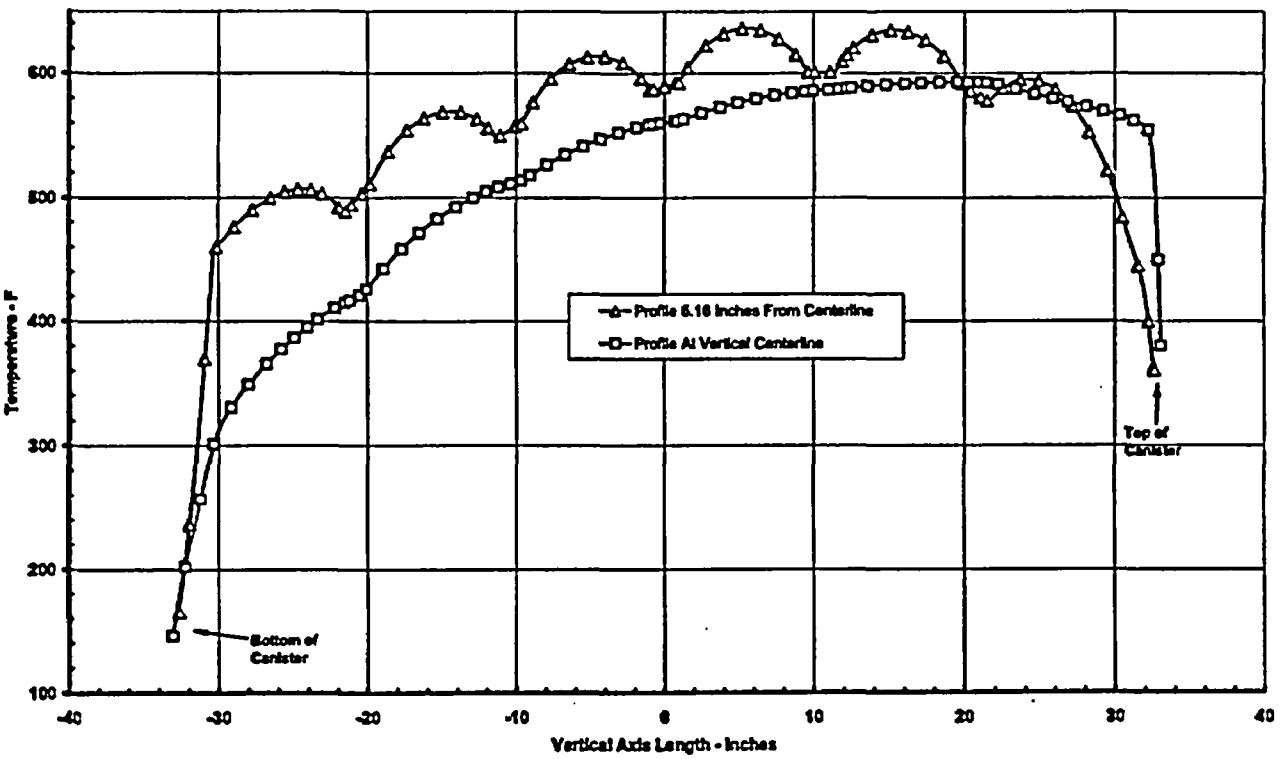


**Figure 4-35 - Temperature Along Vertical Lines Through Basket, Off-Normal Cold Condition in Transfer Cask**

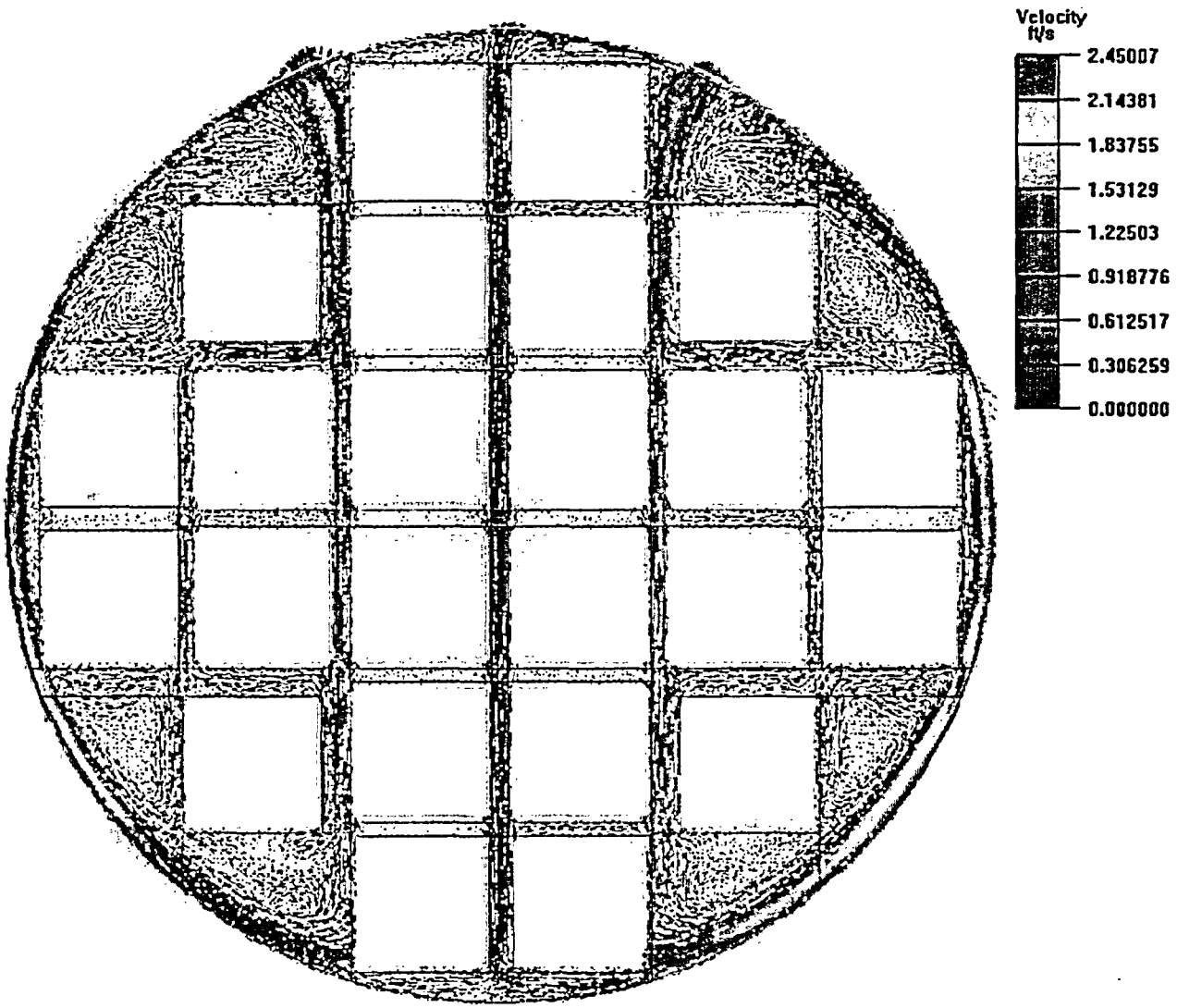


**Figure 4-36 - Velocity Distribution, Off-Normal Cold Condition in Transfer Cask**

C26

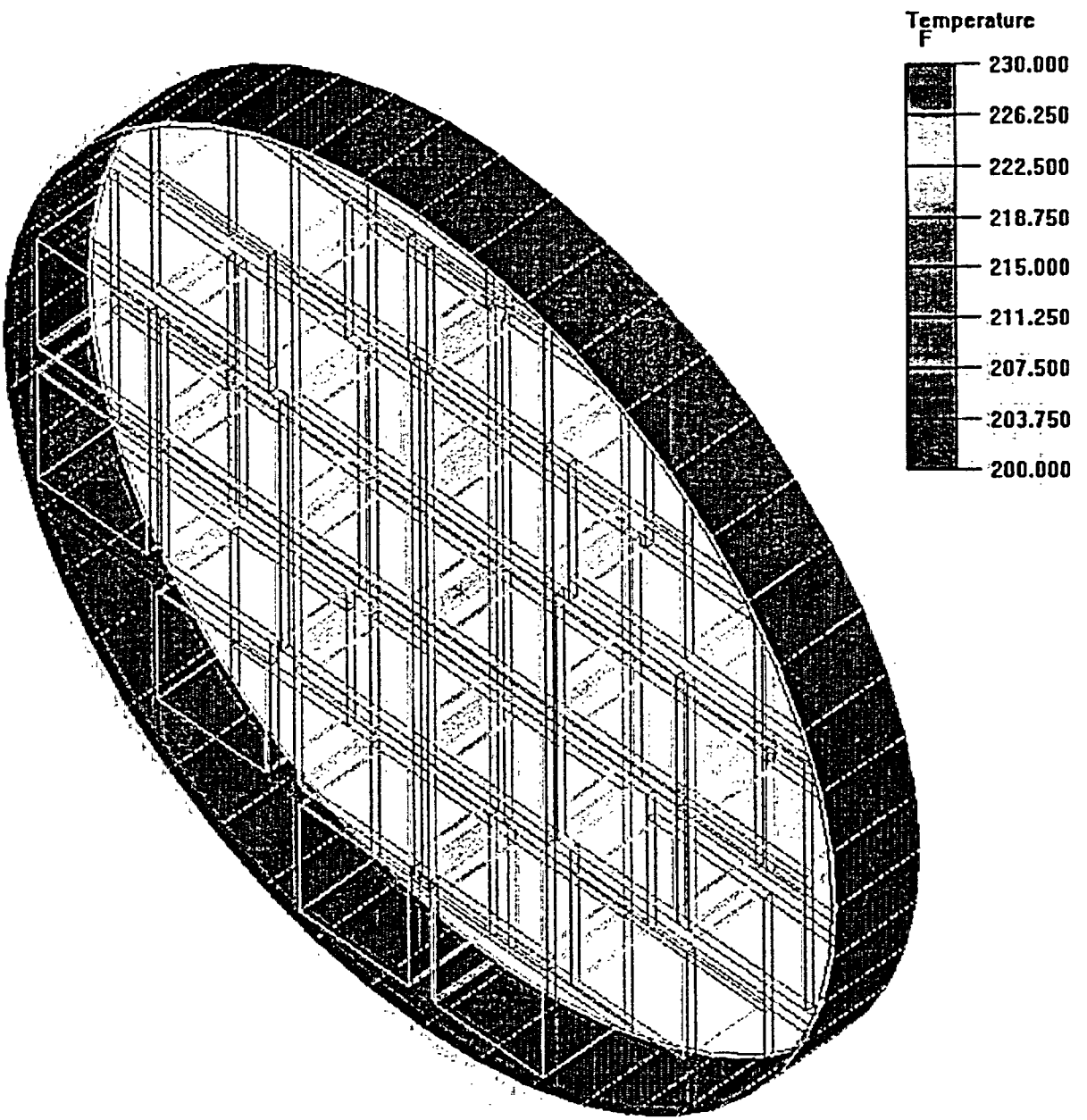


**Figure 4-37 - Imposed Shell Temperatures, Helium Leak Check Operation in Vertical Transfer Cask**

C27

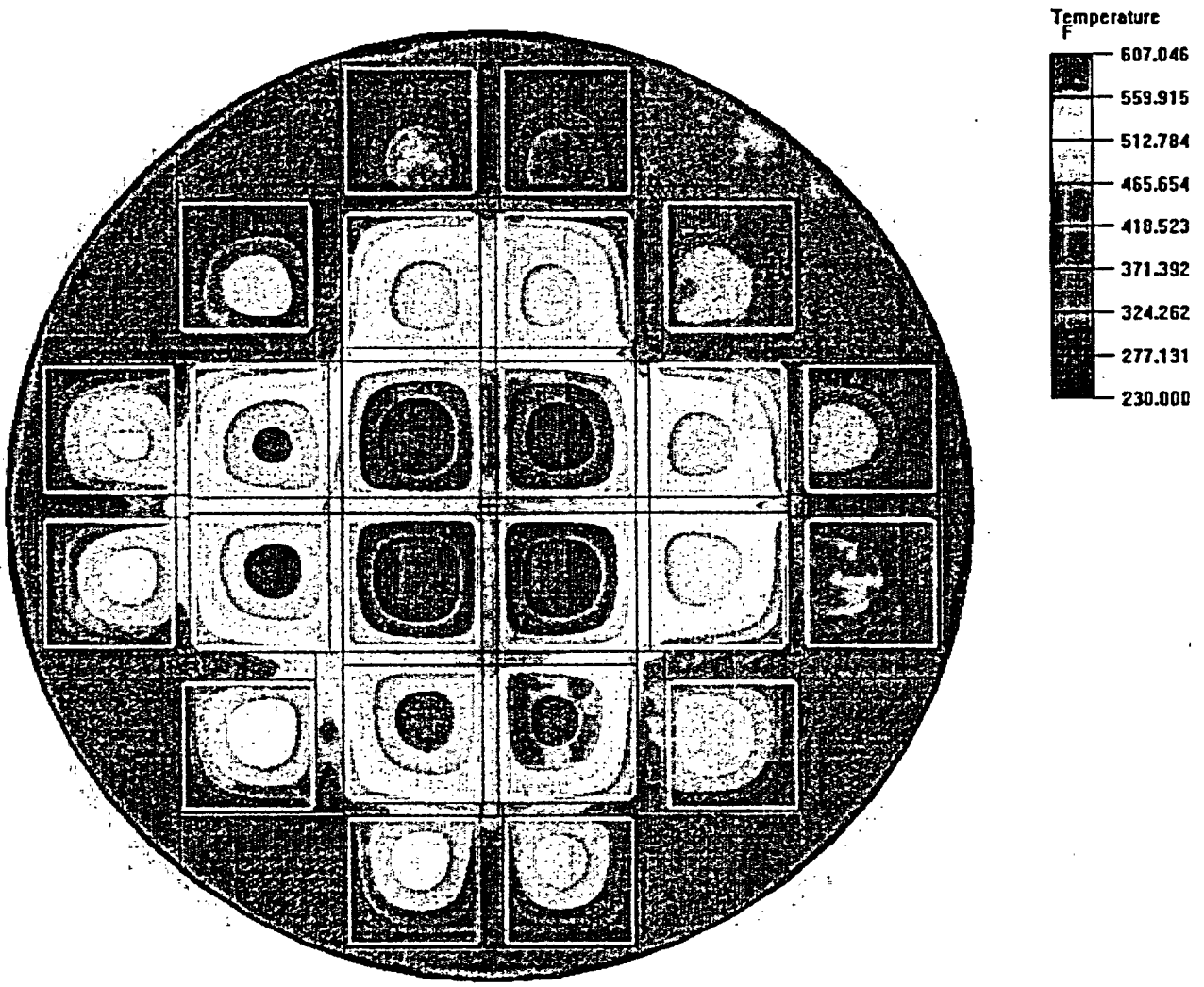


**Figure 4-38 - Temperature Distribution, Helium Leak Check Operation in Vertical Transfer Cask**

C 28

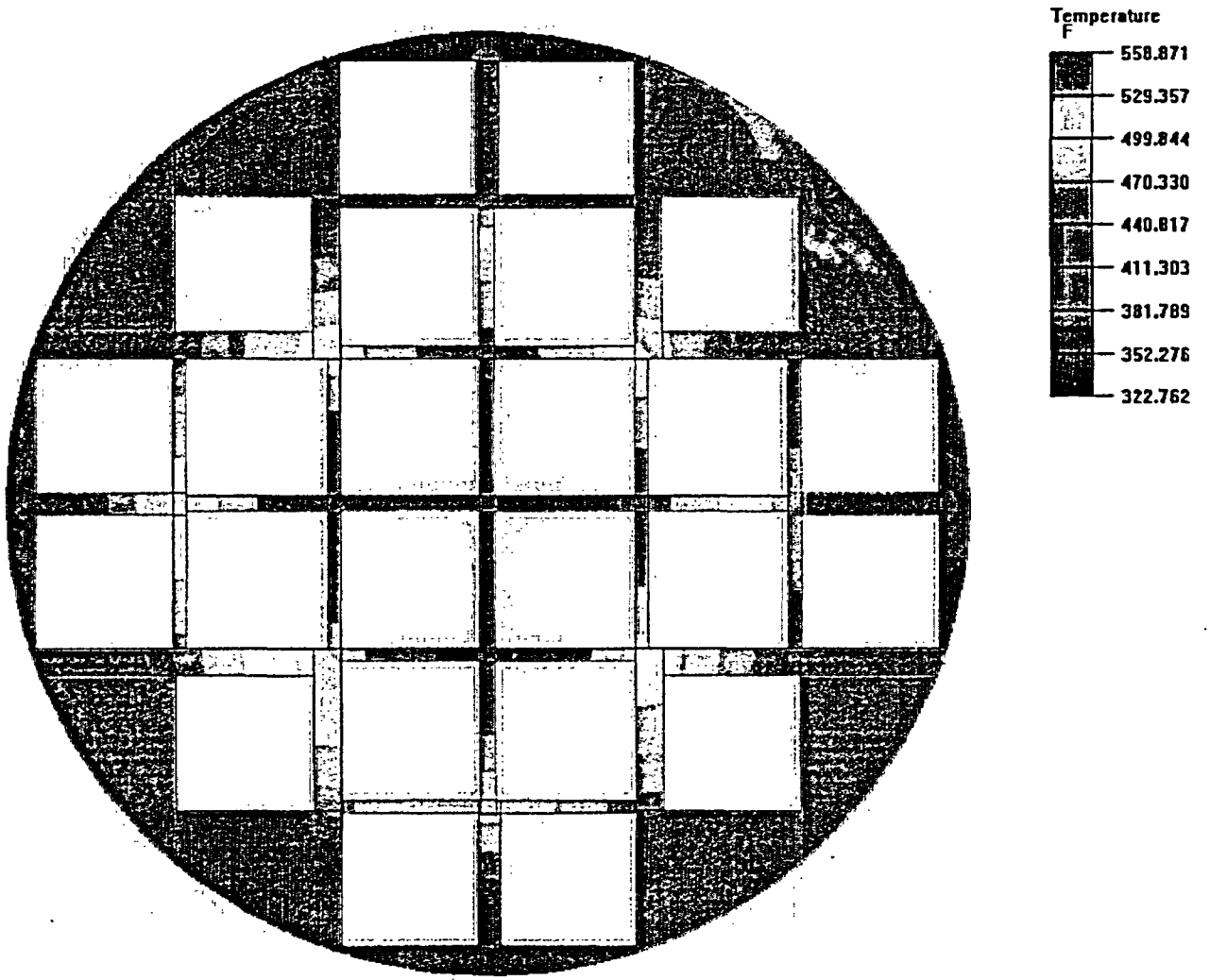


**Figure 4-39 - Spacer Disc Temperature Distribution, Helium Leak Check Operation in Vertical Transfer Cask**

C 29

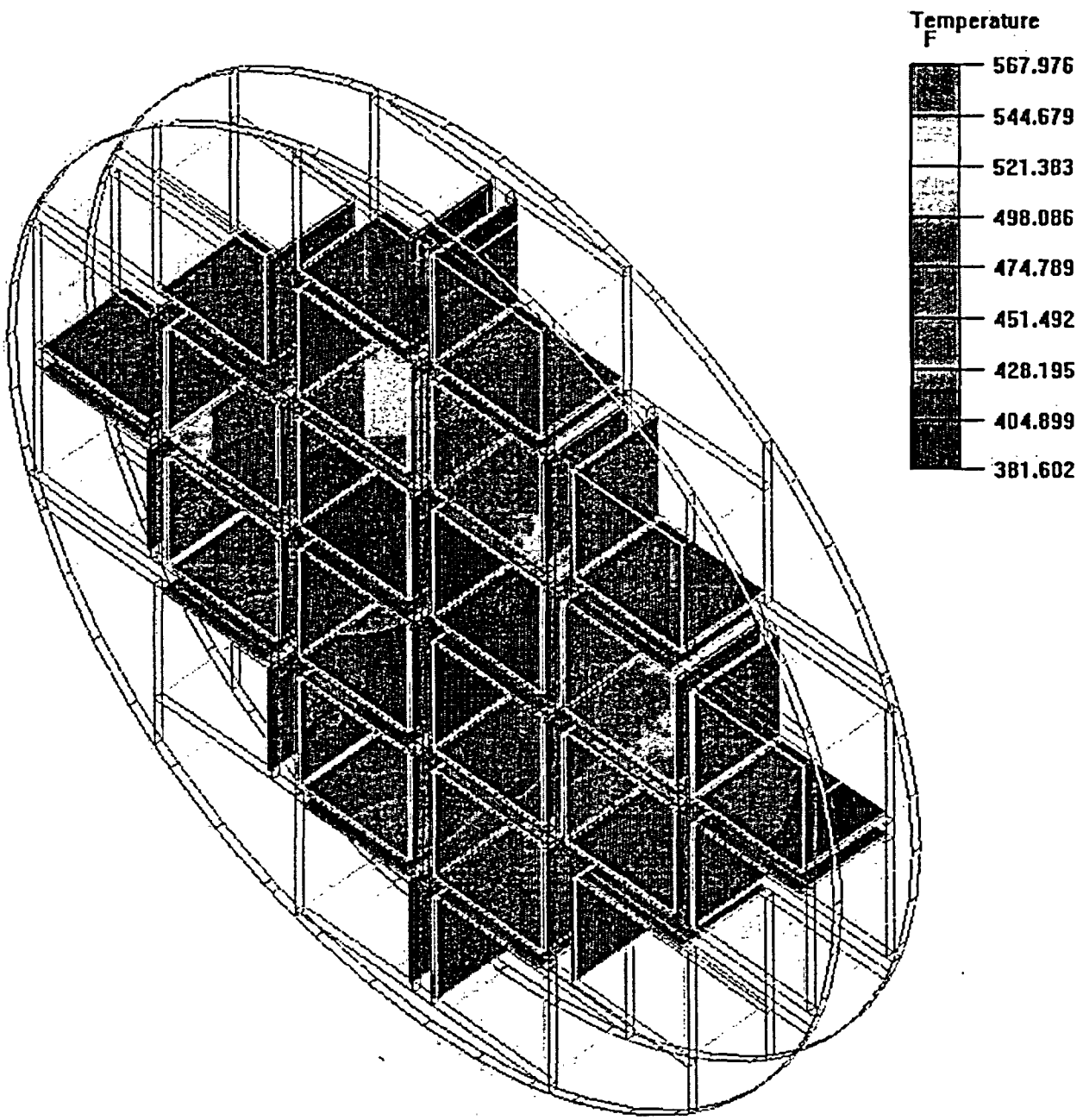


**Figure 4-40 - Poison Sheet Temperature Distribution, Helium Leak Check Operation in Vertical Transfer Cask**

C30

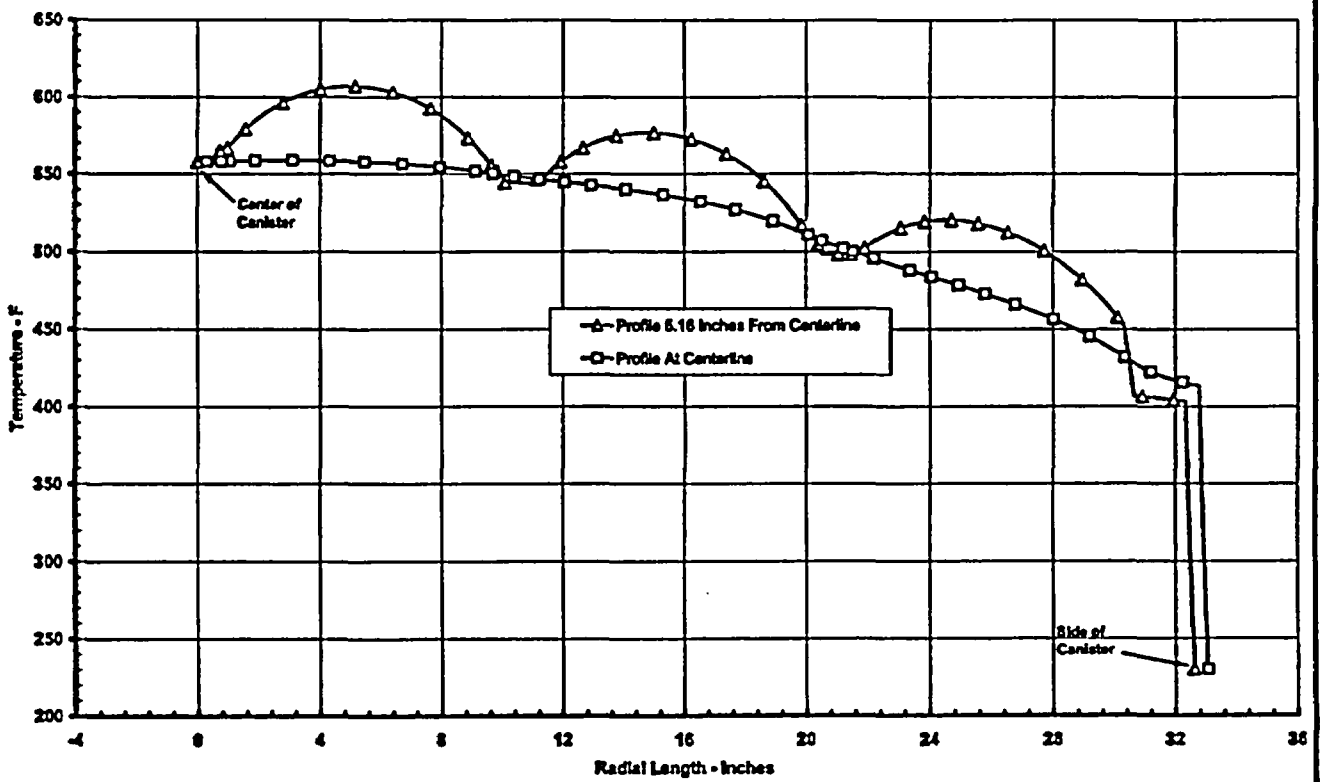


**Figure 4-41 - Temperature Along Radial Lines Through Basket, Helium Leak Check Operation in Vertical Transfer Cask**

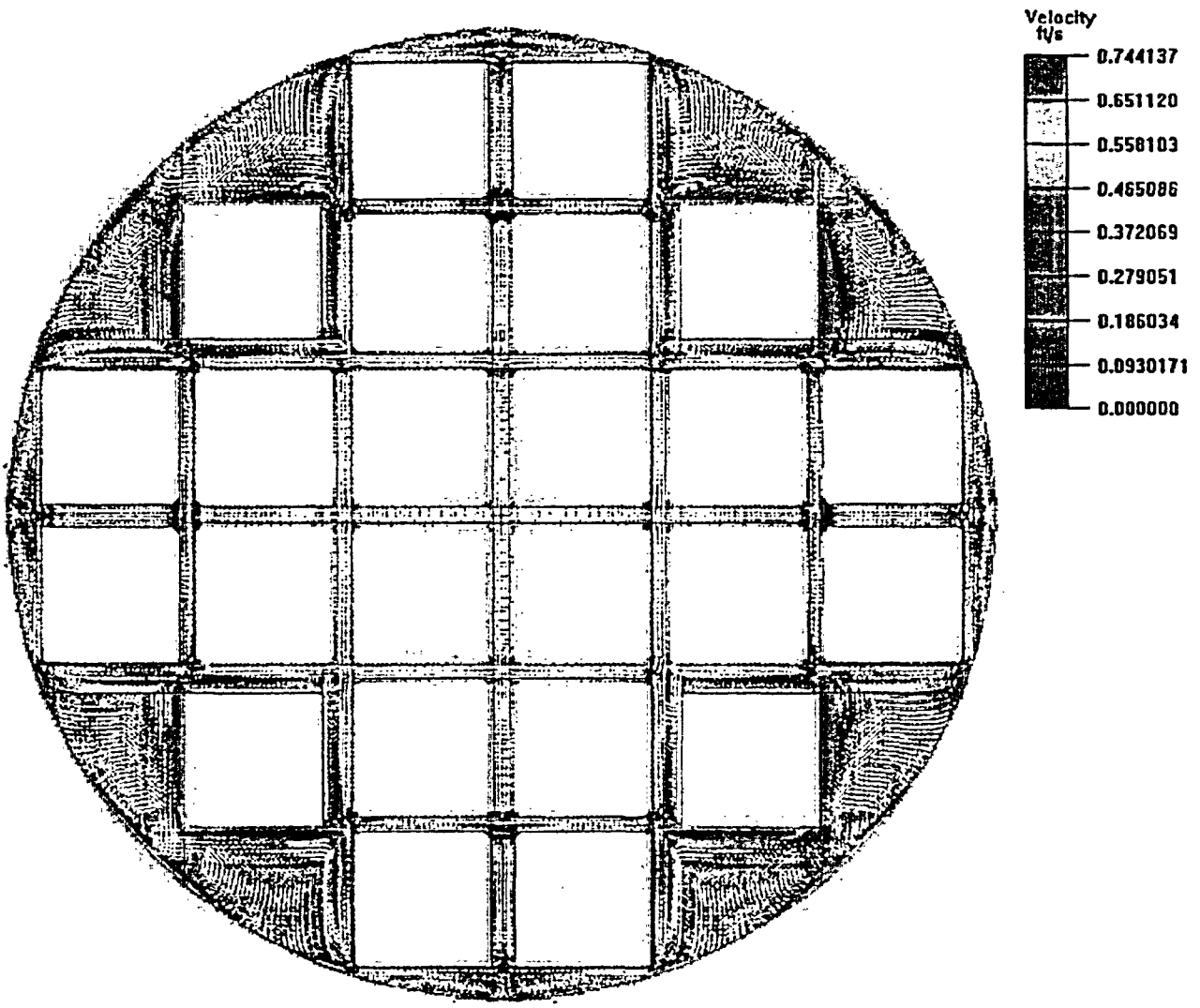


**Figure 4-42 - Z-Plane Velocity Distribution, Helium Leak Check Operation in Vertical Transfer Cask**

C 31

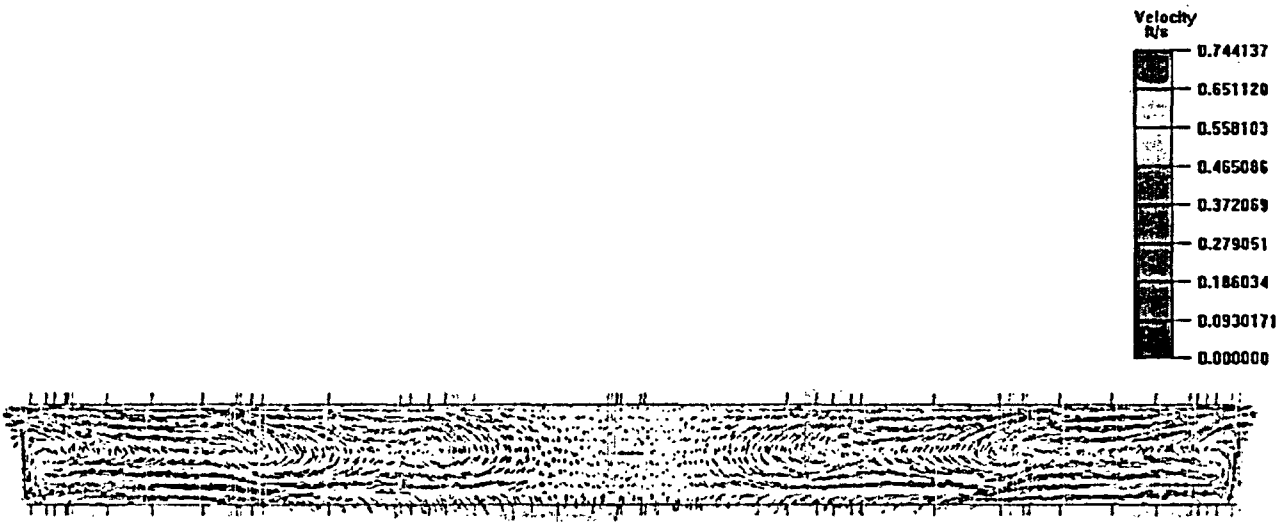


**Figure 4-43 - Y-Plane Velocity Distribution, Helium Leak Check Operation in Vertical Transfer Cask**

C32

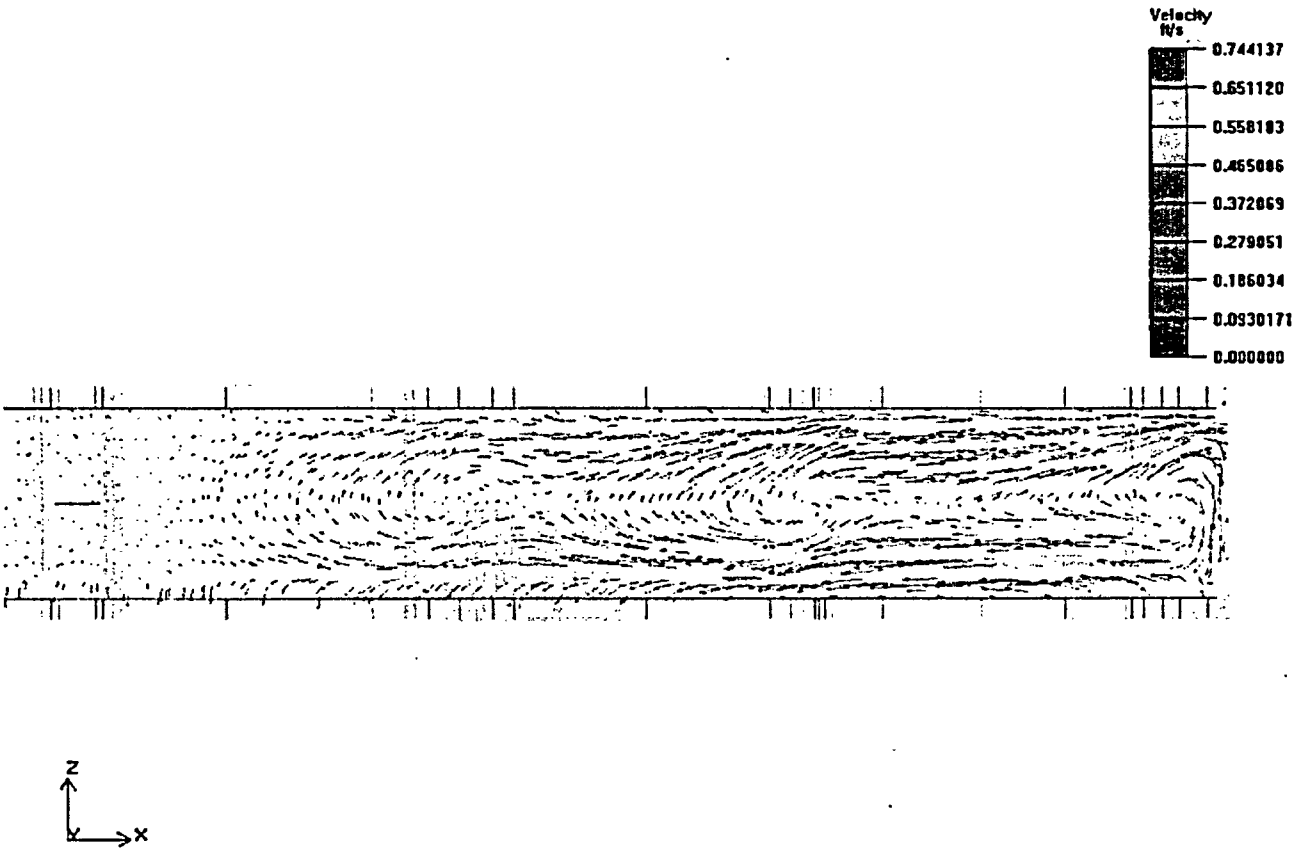


**Figure 4-44 - Y-Plane Velocity Distribution, Helium Leak Check Operation in Vertical Transfer Cask (Enlarged View)**

C 33

## 5. SUMMARY AND CONCLUSION

A thermal model of the thermal-hydraulic environment within the DSC canister has been developed using a CFD methodology. The model has been used to evaluate the design basis thermal performance of the 24PT4 fuel basket during operations within the AHSM and the OS197 transfer cask under bounding conditions (i.e., the thermal condition producing the lowest thermal margin for the fuel cladding) of storage and transfer. The bounding condition for storage is the normal condition with a peak daily temperature of 104°F, a 24-hour average of 97°F, solar insolation, and a decay heat loading of 24 kW within the DSC, while the bounding condition for transfer is the off-normal condition with a peak daily temperature of 117°F, the use of a sun shade, and a decay heat loading of 24 kW. In addition, the steady-state thermal performance of the 24PT4 fuel basket is evaluated for the normal hot condition of storage with the heat load configuration #3, the off-normal cold transfer condition with the heat load configuration #1, and during the helium leak check operation within a vertical transfer cask with the heat load configuration #1.

Table 5-1 to Table 5-3 present a summary of the predicted peak temperatures for the analyzed conditions. As seen, all of the component temperatures are within their allowable limits. The minimum thermal margin seen for the predicted peak fuel cladding temperature is 55°F at the design basis storage condition, while the minimum thermal margins for the guide sleeve, support disc, and support rods (i.e., 125°F, 32°F, and 80°F, respectively) all occur at the off-normal hot transfer condition. .

**Table 5-1 - Summary Of CFD Predicted DSC Component Temperatures For Unit 2/3,Normal Hot Storage Condition**

| DSC Component | Heat Load Configuration #1 [1] | Heat Load Configuration #3 [2] | Allowable Temperature |
|---|---|---|---|
| Max. Fuel Cladding | 697 °F | 697 °F | 752 °F |
| Max. Guide Sleeve | 662 °F | 650 °F | 800 °F |
| Max. Spacer Disc | 653 °F | 635 °F | 700 °F |
| Max. Support Rod | 555 °F | 560 °F | 650 °F |
| Max. Shell | 459 °F | 459 °F | 800 °F |
| Avg. Gas | 530 °F [3] | 590 °F [3] | - |

Table Notes: 1) Decay heat distribution for heat load configuration #1 illustrated in Figure 3-3.

2) Decay heat distribution for heat load configuration #3 illustrated in Figure 3-4.

3) Average gas temperature within modeled segment. Not directly available from the model, but estimated from average spacer disc temperature and subjective averaging of screen display of gas temperature distribution.

**Table 5-2 - Summary Of CFD Predicted DSC Component Temperatures For Unit 2/3, Off-Normal Transfer Condition w/ 117 °F Ambient Temperature**

| DSC Component | Off-Normal Hot Transfer [1] | Off-Normal Cold Transfer [2] | Allowable Temperature |
|---|---|---|---|
| Max. Fuel Cladding | 712 °F | 636 °F | 752 °F |
| Max. Guide Sleeve | 675 °F | 601 °F | 800 °F |
| Max. Spacer Disc | 668 °F | 590 °F | 700 °F |
| Max. Support Rod | 570 °F | 480 °F | 650 °F |
| Max. Shell | 443 °F | 380 °F | 800 °F |
| Avg. Gas | 550 °F [3] | 512 °F | - |

Table Notes: 1) For DSC load configuration 1 with twenty four 1 kW fuel assemblies and peak ambient temperature of 117°F with sunshade.

2) For DSC load configuration 1 with twenty four 1 kW fuel assemblies and ambient temperature of -40°F.

3) Average gas temperature within modeled segment. Not directly available from the model, but estimated from average spacer disc temperature and subjective averaging of screen display of gas temperature distribution.

**Table 5-3 - Summary Of DSC Component Temperatures For Unit 2/3, Helium Leak Check Operations**

| DSC Component | CFD Based Analysis [1] | Allowable Temperature |
|---|---|---|
| Max. Fuel Cladding | 607 °F | 752 °F |
| Max. Guide Sleeve | 568 °F | 800 °F |
| Max. Spacer Disc | 559 °F | 700 °F |
| Max. Support Rod | 376 °F | 650 °F |
| Max. Shell | 230 °F | 800 °F |
| Avg. Gas | 420 °F [2] | - |

Table Notes: 1) For DSC load configuration 1 with twenty four 1 kW fuel assemblies.

2) Average gas temperature within modeled segment. Not directly available from the model, but estimated from average spacer disc temperature and subjective averaging of screen display of gas temperature distribution.

## 6. REFERENCES


*6.1* Final Safety Analysis Report, Standardized Advanced NUHOMS Horizontal Modular Storage System For Irradiated Nuclear Fuel, Transnuclear Inc., ANUH-01.0150, Revision 0, Docket Number 72-1029.

*6.2* Drawings: NUHOMS® 24PT4-DSC, ANUH-01-.4001, Revision 1.

*6.3* ASME Boiler & Pressure Vessel Code, Section II, Part D, Properties, 1998 Edition including 2000 addenda.

*6.4* Calculation No. SCE-23.0402, *"24PT4-DSC Thermal Evaluation"*, Rev. 1, Transnuclear, Inc., Project SCE-23.

*6.5* Calculation No. SCE-23.0410, *"Thermal Analysis of NUHOMS® Advanced Horizontal Storage Module Using A CFD Method"*, Rev. 1, Transnuclear, Inc., Project SCE-23.

*6.6* Transnuclear Inc., Final Safety Analysis Report for the Standardized NUHOMS® Horizontal Modular Storage System for Irradiated Nuclear Fuel, Revision 8, June 2004, NRC Docket No. 72-1004.

*6.7* Calculation No. SCE-23.0406, *"24PT4-DSC Internal Pressure Calculation"*, Rev. 3, Transnuclear West, Project SCE-23.

*6.8* Calculation No. SCE-23.0400, *"Thermal and Pressure Calculation Methodology Document"*, Rev. 0, Transnuclear West, Project SCE-23.

*6.9* *FLUENT™*, Version 6.1, Fluent, Inc., Lebanon, NH, 2003.

*6.10* *ICEPAK™*, Version 4.1, Fluent, Inc., Lebanon, NH, 2003.

*6.11* QA Validation and Verification Report #QA040.229.0001 For Software Codes FLUENT™, Version 6.1, and ICEPAK™, Version 4.1, Transnuclear, Inc., May 2004, Rev. 0.

*6.12* "NUHOMS® Modular Spent-Fuel Storage System: Performance Testing", *Report PNL-7327/UC-812/EPRI NP-6941, Pacific Northwest Laboratory & Carolina Power and Light Company, September 1990.*

*6.13* *Rohsenow, Hartnett, and Choi,* Handbook of Heat Transfer, *3rd edition, McGraw-Hill Publishers, 1998.*

# APPENDIX A: FLUENT™ / ICEPAK™ RUN LOG

INTENTIONALLY LEFT BLANK

## APPENDIX B – EFFECTIVE THERMAL CONDUCTIVITY OF CE 16x16 FUEL ASSEMBLIES

### B1. Purpose

The design basis thermal analysis of the heat transfer within the 24PT4-DSC (dry shielded canister) presented in Section 4 models the CE 16x16 Zircalloy clad fuel assemblies as homogeneous solid regions with uniform internal heat generation. To accurately predict the temperature rise from the fuel guide sleeves to the peak pin location within each fuel assembly using this type of modeling the effective thermal conductivity of the homogeneous solid region must be determined. The effective thermal conductivity calculation accounts for the actual geometry the fuel assembly and the fact that the heat generation occurs only within the fueled pins.

### B2. Assumptions

1. Table B-1 presents a summary of the relevant design information for the CE 16x16 fuel assembly type as obtained from References [B5.1], [B5.2], and [B5.6].
2. The fuel assemblies are assumed to be centered within the guide sleeves.
3. Based on the information in [B5.3], the fuel rods are assumed to have an emissivity of 0.8.
4. The guide sleeve emissivity is 0.40, per Section 3.2.
5. The peaking factor of the fuel is assumed to be 1.08 (see Section 3.3). The CE 16x16 fuel assemblies are assumed to have a decay heat load of 1,000 watts per fuel assembly.
6. Heat transfer from the assembly to the guide sleeve is assumed to be via radiation and conduction only. Neither convection nor axial heat transfer is modeled.
7. To account for the presence of air and/or steam vapor at even low vacuum pressures, the effective conductivity values for vacuum drying are computed assuming the thermal conductivity of air for the void spaces within the assembly and guide sleeve.

### B3. Methodology

The analysis methodology used for this calculation is based on the calculation approach outlined in Section 3.2.2 of reference [B5.5]. A quarter of the CE 16x16 fuel assembly and the surrounding guide sleeve are modeled. The boundaries formed by the guide sleeve are assumed to be at a specified constant temperature, while symmetry conditions are assumed at the remaining two boundaries. The Thermal Desktop™ [B5.7] and SINDA/FLUINT™ [B5.8] computer programs were used to develop and exercise this detailed thermal model of the fuel assembly. Figures B-1 presents a perspective view of the modeled fuel assembly and guide sleeve segment for the CE 16x16 fuel assemblies. Figures B-2 illustrates the finite element modeling used.

The guide tubes are assumed to be filled with helium gas with heat transfer across the interior void volume being via radiation and conduction. Heat transfer across the interiors of the various fuel rods is via conduction through the uranium oxide pellet. While a gap may exist between the cladding and the fuel pellet, the associated thermal resistance is assumed to be negligible since the size of the gap

is small and since, due to swelling of the pellet, it may not even exist. Further, the resistance due to this gap has an insignificant effect on the radial heat transfer within the fuel assembly.

Table B-2 presents the component thermal conductivity values assumed for the thermal modeling. Since the analysis is conducted using a series of steady-state simulations, values for density and specific heat are not required.

The decay heat loading is applied as a volumetric heat load assuming a 1.08 peaking factor and an active fuel length from Table B-1. The design volumetric heat loading used for the fuel assembly types are as follows:

$$\text{Design volumetric heat load} = \left[\frac{(\text{Decay Heat per Assembly}) \times (\text{Peaking Factor})}{(\text{No. of fueled rods}) \times (\text{Volume per rod})}\right]$$

For the 24PT4 with a decay heat loading of 1.0 kW/assembly:

$$\text{Volume per rod} = \text{Active Fuel Lenght} \times \pi \times (\text{Fuel rod OD} - 2 \times \text{Cladding Thickness})^2 / 4$$
$$= 149" \times \pi \times (0.382 - 2 \times 0.025)^2 / 4$$
$$= 12.89889\ \text{in}^3$$

$$\text{24PT4 Design volumetric heat load w/ 1.0 kW} = \left[\frac{(1000\ \text{watts}) \times (1.08)}{(236) \times (12.89889\ \text{in}^3)}\right]$$
$$= 0.35478\ \text{watts/in}^3$$

B4. Effective Thermal Conductivity Calculation

The thermal model described above was exercised for nine guide sleeve temperature levels (i.e., 150, 200, 275, 350, 425, 500, 575, 650, and 725°F) for the case with helium backfill and eleven guide sleeve temperature levels (i.e., the previous nine levels plus 800 and 875 °F) for the vacuum drying condition. The resulting peak temperatures are presented in Table B-3. In accordance with the development of the equation for effective conductivity presented on page II-127 of [B5.4] and equation 6.1-5 of [B5.5], the effective thermal conductivity can be computed as:

$$k_{effective} = \left[\frac{0.29468 \times \text{Volumetric Heat Generation Based On Assembly Width} \times \left(\frac{\text{Assembly Width}}{2}\right)^2}{(T_{peak} - T_{sleeve})}\right]$$

This equation can be restated as:

$$k_{effective} = \left[ \frac{0.29468 \times \text{Decay Heat Loading For Modeled Section} \times 4}{4 \times \text{Length of Modeled Segment} \times (T_{peak} - T_{sleeve})} \right]$$

The decay heat loading computed from the model, the length of the modeled segment (i.e., 0.5 inches), and the noted peak temperature and boundary sleeve temperature are substituted to yield the computed effective thermal conductivity. Table B-3 presents the computed effective thermal conductivity for each guide sleeve boundary temperature under the helium filled and vacuum drying conditions.

For use in finite element modeling, Section 6.2.2 of [B5.5] recommends that the effective thermal conductivity values be made a function of the mean assembly temperature, or $(T_{peak} + T_{sleeve})/2$. Figure B-3 illustrates the correlation between the computed effective thermal conductivity and the median assembly temperature for the helium filled conditions, while Figure B-4 illustrates the correlation for the vacuum drying condition. The recommended effective thermal conductivity for PWR fuel assemblies from Table S-2 of [B5.5] is also presented in the figures for comparison purposes.

Tables B-4 presents the same effective thermal conductivity data in Table B-3, but interpolated for specific values of the median assembly temperature.

B5. References

B5.1. "Characteristics of Spent Fuel, High Level Waste, And Other Radioactive Wastes Which May Require Long-Term Isolation," DOE/RW-0184, Volume 3 of 6, dated December 1987.

B5.2. "Domestic Light Water Reactor Fuel Design Evolution, Volume III," Nuclear Assurance Corporation, September 1981, DOE/ET/47912-3.

B5.3 NUREG/CR-0497, A Handbook of Materials Properties for Use in the Analysis of Light Water Reactor Fuel Rod Behavior, MATPRO - Version 11 (Revision 2), EG&G Idaho, Inc., TREE-1280, August 1981.

B5.4. SAND90-2406, Sanders, T. L., et al., A Method for Determining the Spent-Fuel Contribution to Transport Cask Containment Requirements, TTC-1019, UC-820, November 1992.

B5.5. *"Spent Nuclear Fuel Effective Thermal Conductivity Report"*, prepared TRW Environmental Safety Systems, Inc. for DOE Civilian Radioactive Waste Management System (CRWMS), Report BBA000000-01717-5705-00010, Rev. 0, July 1996

B5.6. "SONGS Unit 2/3 Fuel Assembly Materials and Masses" SCE No. N-1020-162. Transnuclear, Inc. No. SCE-23.0100-11

B5.7. Thermal Desktop™, Version 4.4, Cullimore & Ring Technologies, Inc., Littleton, CO, 2001.

B5.8. SINDA/FLUINT™, *Systems Improved Numerical Differencing Analyzer and Fluid Integrator*, Version 4.4, prepared for NASA, Johnson Spacecraft Center, Contract NAS9-19365, prepared by Cullimore & Ring Technologies, Inc., Littleton, CO, 2001.

B6. Computational Run Summary

The table below lists the computer runs performed for the CE 16x16 fuel assembly effective thermal conductivity calculation. The list includes the input, database, and output files associated with the Thermal Desktop™ and SINDA/FLUINT™ generated results. The files are contained on an optical disk that accompanies this calculation.

**Thermal Desktop & SINDA/FLUINT Run Log**

| Case # | Operating Condition | File Name | Date |
|---|---|---|---|
| Case B1 | CE 16x16 Fuel Assembly w/ 1000 Watts Decay Heat & Helium Backfill | CE16x16.dwg | 1/27/2003 |
| | | CE16x16_24PT4.inp | " " |
| | | CE16x16_24PT4.cc | " " |
| | | CE16x16_K-eff.rad | " " |
| | | CE16x16_24PT4.out | " " |
| | | CE16x16_24PT4.sav | " " |
| | | k-eff_Materials_24PT.tdp | " " |
| | | k-eff_Materials_24PT.rco | " " |
| Case B2 | CE 16x16 Fuel Assembly Under Vacuum Drying Operations w/ 1000 Watts Decay Heat | CE16x16_Rev1.dwg | 6/24/2004 |
| | | CE16x16_24PT4_vac-air.inp | " " |
| | | CE16x16_24PT4_vac-air.cc | " " |
| | | CE16x16_K-eff.rad | " " |
| | | CE16x16_24PT4_vac-air.out | " " |
| | | CE16x16_24PT4_vac-air.sav | " " |
| | | k-eff_Materials_24PT.tdp | 1/27/2003 |
| | | k-eff_Materials_24PT.rco | " " |

## Table B-1 - Summary of Design Data For CE 16x16 Fuel Assembly Type

| Parameter | Value For CE 16x16 Fuel Assembly |
|---|---|
| Number of fuel rods | 236 |
| Number of guide tubes | 5 |
| Number of instrument tubes | 0 |
| **Parameter** | **Inches** |
| Pellet diameter | 0.325 |
| Active fuel length | 149 |
| Cladding thickness | 0.025 |
| Fuel rod OD | 0.382 |
| Fuel rod pitch | 0.506 |
| Guide tube OD | 0.98 |
| Guide tube thickness | 0.040 |
| Instrument tube OD | – |
| Instrument tube thickness | – |

Note: Assembly geometry obtained from References [B5.1], [B5.2], and [B5.6]

## Table B-2 - Thermal Properties Used In Calculation of Fuel Effective Conductivities

| Temperature (°F) | Conductivity (BTU/min -in-°F) |
|---|---|
| Zircalloy [B5.3] | |
| 200 | 0.0109 |
| 300 | 0.0115 |
| 400 | 0.0121 |
| 500 | 0.0126 |
| 600 | 0.0131 |
| 800 | 0.0142 |
| Fuel Pellet, UO2 [B5.3] | |
| 200 | 5.537e-3 |
| 300 | 5.038e-3 |
| 400 | 4.622e-3 |
| 500 | 4.270e-3 |
| 600 | 3.968e-3 |
| 700 | 3.707e-3 |
| 800 | 3.478e-3 |
| Type 304/304L Stainless Steel [See Table 3-1] | |
| Helium [See Table 3-2] | |
| Air [See Table 3-2] | |

## Table B-3 - Computed Effective Thermal Conductivity

| Conditions | Sleeve Temperature, F | Peak Temperature, F | Medium Assembly Temperature, F | Effective Thermal Conductivity, Btu/min-in-F |
|---|---|---|---|---|
| Helium Filled | 150 | 234.8 | 192.4 | 0.000349 |
| | 200 | 279.5 | 239.8 | 0.000372 |
| | 275 | 345.9 | 310.5 | 0.000418 |
| | 350 | 413.2 | 381.6 | 0.000469 |
| | 425 | 481.2 | 453.1 | 0.000527 |
| | 500 | 550 | 525.0 | 0.000592 |
| | 575 | 619.7 | 597.4 | 0.000662 |
| | 650 | 690.1 | 670.1 | 0.000738 |
| | 725 | 761 | 743.0 | 0.000823 |
| Vacuum Drying Conditions | 150 | 347.6 | 248.8 | 0.000150 |
| | 200 | 376.3 | 288.2 | 0.000168 |
| | 275 | 423.5 | 349.3 | 0.000199 |
| | 350 | 475.2 | 412.6 | 0.000237 |
| | 425 | 530.9 | 478.0 | 0.000280 |
| | 500 | 589.8 | 544.9 | 0.000330 |
| | 575 | 651.5 | 613.3 | 0.000387 |
| | 650 | 715.5 | 682.8 | 0.000452 |
| | 725 | 781.4 | 753.2 | 0.000525 |
| | 800 | 848.9 | 824.5 | 0.000606 |
| | 875 | 917.6 | 896.3 | 0.000695 |

## Table B-4 - CE 16x16 Fuel Assembly Effective Conductivities

| | K-effective, (Btu/min/in/°F) | |
|---|---|---|
| Median Temperature (°F) | Helium Filled | Vacuum Conditions |
| 200 | 0.000353 | 0.000127 |
| 275 | 0.000395 | 0.000161 |
| 350 | 0.000446 | 0.000200 |
| 425 | 0.000504 | 0.000245 |
| 500 | 0.000570 | 0.000296 |
| 575 | 0.000641 | 0.000355 |
| 650 | 0.000717 | 0.000421 |
| 725 | 0.000802 | 0.000496 |
| 800 | 0.000886 | 0.000578 |
| 875 | — | 0.000669 |

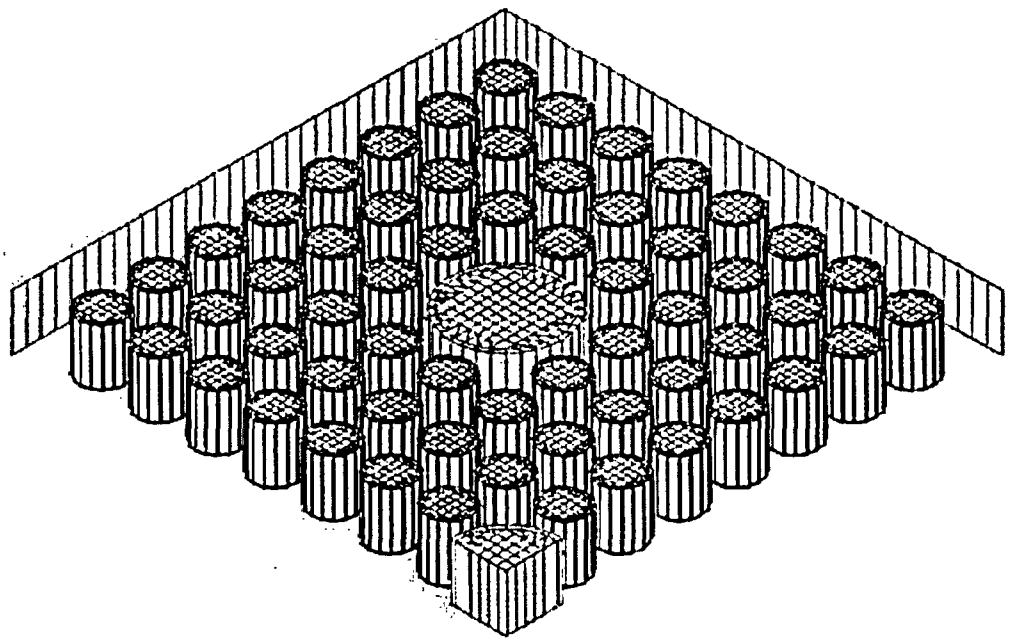

**Figure B-1 - Perspective View Of CE 16x16 Thermal Model (1/4 Segment)**

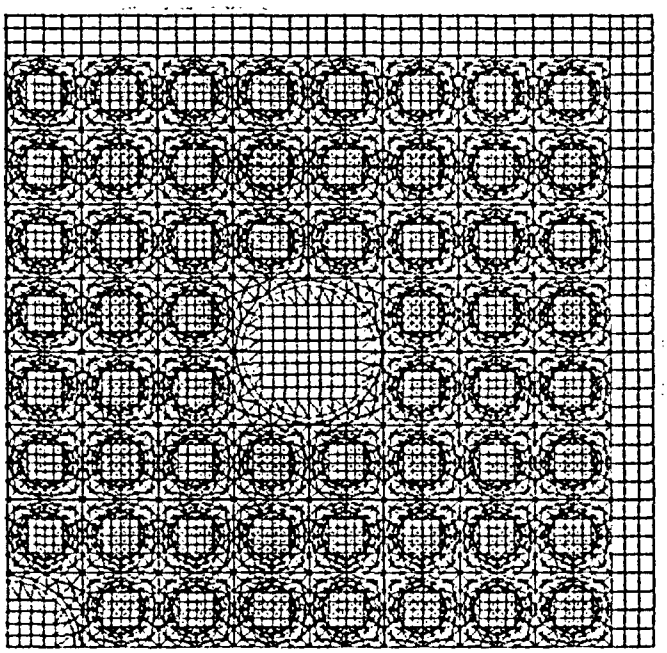

**Figure B-2 - Finite Element Modeling Of 1/4 Segment CE 16x16 Assembly**

C 34

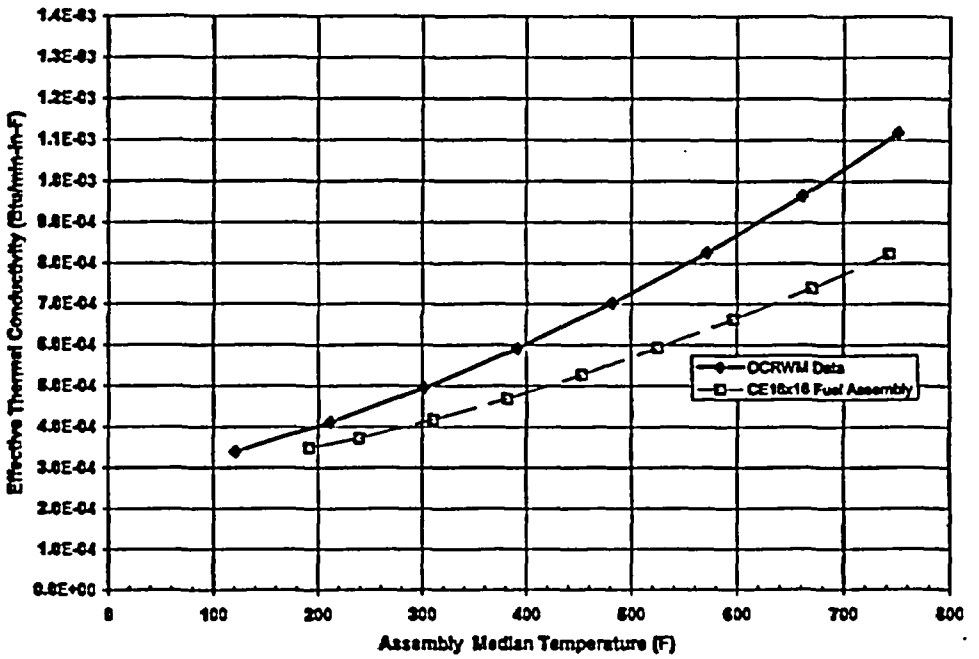


**Figure B-3 - Effective Radial Thermal Conductivity For Helium Filled Conditions**

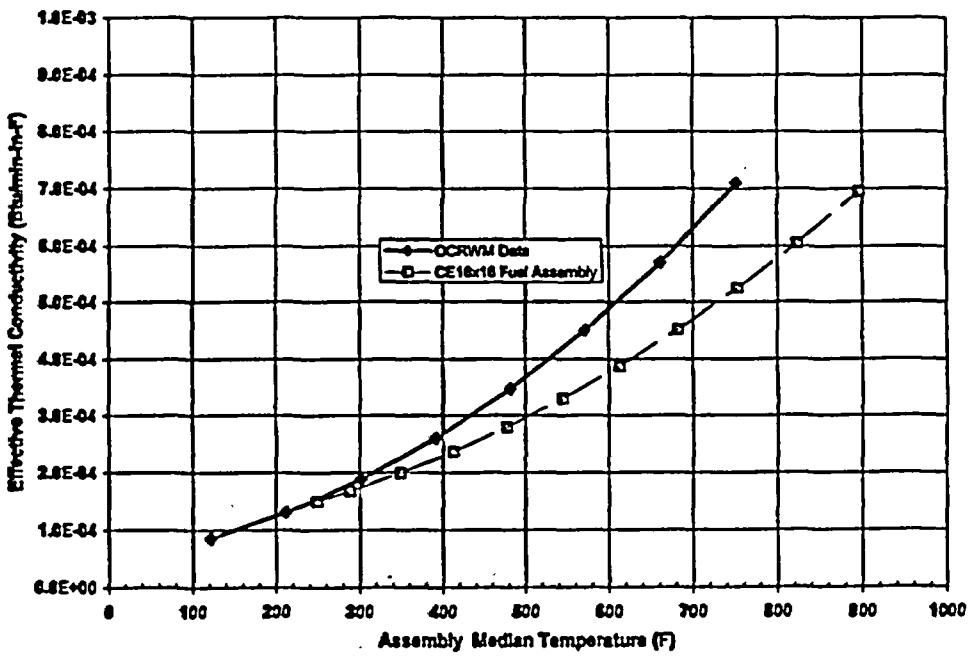


**Figure B-4 - Effective Radial Thermal Conductivity For Vacuum Conditions**